Dynamics Of Synaptically Coupled McKean Neurons

Matthew Denman-Johnson

Ph.D. in Mathematics

Mathematical Biology Group

Department of Mathematical Sciences
Loughborough University - 2004

Dynamics Of Synaptically Coupled McKean Neurons

by

Matthew Denman-Johnson

A Doctoral Thesis

Submitted in partial fulfillment of the requirements

for the award of

Ph.D. in Mathematics of Loughborough University

August 2004

Abstract

The work in this thesis uses geometric dynamical systems methods to derive phase equations for networks of weakly connected McKean relaxation oscillators. Importantly, this particular single neuron model, with appropriate modifications, is shown to mimic very closely the behaviour of the more biophysically complicated Hodgkin-Huxley model, whilst remaining analytically tractable (albeit in some singular limit). We consider realistic forms of axo-dendritic synaptic coupling with chemical synapses modelled as the convolution of some input spike train with an appropriate temporal kernel. Using explicit forms for the phase response curves (PRCs), for a range of single neuron models, we are able to derive explicit formulas for the phase interaction function in an arbitrary synaptically interacting network of neural oscillators. The PRC for the McKean model is calculated exactly, whilst those for other models is found numerically. In both cases we make extensive use of Fourier representations for synaptic currents, to investigate the effects of axonal, synaptic and dendritic delays on the existence and stability of phase-locked states. Results are obtained for both discrete networks and a one dimensional continuum with space-dependent axonal delays using the theory of weakly coupled oscillators. Moreover, we show how strongly coupled inhibitory neurons, with an underlying excitable structure, can interact to produce a robust anti-phase rhythm. We describe this process exactly for the McKean model, and are thus able to quantify the process of anode break excitation for this model. We investigate in some detail the dynamics of so-called half-center oscillators, built out of reciprocally interacting inhibitory non-oscillatory neurons. Importantly this forms the basis for the study of the central pattern generator (CPG) underlying swimming in the Xenopus tadpole. A model is developed based around weakly

interacting half-center oscillators, themselves built from non-oscillatory modified McKean neurons. This latter model is a natural extension of the McKean model that more closely reproduces neuronal output from neurons within the CPG of the tadpole swimming circuit. The theory of weakly coupled chains is generalised to incorporate the important distinction between left and right sides of the spinal cord, and shown to yield patterns consistent with those observed during fictive swimming. Throughout the thesis results from any exact mathematical analysis are always compared to both direct numerical simulations of the McKean model and the more biologically complicated Hodgkin-Huxley model. There is always excellent agreement between theory and numerical experiment in the weak coupling regime, as expected. Moreover, results from the weak-coupling theory are found to have good predictive power even for moderately strong forms of coupling.

Contents

Chapter 1

Introduction

1.1 Background On Coupled Oscillators

Coupling : *A method of linking objects together.*

Oscillator *: A device or mechanism for producing or controlling oscillations.*

Oscillation *: To vary or fluctuate between fixed limits.*

In 1665 Dutch astronomer and physicist Christiaan Huygen was recovering from illness when he noticed something odd about the two pendulum clocks on his wall. Huygen noticed that the pendulums were perfectly synchronised and so he started to experiment. He perturbed both pendulums in various ways and found that the regardless of the disturbance, the pendulums would always synchronise after a while. He came to the conclusion that there were imperceptibly small vibrations that were 'coupling' the motion of the pendulums.

After this discovery there was very little scientific investigation into the field of coupled oscillators for 300 years. In the 1960's biologist Arthur Winfree worked on the proposal that coupled oscillators were not a curiosity of limited interest, but were in fact prevalent in the natural world [1] [2]. The most famous example is of the Malaysian fireflies and how a large populations will eventually flash in synchrony as the night-time progresses [3, 4] [5]. He was the first to look at large populations of oscillators and suggested that in limit of weak coupling, amplitude variations could be neglected. This meant that oscillators could be described simply by a phase along their limit cycle. He also discovered that, in a population of oscillators with a distribution of natural frequencies, at some critical level as the variance is reduced, the oscillators will synchronise spontaneously. Winfree noted that this behaviour was reminiscent of a thermodynamic phase transition and this is still an active research area [6].

There are many areas of scientific work that coupled oscillator theory is used today. The heart can be modelled by systems such as the Bonhoeffer Van-Der-Pol equation [7] [8] [9]. Calcium dynamics can also be modelled with oscillatory systems [10] [11]. The work in this thesis looks at using coupled oscillators to model neural networks.

The first electroencephalograph of a human showed that the brain generated a rhythmic pattern of 8-12Hz [12]. From these scalp recordings various oscillatory patterns were identified, both in rest and sleep. There was however a conspicuous lack of these patterns during normal consciousness and the rhythms that were observed, were low amplitude and de-synchronised. The trend of observed patterns being non-cognitive was further shown when the rhythms were observed in loss of consciousness states such are during epileptic fits and in anathematised patients. Such discoveries about the oscillatory nature of the human brain engaged the scientific community. Biologists became interested in large-scale models of neural

activity and this in turn prompted physicists and mathematicians to investigate the underlying dynamics.

There are many levels at which this neural activity can be modelled, from detailed single-ion channel models [13], up to the 'black box' models that help to understand psychological phenomena [14]. Between these two extremes lies the use of low dimensional models to represent individual neurons. It is the theory of coupled phase oscillators that provides a substantial framework for understanding the emergent properties of such neural networks [15]. Moreover it is known that in many systems synchrony tends to dominate in the presence of strong stimuli. However when there is no active stimulation, waves are often observed [16]. It is now known from theoretical work that a network of weakly coupled oscillators with spatially restricted connections can produce these travelling waves [16]. This generation of travelling waves has resulted in oscillatory neural networks being widely studied, especially since it is the travelling wave phenomenon that is observed in many biological experiments. For example a vast array of travelling waves of electrical activity are observed in the visual and visuomotor as well as the olfactory areas of cortex [17]. In vertebrates the temporal frequencies of these stimuli driven oscillations range between 10-100Hz.

These synchronies and travelling waves occur at the network level, yet it is the oscillatory nature of the individual neurons that enables these properties to exist. It is well established that there are a large number of neurons in the brain, estimated at around 10^{10} neurons and 10^{15} synapses. It is interesting that as well as there being a large quantity of neurons, they are also densely packed. In just 1mm^3 of cortical tissue there are about 10^5 neurons.

For the work in this thesis we consider three fundamental components of the single neuron:

The DENDRITIC TREE : A branched structure that forms the main input pathway of a neuron receiving signals from other neurons [18]. It sums the output signals received from surrounding neurons in the form of an electrical potential, which diffuses along the tree to the SOMA.

The SOMA : The main body of the neuron. If the total potential at the soma exceeds a certain threshold value, the neuron produces a short electrical spike or *action potential* , which is then conducted along the AXON.

The AXON : When the soma fires it causes a potential difference in an area called the *axon hillock* . This causes the action potential to travel down the axon and terminate in a regions called *synaptic terminals* . This potential causes neurotransmitters (chemicals) to be released which bind to the dendritic tree and cause a change in potential of the target neuron.

Figure (1.1.1) shows some of the many different types of neurons. Note, however, that their fundamental structure is the same. Namely, they all have a single axon, cell body and branched dendritic tree. The electrophysiological understanding of the nature of neurons allowed the creation of realistic mathematical models that could mimic experimental data. In the 1950's Hodgkin-Huxley constructed the first bio-physical model of a neuron and this is the starting point for chapter 2.

In this thesis we derive phase equations for networks of weakly connected McKean relaxation oscillators. This model is both analytically tractable and mimics the more detailed Hodgkin-Huxley model.

We calculate the explicit form of the phase response curves (PRC) for the McKean model using geometric techniques. For other single neuron models we do this numerically. These are used to derive explicit formulae for the phase interaction functions in networks of synaptically interacting neural oscillators. In all cases we will show that Fourier representations are useful for performing network cal-

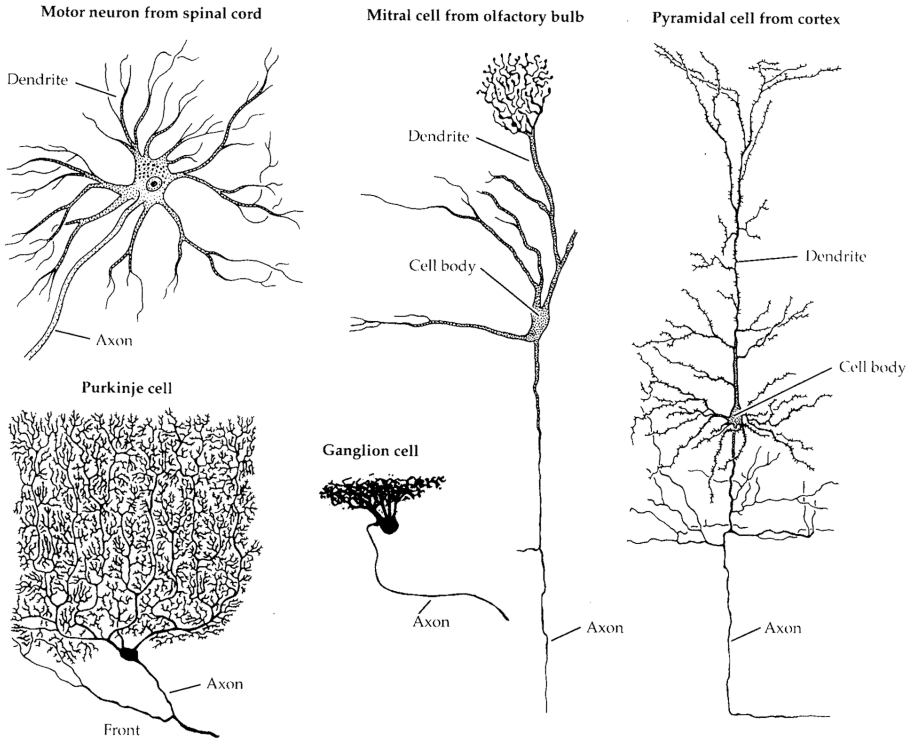

Figure 1.1.1: Caricatures of different types of neurons [18].

culations. This allows the investigation of how axonal, as well as synaptic and dendritic delays effect the existence and stability of phase-locked states. We use the theory of weak coupling to obtain results for both discrete networks and a one dimensional continuum.

We also investigate strongly coupled inhibitory neurons, possessing an underlying excitable structure, and show how these can interact to produce a robust anti-phase rhythm. We describe this process exactly for the McKean model, and thus are able to quantify the process of anode break excitation for this model. We investigate the dynamics of so-called half-center oscillators, and build our own out of reciprocally interacting inhibitory non-oscillatory neurons. Importantly this forms the basis for a study of the central pattern generator (CPG) underlying swimming in the

Xenopus tadpole. A model is developed based around weakly interacting half-center oscillators, themselves built from modified McKean neurons. This latter model is a natural extension of the McKean model. It more closely reproduces neuronal output from neurons within the CPG of the tadpole swimming circuit. The theory of weakly coupled chains is generalised to incorporate the significant distinction between left and right sides of the spinal cord. We apply our abstract formalism to the concrete example of swimming in the Xenopus tadpole.

Next we give a more detailed overview of the content of each chapter

1.2 Review Of Chapters

1.2.1 Chapter 2 : Single Neuron Models

In this chapter we introduce and investigate the properties of several oscillatory models. Starting with the classic Hodgkin-Huxley model, we show how the FitzHugh-Nagumo, Integrate-and-Fire and McKean models can all be seen to be obtained by logical reductions of the Hodgkin-Huxley model. For each model we look at the effect of applied input and how the all models have the ability to produce spikes or 'action potentials'. We introduce the notion of the response function and discuss how, for every oscillatory model, one can be calculated either numerically or analytically.

1.2.2 Chapter 3 : Small Discrete Networks

In this chapter we start with a review of coupled oscillator theory in the weak coupling limit. We show that Fourier transforms are a powerful tool with which to

solve the synaptically coupled network equations of any oscillatory neuron model. We go on to show that, for certain models such as the Integrate-and-Fire and McKean models, the network equations can be solved explicitly for phase-locked states. For these two models we simulate networks of 2 and 3 neurons and in the case of the McKean model we look at the effect of discrete delays.

1.2.3 Chapter 4 : Continuum Networks and Dendrites

In this chapter we examine the logical extension of large networks, namely a continuum description of neural tissue. We look at the stability of travelling waves for the parameter space of the wave speed and phase gradient. We then look at the dendritic tree and simplify the complicate notion of the dendritic tree to a single dendritic coordinate. We look at the effects of dendrites on small discrete networks and then on continuous networks.

1.2.4 Chapter 5 : Half-Center

In this chapter we define a half-center oscillator and show how to construct one for both the McKean and Hodgkin-Huxley models. We describe how an anti-phase rhythm is generated through the mechanism of post inhibitory rebound. We show that phase response curve of the McKean half-center can be calculated explicitly in the singular limit. We then propose a small network of half-centers and try to reproduce behaviour that is seen in a similarly constructed but biologically realistic network.

1.2.5 Chapter 6 : Locomotion In The Embryonic Xenopus Tadpole

In this chapter we look at the simplest vertebrate, the tadpole. We review the current biological knowledge of the anatomical and chemical mechanisms for locomotion. We propose a new two variable model of an excitable neuron which more closely matches the Hodgkin-Huxley behaviour than the McKean model. We then construct a half-center using this new model and show that, unlike the original McKean model, it can reproduce biologically realistic behaviour. We bring together the work of the previous chapters to the task of modelling the tadpole with a chain of half-centers, with both explicit solutions and brute force simulations. We investigate travelling waves and how a frequency gradient effects the solutions.

1.2.6 Chapter 7 : Conclusions and Further Work

In this chapter we review the previous chapters. We highlight several interesting results and conclusions, and suggest how they can be investigated in further work.

Chapter 2

Single Neuron Models

When studying the dynamics of excitable or oscillatory neural processes there are a myriad of models that one can choose from. The choice of model depends largely on the behaviour one wishes to investigate, such as excitability, bursting and bistability. In this chapter I focus on four particular models, three of which can be seen as reductions of the Hodgkin-Huxley model. Each model has its own benefits and drawbacks,

- Hodgkin-Huxley Model : A good choice for biological realism with the ability to fit variables to experimental data [19] [20]. However it is a four dimensional non-linear ODE system and as such is not very analytically tractable.
- FitzHugh-Nagumo : A more simple two dimensional ODE model that allows a geometric interpretation of dynamics (firing) in the phase plane [21] [22] [23]. It is versatile in the sense that as well as neurons it has also been used to model cells including those in the heart [24]. Unfortunately parameters of the model cannot be directly linked to biophysical experiments. As such the results are not as similar to experiments as with the Hodgkin-Huxley model.

- Integrate and Fire : A one dimensional ODE model that is useful to simulate large networks [25]. It has no innate ability to spike instead it has a threshold and reset condition. It has the disadvantage that it is quite abstract from the biology it is representing.
- McKean : A piece-wise linear version of the FitzHugh-Nagumo model that has the benefit of being analytically tractable [26]. However it suffers from the same drawbacks as the FitzHugh-Nagumo model.

Each of these models will be studied under the conditions where it oscillates in isolation. As such it is natural to compare the Phase Response Curve (PRC) of each. The PRC provides a measure of the response of a system to pulsatile input and is described below.

The Phase Response Curve

For every oscillatory model the periodic phase response curve can be calculated. The PRC of an oscillatory model describes how the system responds to pulsatile input at a fixed point of the input [27]. It is calculated by perturbing the oscillator with a brief depolarising infinitesimally small (in duration and amplitude) stimulus at different times in its cycle and measuring the resulting phase shift from the unperturbed system. The PRC has the same period as the periodic oscillator. There are two types [27],
Type I Phase Response : An all positive curve, indicating that any input will advance the next firing event.
Type II Phase Response : Both a positive and negative curve, indicating that any input may advance or retard the next firing event. (Depending upon where it occurs in the cycle).
For a phase variable $\theta(t)$ in a periodic system, there is freedom to choose the origin

where $\theta(0) = 0$ In this work we will always have the response function starting at the point when the model starts to spike. In most cases this occurs at the maximum of the PRC. In cases where the explicit calculation of the PRC is not possible we use XPP [28] to calculate it numerically. A full discussion discussion of the numerical techniques for computing PRC's for limit cycle oscillators is given in [27] [29].

2.1 The Hodgkin-Huxley Model

Accredited as the first bio-physical model of a neuron, the Hodgkin and Huxley model was engineered by Hodgkin-Huxley to match experimental results that the pair had observed whilst working on the squid giant axon [30, 31] [32, 33]. Since the 1950's their model has been established as the most widely used for neuron modelling when biological realism is needed. The Hodgkin-Huxley model is also often modified with extra dynamical expressions to elicit various real-world behaviour such as bursting, not naturally seen in the original model (i.e. with other ionic currents [34]).

The form of the Hodgkin-Huxley model can be seen to be based on the conservation of electrical charge. It describes a neuron as a spatially isopotential cell with membrane potential v and has the form

$$C\frac{\mathrm{d}v}{\mathrm{dt}} = -F + I_s + I, \tag{2.1}$$

where C is the cell capacitance, F the membrane current, I_s the sum of external synaptic currents entering the cell and I describes any external injected currents. The membrane current arises mainly through the conduction of sodium and potassium ions through voltage dependent channels in the membrane and the contribu-

tion form other ionic currents is assumed to obey Ohm's law. F is function of v and of three time and voltage dependent conductance variables m, n and h:

$$F(v, m, n, h) = g_L(v - v_L) + g_K n^4(v - v_K) + g_{Na} h m^3(v - v_{Na}). \tag{2.2}$$

With the experimentally determined constants g_L, g_K, g_{Na} in (mmho/cm^2) and v_L, v_K, v_{Na} in mvolt, v_L, v_K and v_{Na} represent the membrane reversal potentials associated with the leakage, potassium and sodium channels respectively. The values of these constants are given in Appendix A.

The conductance variables m, n and h take values between 0 and 1 and approach the asymptotic values $m_\infty(v)$, $n_\infty(v)$ and $h_\infty(v)$ with time constants $\tau_m(v)$, $\tau_n(v)$ and $\tau_h(v)$ respectively. The six functions $\tau_X(v)$ and $X_\infty(v)$, $X \in \{m, n, h\}$, are obtained from fits with experimental data:

$$\tau_X(v)\frac{\mathrm{d}X}{\mathrm{dt}} = X_\infty(v) - X,$$

where

$$\tau_X(v) = \frac{1}{\alpha_X(v) + \beta_X(v)}, \qquad X_\infty(v) = \frac{\alpha_X(v)}{\alpha_X(v) + \beta_X(v)},$$

Where $X \in \{m, n, h\}$ The functions $\alpha_X(v)$ and $\beta_X(v)$ are given by

$$\alpha_X(v) = (a_X A + a_X B v)/(a_X C + \mathrm{e}^{((v + a_X D)/a_X F)}),$$
$$\beta_X(v) = (b_X A + b_X B v)/(b_X C + \mathrm{e}^{((v + b_X D)/b_X F)}).$$

One of the important contributions of Hodgkin-Huxley was to obtain the coefficients experimentally.
The values of $a_X A, a_X B, a_X C, a_X D, a_X F$ and $b_X A, b_X B, b_X C, b_X D, b_X F$ used are given in Appendix A.

The Hodgkin-Huxley model is an excitable model, i.e. when there is a sufficiently large transient input the system will produce action potentials. These can be seen in figure (2.1.1).

Depending on the value of a constant external input the stable state of the Hodgkin-

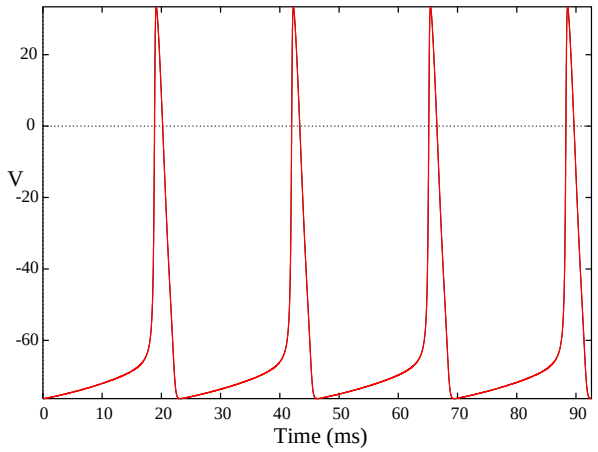

Figure 2.1.1: The action potentials created by the Hodgkin-Huxley model when $I = 20$.

Huxley model is either a fixed point or a limit cycle. Looking at a bifurcation diagram (2.1.2) shows that there is a critical value or threshold value I_* at which the system undergoes a Hopf bifurcation and the stable fixed point becomes a stable limit cycle. The stable limit cycle persist as I increases until the value I^* at which point it becomes a stable fixed point again. One thing to note is that at the onset of spikes there is an instantaneous jump to a non-zero frequency (2.1.3), this is an example of *Class II neural excitability* [35]. There are other oscillatory models such as the Moris-Lecar model [36] for which there are arbitrarily low frequency oscillations in the neighbourhood of the bifurcation point. This is known as *Class I neural excitability* and is common to many cortical neuron models.

The PRC of the Hodgkin-Huxley model cannot be calculated analytically. How-

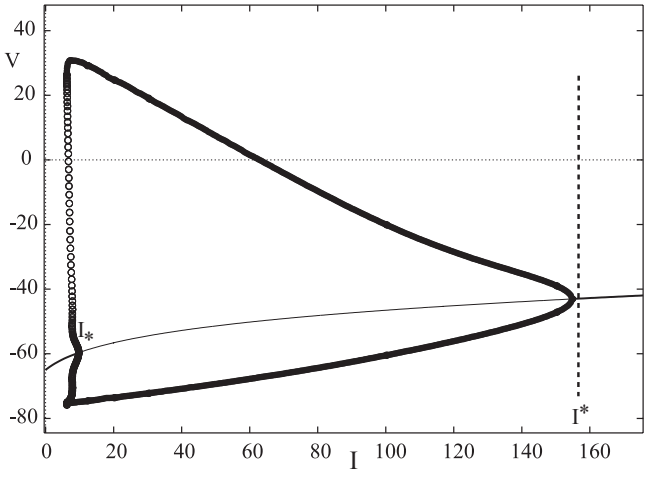

Figure 2.1.2: Bifurcation diagram of the Hodgkin-Huxley model as a function of the external drive I. Black circles and open circles denote stable and unstable limit cycles respectively. Thick (thin) lines show stable (unstable) fixed point behaviour. The onset of oscillations start at the input value I_* and stop at I^*.

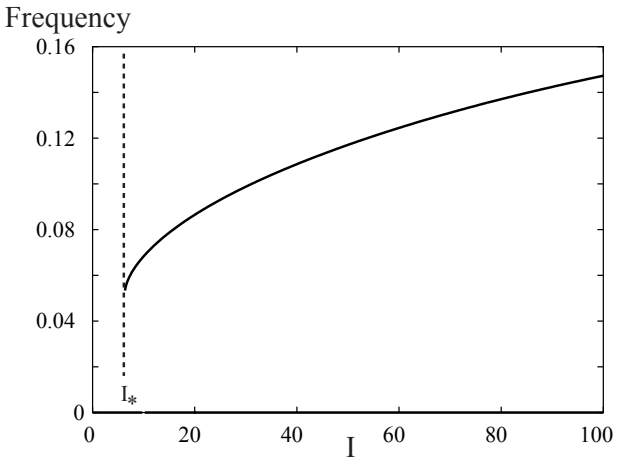

Figure 2.1.3: Diagram showing the effect of constant external drive on the frequency of a Hodgkin-Huxley neuron.

ever it can calculated numerically. This can be seen in figure (2.1.4) and it is clear that it is a Type II PRC. Directly as the spike starts the PRC is positive, going neg-

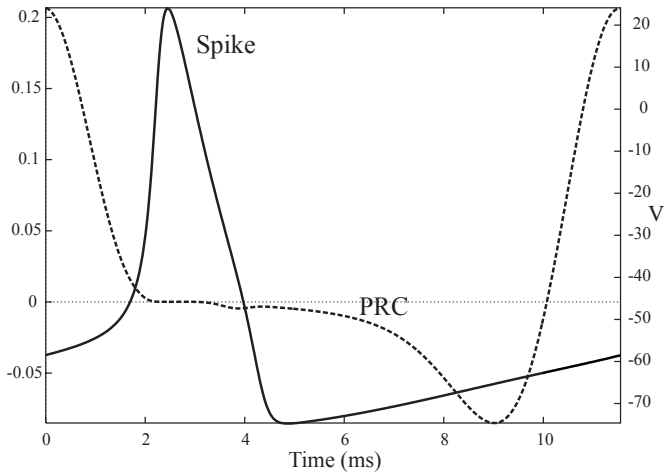

Figure 2.1.4: The numerically calculated PRC of the Hodgkin-Huxley with a spike superimposed onto the diagram for $I = 20$. The PRC was calculated using XPP [28].

ative as the spike dies away and the system relaxes.

2.1.1 Reduction Of The Model

Whilst the Hodgkin-Huxley model is a good choice of model when a balance between biological realism and simplicity of form is needed, its number of degrees of freedom are a drawback.

Reducing the model is clearly advantageous to facilitate both analytical progress and large network simulations. A look at the dynamics of the m, n and h variables suggests a first reduction. The m, h and n time derivatives have voltage dependent time constants $\tau_m(v)$, $\tau_h(v)$ and $\tau_n(v)$ respectively. These have the effect of scaling

the rate at which the variables m, n and h approach their asymptotic values. The smaller this value the faster the convergence. This prompts a look at how the dynamics of the τ's vary with v. This is shown in Figure (2.1.5),where it is illustrated that $\tau_m(v)$ is significantly smaller over the range of v compared to h and n, causing m to reach its asymptotic value more more rapidly than h and n. This prompts the

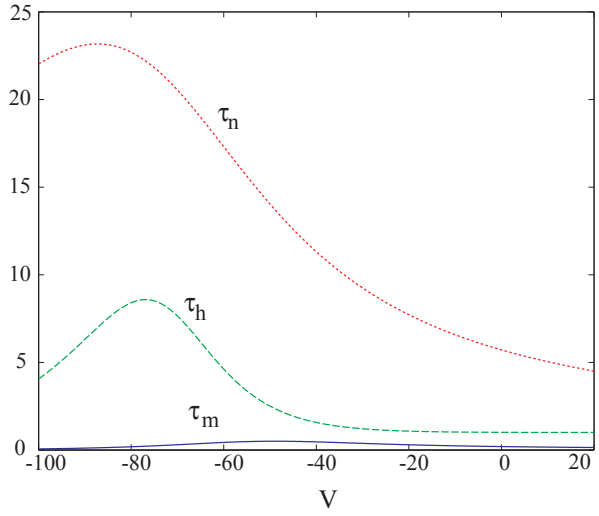

Figure 2.1.5: The τ's vary in value with voltage. It is clear that the τ_m curve is significantly lower in magnitude over the whole range.

simplification of replacing m by its asymptotic value m_∞.

In figure (2.1.6) it can be seen that replacing m by $m_\infty(v)$ has little effect on the dynamics of the system. The period of the orbits is slightly effected but the spiking nature behaviour itself persists. So under this simplification (2.2) now becomes

$$F(v,m,n,h) = F(v,n,h) = g_L\,(v - v_L) + g_K n^4\,(v - v_K) + g_{Na} h m_\infty^3(v)\,(v - v_{Na})\,. \tag{2.3}$$

Our next reduction is motivated by noting the similar nature of n and h.

It can be seen from figure (2.1.7) that there is an approximately linear relation be-

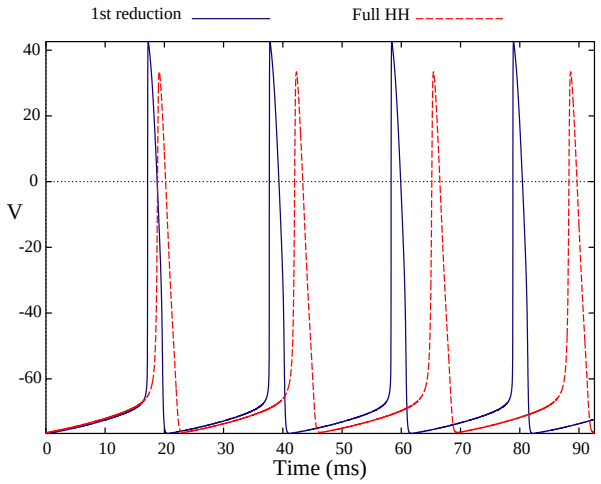

Figure 2.1.6: The comparison between the action potentials produced by the full Hodgkin-Huxley model (HH) and the first reduction made where $m \to m_\infty(v)$ (HHR).

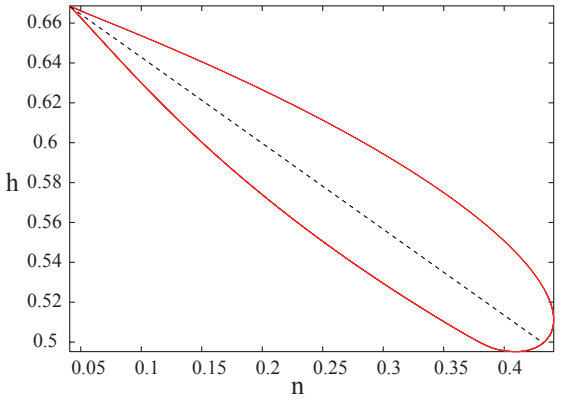

Figure 2.1.7: The n and h variables have a periodic relationship.

tween n and h. The simplest approximation to this relationship is an equation of the form

$$h = \alpha n + \beta. \tag{2.4}$$

The value of α and β can be determined using a method such as least squares,

which minimises the error between the actual and approximate solutions over one period.

It follows from (2.3) that

$$F(v,n) = g_L\left(v - v_L\right) + g_K n^4\left(v - v_K\right) + g_{Na} m_\infty^3\left(\alpha n + \beta\right)\left(v - v_{Na}\right). \tag{2.5}$$

This new form for the equations now involves only two variables v and n. This approximation with a linear relationship is simple but not very accurate. There is a more rigourous method of reducing the three variable system [37] that is more general than the above approach, by noting that the system effectively work on two time scales. Having n and h replaced by asymptotic forms $n_\infty(v)$ and $h_\infty(v)$ would stop the generation action potentials, so we define a new variable u as an auxiliary potential on a different time scale to that of v. Introducing this new potential u and making the replacement

$$X = X_\infty(u), \qquad X \in \{n, h\},$$

it is possible simplify the equations. Note that the functions X_∞ are monotonic and can be inverted. We now define f such that

$$f(v,u) = F(v, m_\infty(v), n_\infty(u), h_\infty(u)).$$

To find an equation for u we assume that the time dependence of f follows that of F at fixed v. That is we choose

$$\frac{\partial F}{\partial t} = \frac{\partial f}{\partial t}.$$

This is equivalent to

$$\frac{\partial F}{\partial h}\frac{\mathrm{d}h}{\mathrm{dt}} + \frac{\partial F}{\partial n}\frac{\mathrm{d}n}{\mathrm{dt}} = \left[\frac{\partial f}{\partial h_\infty}\frac{\mathrm{d}h_\infty(u)}{\mathrm{du}} + \frac{\partial f}{\partial n_\infty}\frac{\mathrm{d}n_\infty(u)}{\mathrm{du}}\right]\frac{\mathrm{d}u}{\mathrm{dt}}. \tag{2.6}$$

Where the partial derivatives on the right hand side are evaluated at $X = X_\infty(u)$.

Now

$$\frac{\partial F}{\partial h} = g_{Na} m^3 (v - v_{Na}) \qquad \text{Similarly for } n \qquad \frac{\partial F}{\partial n} = 4 g_K n^3 (v - v_K),$$
$$\frac{\mathrm{d}h_\infty}{\mathrm{du}} = \frac{\mathrm{d}\alpha_h}{\mathrm{du}}\tau_h + \frac{\mathrm{d}\tau_h}{\mathrm{du}}\alpha_h.$$

So we have that

$$\frac{\mathrm{d}\tau_h}{\mathrm{du}} = \frac{\mathrm{d}}{\mathrm{du}}\left(\frac{1}{\alpha_h + \beta_h}\right) = -\left(\frac{\mathrm{d}\alpha_h}{\mathrm{du}} + \frac{\mathrm{d}\beta_h}{\mathrm{du}}\right)\frac{1}{(\alpha_h + \beta_h)^2},$$

and by the same reduction

$$\frac{\mathrm{d}\tau_n}{\mathrm{du}} = -\left(\frac{\mathrm{d}\alpha_n}{\mathrm{du}} + \frac{\mathrm{d}\beta_n}{\mathrm{du}}\right)\frac{1}{(\alpha_n + \beta_n)^2}.$$

where

$$\frac{\mathrm{d}\alpha_X}{\mathrm{du}} = \frac{a_X B\left(a_X C + \mathrm{e}^{(v+a_X D)/a_X F}\right) - (a_X A + a_X B v)\,\mathrm{e}^{(v+a_X D)/a_X F}/a_X F}{\left(a_X C + \mathrm{e}^{(v+a_X D)/a_X F}\right)^2},$$
$$\frac{\mathrm{d}\beta_X}{\mathrm{du}} = \frac{b_X B\left(b_X C + \mathrm{e}^{(v+b_X D)/b_X F}\right) - (b_X A + b_X B v)\,\mathrm{e}^{(v+b_X D)/b_X F}/b_X F}{\left(b_X C + \mathrm{e}^{(v+b_X D)/b_X F}\right)^2}.$$

Rearranging (2.6) gives

$$\frac{\mathrm{d}u}{\mathrm{dt}} = g(u, v) = \frac{A(u, v)}{B(u, v)}, \tag{2.7}$$

where

$$A(u, v) = \frac{\partial F}{\partial h}\left[\frac{h_\infty(v) - h_\infty(u)}{\tau_h}\right] + \frac{\partial F}{\partial n}\left[\frac{n_\infty(v) - n_\infty(u)}{\tau_n}\right],$$

and

$$B(u, v) = \frac{\partial f}{\partial h_\infty}\frac{\mathrm{d}h_\infty(u)}{\mathrm{du}} + \frac{\partial f}{\partial n_\infty}\frac{\mathrm{d}n_\infty(u)}{\mathrm{du}}.$$

Hence the reduced Hodgkin-Huxley model has the form

$$C\frac{\mathrm{d}v}{\mathrm{dt}} = -f(v, u) + I_s + I,$$
$$\frac{\mathrm{d}u}{\mathrm{dt}} = g(v, u). \tag{2.8}$$

This system still produces action potentials and the comparison in figure (2.1.8) shows that there is still a reasonable quantitative similarity between the four and

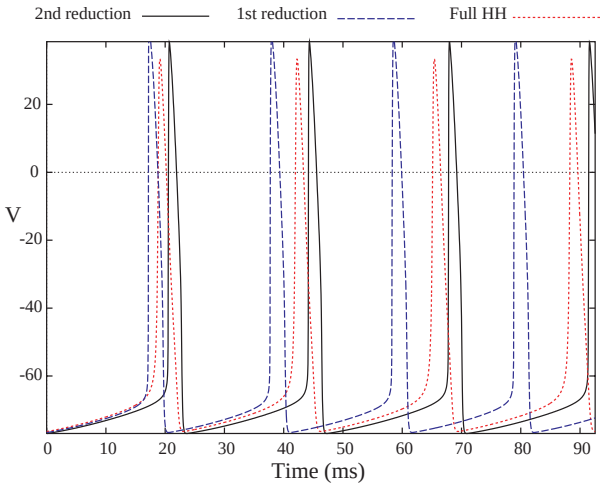

Figure 2.1.8: A comparison of all three reductions

two dimensional models. Moreover, it is better than the previous approximation $h = \alpha n + \beta$.

Being that the model is now a two variable system, it is appropriate to consider the dynamics in the phase plane. The nullclines have the form of a cubic and a straight line as shown in figure (2.1.9).

As with the Hodgkin-Huxley model, the PRC of this system may be calculated numerically. This can be seen in figure (2.1.10) and it is clear that it is a Type II PRC. One natural consequence of (2.7) is that the nullcline for u is simply $v = u$ Just as with the full Hodgkin-Huxley model, as the spike starts the PRC is positive going negative as the spike dies away and the system relaxes. This suggests that the reduction keeps many of the same traits as the full model. These oscillations can be interpreted on the phase plane in figure (2.1.9), as I is increased its has the effect of moving the cubic v nullcline up, this moves the equilibrium point to the right. When the equilibrium point is on the left (right) 'branch' of the nullcline there are stable fixed point solutions, but on the middle section there are periodic

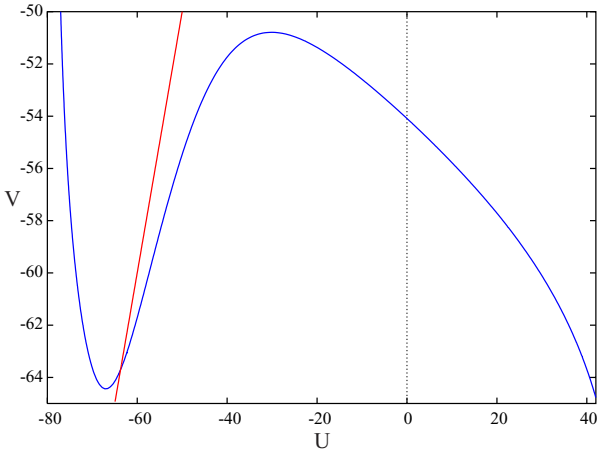

Figure 2.1.9: The nullclines of the reduced HH model for $I = 20$. This shows there is no stable equilibrium and hence why the system oscillates.

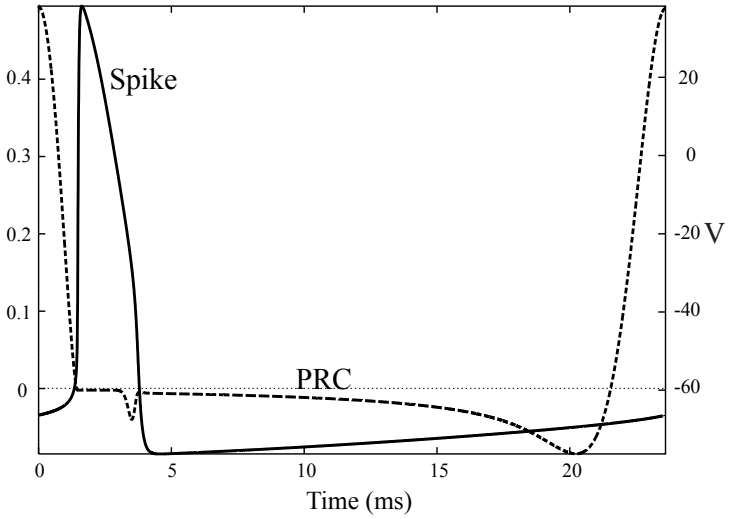

Figure 2.1.10: The numerically calculated PRC of the reduced Hodgkin-Huxley with a spike superimposed onto the diagram for $I = 20$.

orbits. This explains figure (2.1.2) for the full model, where between I_* and I^* there are oscillations. The same figure can be produced the reduced model but it has qualitatively the same behaviour so is not shown.

It can be seen from the action potentials that motion in v happens fast time scale, so this system can be thought of as comprising of the fast variable v, and a slow variable u. The variable v has a cubic nullcline and u has a nullcline that is monotonically increasing. These two variables are both needed for the generation of an action potential. The variable v can be considered the capacitance of the cell whilst u can be regarded as responsible for the refractory period. The notion that v acts on a much shorter time scale than u intimates to the fact that v creates the sudden excursion of the spike while u contributes more to the shape. The spike occurs when the initial conditions are such that u is below its nullcline and when v has a sufficient value so that it can not reach the steady state without performing an excursion (action potential).

Even in this reduced system there is scope for more reduction. The function $f(v, u)$ is cumbersome, but from (2.1.9) it can be seen that it has an approximately cubic shape. This cubic can be fitted by a function using any method such as method of least-squares, and is then analogous to the FitzHugh-Nagumo model [21].

2.2 The FitzHugh-Nagumo model

The FitzHugh-Nagumo model is a versatile model not only well used in neuroscience, but because it is a simple form for an excitable system, it is also used in other areas such as heart dynamics [38], calcium oscillations [10] and even the pulsatile release of luteinizing hormone releasing hormone [39]. The simplicity of this model does, however, mean that all quantitative links to biological data are lost.

The model is given by

$$\mu \dot{v} = f(v) - w - w_0 + I, \tag{2.9}$$

$$\dot{w} = v - \gamma w - v_0, \tag{2.10}$$

where $f(v) = Cv(v - \alpha)(1 - v)$. The variable v corresponds to membrane potential whilst w is associated with the refractory properties of a neuron. The parameters C, α, μ, w_0, v_0 and γ may be considered as combinations of the membrane reversal potentials and conductance properties whilst I is any externally injected current. All of the parameters used are in the Appendix. This model still has the ability to generate action potentials, as seen in figure (2.2.1). Moreover comparing the cubic form of the v nullclines in figures (2.1.9) and (2.2.2) shows the similar forms between the HHR and FHN models.

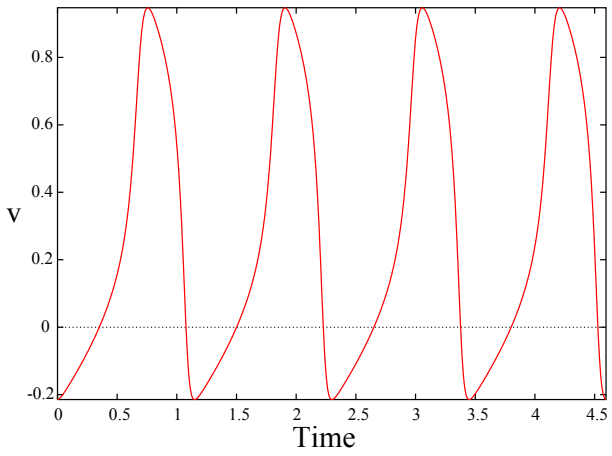

Figure 2.2.1: The action potentials created by the FitzHugh-Nagumo model for $I = 1$.

It can be seen in figure (2.2.3) that the oscillations occur in a window of external input between I_* and I^*. In figure (2.2) the model can be seen to have Class II

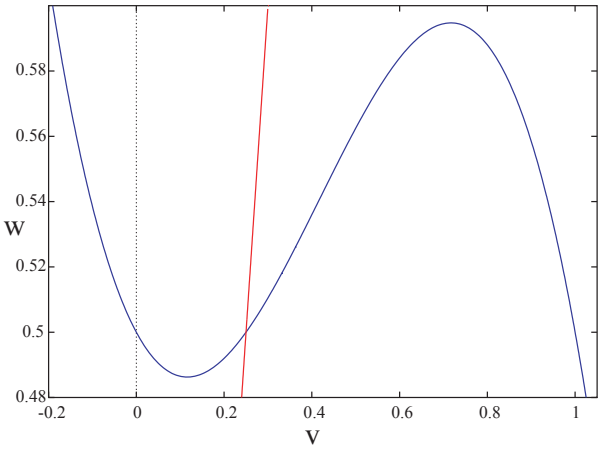

Figure 2.2.2: The nullclines of the FitzHugh-Nagumo model for $I = 1$

neural excitability.

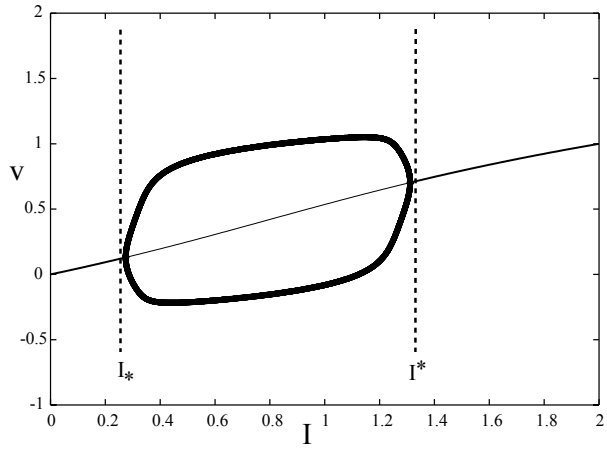

Figure 2.2.3: Bifurcation diagram of the FitzHugh-Nagumo model as a function of the external drive I. Circles denote stable limit cycles, thick (thin) lines show stable (unstable) fixed point behaviour. The onset of oscillations start at the input value I_* and stop at I^*.

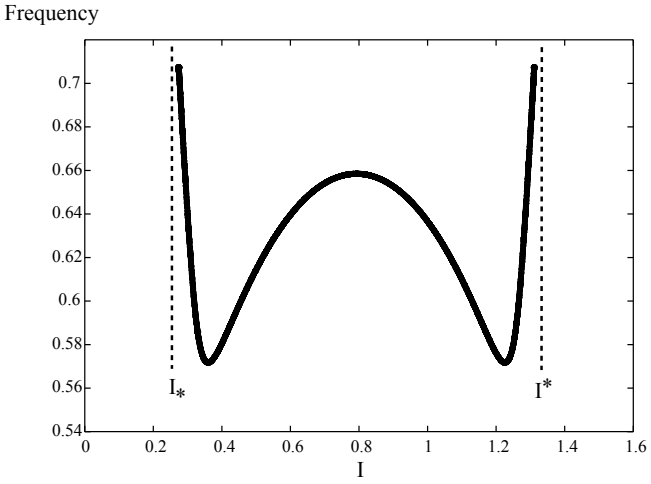

Figure 2.2.4: Diagram showing the effect of the external drive on the frequency of oscillations of the FitzHugh-Nagumo model.

The PRC of the FHN model is numerically calculated in Figure (2.2.5). It can be seen that, like the Hodgkin-Huxley model, the FHN model has a type II response function.

2.3 The Integrate and Fire model

In order to reduce the system further a simple method is to eliminate one of the variables. Setting w to the equilibrium point, eliminates the w variable giving a single equation of the form

$$\mu\dot{v} = f(v) - w^* + I,$$

where $w^* = w_0 + (v - v_0)/\gamma$. If the w variable is removed then there is no way to determine the critical transition value of v which marks the onset of spikes. It is therefore an necessary to introduce an artificial threshold h, for which v must

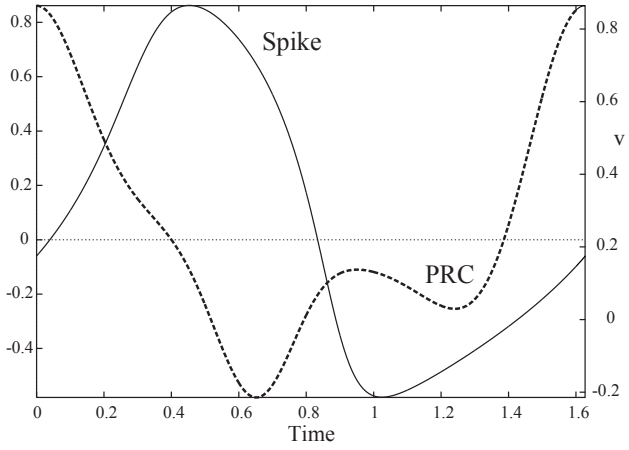

Figure 2.2.5: The numerically calculated PRC of the FitzHugh-Nagumo model with a spike superimposed onto the diagram.

exceed to illicit an action potential. This threshold can be calculated by taking the largest value of v for which $w = w^*$ and $\dot{v} = 0$, since $\mathrm{d}v/\mathrm{d}t > 0$ for larger values of v. However this reduced system will not produce spikes themselves so a reset condition must be introduced so that the system is reset back to initial conditions after reaching h. What in higher dimensional models is the characteristic large excursion of the spike does not occur in this model, effectively it is replaced by a delta Dirac function. The reset condition has the form

$$\lim_{\delta \to 0^+} v(T^m + \delta) = v_{reset}, \tag{2.11}$$

where T^n are the times at which the system reaches h. This means that T^n is effectively the definition of the nth firing time, defined by

$$T^n = \inf\left\{t \mid v(t) \ \geq \ h \ ; \ t \ \geq \ T^{n-1} + \tau_R\right\}. \tag{2.12}$$

The quantity τ_R represents the absolute refractory period of the neuron and effects the duration of the spikes. It can be calculated from any if the higher dimensional

models by calculating the period of oscillation for constant external drive. Another popular way that the lost refractory properties are re-introduced is by having a time dependant threshold function $h = h(t)$ [40]. This function typically has a large positive value after an action potential which decays at a rate τ_h.

Using the more simple notion of a constant threshold and linearising the cubic form of the function $f(v)$ about the threshold value (for even more simplicity), gives a linear IF model with $f(v)$ of the form $f(v) = \alpha v$ where $\alpha < 0$.

The standard linear integrate and fire model is defined as

$$\frac{\mathrm{d}v}{\mathrm{dt}} = -\frac{v}{\tau} + I, \tag{2.13}$$

where τ is the membrane time constant and the system is subject to the restraints of spiking at the threshold value then resetting to the rest value.

2.3.1 The Driven Integrate and Fire Model

Here we consider driving (2.13) with input $I(t) = I + \epsilon X(t)$. To calculate the firing times we multiply (2.13) by the integrating factor $e^{t/\tau}$ to obtain

$$e^{t/\tau}\dot{v} = -\mathrm{e}^{t/\tau}\frac{v(t)}{\tau} + \mathrm{e}^{t/\tau}I(t),$$

which may be re-arranged to give

$$\frac{\mathrm{d}}{\mathrm{dt}}\left(\mathrm{e}^{t/\tau}v(t)\right) = I(t)\mathrm{e}^{t/\tau}.$$

Integrating between firing times T_n and T_{n+1} gives

$$e^{t/\tau}v(t)\Big|_{T_n}^{T_{n+1}} = \int_{T_n}^{T_{n+1}} I(s)\mathrm{e}^{s/\tau}\mathrm{d}s.$$

Evaluating this integral gives

$$he^{T_{n+1}/\tau} = \int_{T_n^+}^{T_{n+1}^-} I(s)\mathrm{e}^{s/\tau}\mathrm{d}s,$$

where we have chosen $v_{reset} = 0$ This gives an implicit map for the firing times. For the case where $\epsilon = 0$ we have a simple oscillator with period $T = T_{n+1} - T_n =$ constant $\forall\ n$ where

$$T = \ln\left[\frac{I\tau}{I\tau - h}\right], \qquad I\tau > h.$$

We therefore have the condition that $I\tau > h$ for an oscillation to exist. Note that between firing events the general solution of the IF model is given by

$$\int_0^{v(t)} \frac{\mathrm{d}v}{f(v) + I} = \int_0^t \mathrm{d}t,$$

with $f(v) = -v/\tau$ for the linear IF model.

Assuming that the model oscillates, this suggests a change of variables. Introduce

$$\theta(t) = \frac{1}{T}\int_0^{v(t)} \frac{\mathrm{d}v}{f(v) + I} = \Psi(v). \tag{2.14}$$

When $v(t) < h$ it means that $\theta < 1$ for $0 < t < T$ and so can be though of as on a circle providing we restrict θ to the circle for $t > T$. Differentiating (2.14) gives

$$\dot{\theta} = \frac{\dot{v}}{T}\left[\frac{1}{f(v) + I}\right] = \frac{1}{T}.$$

By definition of $\dot{v} = f(v) + I$, a constant input will yield a linear rise to fire time. Suppose now that $\epsilon \neq 0$ the change of variables (2.14) gives

$$\dot{\theta} = \frac{\dot{v}}{T}\left[\frac{1}{f(v) + I}\right] = \frac{1}{T}\left[\frac{f(v) + I + \epsilon X(t)}{f(v) + I}\right] = \frac{1}{T} + \frac{\epsilon X(t)}{T(f(v) + I)}, \tag{2.15}$$

This enable the calculation of

$$v = \Psi^{-1}\left(\theta(t)\right).$$

We have to assume that Ψ^{-1} is single valued. The calculation of Ψ^{-1} is needed to be able to resolve the phase equations for v. For a general $f(v)$ this calculation may not be possible but in the linear integrate and fire case it is. Let $f(v)$ be as (2.13) i.e.

$$\theta(t) = \frac{1}{T}\int_0^{v(t)} \frac{\mathrm{d}v}{-v/\tau + I} = \frac{-\tau}{T}\ln\left[\frac{-v/T + I}{I}\right] = -\frac{\tau}{T}\ln\left[\frac{-v + I\tau}{I\tau}\right].$$

Which gives

$$v(t) = \tau I\left(e^{-T\theta(t)/\tau} - 1\right).$$

So replacing this in (2.15) gives

$$\dot{\theta}(t) = \frac{1}{IT}\left[I + \epsilon X(t) e^{T\theta(t)/\tau}\right].$$

This gives the equation for $\dot{\theta}$,

$$\frac{\mathrm{d}\theta}{\mathrm{dt}} = \frac{1}{T}\left[1 + \epsilon X(t) R(\theta)\right],$$

where

$$R(\theta) = \frac{e^{T\theta/\tau}}{I}, \tag{2.16}$$

$R(\theta)$ is the response function of the IF model, and it is clear from the form of (2.16) that it is always positive and hence a type I phase response function.

2.4 The McKean Model

As stated in the last section the response of the IF model is type I. However as seen in section (2.1), the Hodgkin-Huxley model is type II. This poses the question of whether the IF is a good single neuron model and whether it would be better to find a model that has more commonalities with HH but still has an analytically

solvable form. With this in mind we consider a different simplification of the FHN model, obtained by a piecewise linear approximation of the cubic nullcline. The McKean model has the same form as the FHN model (2.9) and (2.10), except that

$$f(v) = \begin{cases} -v & v < \alpha\ 2, \\ v - \alpha & \alpha/2 < v < (1+\alpha)/2, \\ 1 - v & v > (1+\alpha)/2. \end{cases} \tag{2.17}$$

This new form for the model will still generate spikes, and again it does so between I_* and I^*. This is shown in figure (2.4.1)

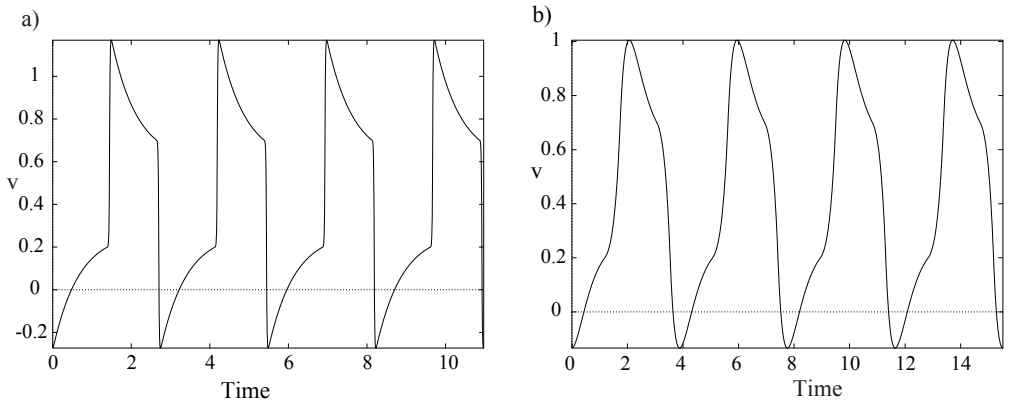

Figure 2.4.1: This shows the spike shapes generated by the piece-wise linear McKean model with $I = 0.8$. a) $\mu = 0.01$ near singular limit, b) $\mu = 0.2$ away from singular limit .

Looking at the phase plane and nullclines of the reduced system can be useful to interpret the dynamics in a geometric way. It can be seen in figure (2.4.2) that the cubic nullcline allows the generation of spikes in the same way as described earlier in this chapter.

As before figure (2.4.3) shows that the oscillations occur in a window of external

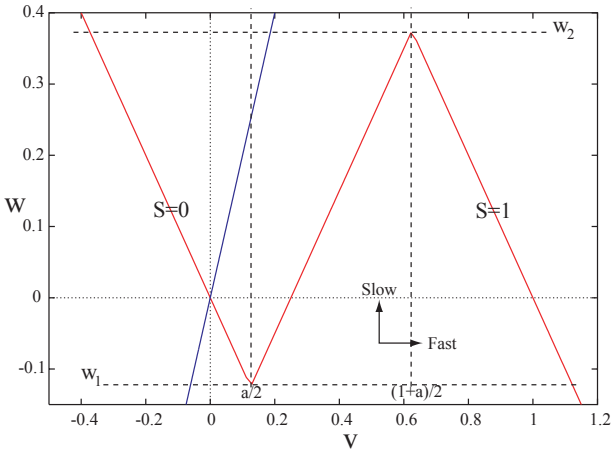

Figure 2.4.2: The phase plane v against w showing the limit cycle and the the nullclines of the system. There is the clearly the N shape linearisation of the cubic FHN $\dot{v} = 0$ nullcline.

input I. Just as with the Hodgkin-Huxley model and FHN figure (2.4.4) shows that the McKean model has Class II neural excitability and has similar properties to that if the FHN model.

If there is no other input the system has nullclines defined by $f(v) = w + w_0 - I$ and $w = (v - v_0)/\gamma$. When the fixed point of this piecewise linear function is such that $v < a/2$, then this is said to define the excitable regime. If we take the singular limit $\mu \to 0$, the system is restricted to the left and right branches of the cubic nullcline. In Abbot [37] a binary variable is introduced for this system

$$S = \begin{cases} 1, & v > (1+\alpha)/2, \\ 0, & v < \alpha/2, \end{cases}$$

to label the left and right branches. Assuming the time scale for the v dynamics is fast compared to the w dynamics, i.e. $\mu \to 0$. We may write $f(v) = S - v$ (that is we assume $\varepsilon \ll \mu \to 0$). Introducing $S^+(t) = \lim_{\delta \to 0^+} S(t+\delta)$, it is possible to write the dynamics for $S(t)$ in the form

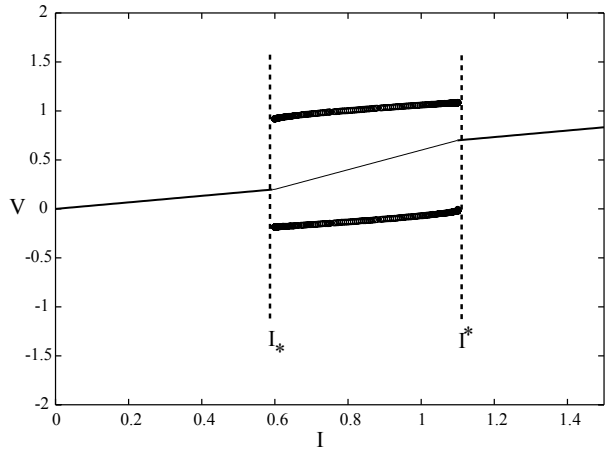

Figure 2.4.3: Bifurcation diagram of the McKean model as a function of the external drive I. Circles denote stable limit cycles, thick (thin) lines show stable (unstable) fixed point behaviour. The onset of oscillations start at the input value I_* and stop at I^*.

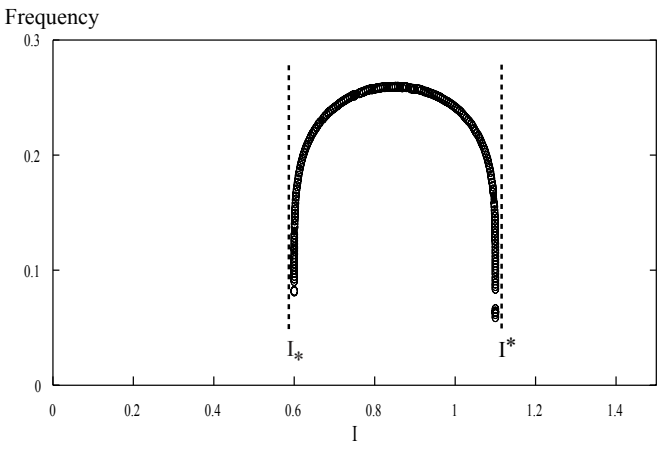

Figure 2.4.4: Diagram showing the effect of the external drive on the frequency of oscillations of the McKean model. The onset of oscillations start at the input value I_* and stop at I^*.

$$S^+ = \Theta(I - w_0 + (S - a)/2 - w). \tag{2.18}$$

where $\Theta(x)$ is a heaviside function such that $\Theta(x) = 1$ if $x \geq 0$ and 0 otherwise. To check the validity of (2.18).The variable S can be seen to change from 0 to 1 as w decreases through w_1, and this is reversed as w increases through w_2. The points w_1 and w_2 are shown in figure (2.4.2) and can easily be calculated as $I - w_0 - a/2$ and $I - w_0 - a/2 + 1/2$ respectively they are the w values at which the left and middle, middle and right branches meet. On the branches $S = 0$ and $S = 1$ v evolves as

$$v = S - w - w_0 + I. \tag{2.19}$$

Using this we can write

$$\dot{w} \equiv G(w; s) = -\beta w + A + S, \tag{2.20}$$

with $\beta = 1 + \gamma$ and $A = I - w_0 - v_0$. When $\mu = 0$ there is an invariant manifold, which can be written $v = m(w)$ with

$$m(w) = \begin{cases} m(w; 0), v < \alpha\ 2, \\ v_c(w), \alpha/2 < v < (1 + \alpha)/2, \\ m(w; 1), v > (1 + \alpha)/2. \end{cases} \tag{2.21}$$

Where $m(w; S) = S - w - w_0 + I$ and $v_c(w) = w + a + w_0 - I$. It should be noted that for $\mu = 0$ the two branches defined by $S = 0$ and $S = 1$ are attracting, whilst the branch defined by $v \equiv v_c(w)$ is repelling.

In the singular limit the period of oscillation can be calculated explicitly as

$T = T_1 + T_2$ where

$$T_1 = \int_{w_2}^{w_1} \frac{1}{G(w; 0)} dw = \frac{1}{\beta} \left[\frac{(-\beta w_2 + A)}{(-\beta w_1 + A)} \right],$$
$$T_2 = \int_{w_1}^{w_2} \frac{1}{G(w; 1)} dw = \frac{1}{\beta} \left[\frac{(-\beta w_1 + A + 1)}{(-\beta w_2 + A + 1)} \right].$$

There are the obvious conditions that the value of I has to be between I_* and I^* as in figure (2.4.3). Without any extra input the model with $\mu = 0$ will evolve on the invariant manifolds. When looked at in the oscillatory regime the equations take the simple form

$$w(t) = \begin{cases} w_2 \exp(-\beta t) + \frac{A}{\beta}[1 - \exp(-\beta t)], \\ w_1 \exp(-\beta(t - T_1)) + \frac{A+1}{\beta}[1 - \exp(-\beta(t - T_1))], \end{cases} \tag{2.22}$$

$$v(t) = S - w(t) - w_0 + I. \tag{2.23}$$

Here the functions $v(t)$ and $w(t)$ are periodically extended such that $v(t+T) = v(t)$ and $w(t+T) = w(t)$. Being periodic, it is possible to rewrite the trajectory in terms of a phase variable $\theta \in [0, 1)$ such that $\theta(t) = \Omega t$ with $\Omega = T^{-1}$. So therefore for a particular T and some periodic functions Γ_v and Γ_w, it is possible to write

$$\begin{aligned} w(t) &= \Gamma_w(\theta(t)), \\ v(t) &= \Gamma_v(\theta(t)) = -\Gamma_w(\theta(t)) + S - w_0 + I. \end{aligned} \tag{2.24}$$

Differentiating we get

$$\begin{aligned} \dot{w} &= \Omega \frac{\mathrm{d}\Gamma_w}{\mathrm{d}\theta} = G(\theta; S), \\ \dot{v} &= \Omega \frac{\mathrm{d}\Gamma_v}{\mathrm{d}\theta} = -G(\theta; S) + \frac{\mathrm{d}S}{\mathrm{d}\theta}. \end{aligned}$$

This system will instantaneously jump between slow manifolds when S changes value. This effectively means, the problem is now an algebraic-differential system which is given by (2.19) and (2.20). For an input with small but non zero ϵ, we would expect the persistence of the limit cycles. A co-ordinate system is needed that comprises a phase on the limit cycle ($\theta \in [0, 1)$) and some normal co-ordinate $b \in \mathbb{R}$ (which needs to vanish on the limit cycle) Following [41] [42], we introduce the change of variables $(v, w) \to (\theta, b)$ (discussed more generally in chapter 3). Us-

ing this change of variables we have

$$\begin{bmatrix} v \\ w \end{bmatrix} = \begin{bmatrix} \Gamma_v(\theta) \\ \Gamma_w(\theta) \end{bmatrix} + \begin{bmatrix} M_v(\theta) \\ M_w(\theta) \end{bmatrix} b + \begin{bmatrix} 1 \\ 1 \end{bmatrix} O(b^2) \tag{2.25}$$

Subject to the constraints $M_v^2 + M_w^2 = 1$ and $\Gamma'_v M_v + \Gamma'_w M_w (' \equiv \frac{\mathrm{d}}{\mathrm{d}\theta})$. Evaluating the Jacobian of transformation and its inverse in the case of small b shows that

$$\begin{bmatrix} \frac{\partial\theta}{\partial v} & \frac{\partial b}{\partial v} \\ \frac{\partial\theta}{\partial w} & \frac{\partial b}{\partial w} \end{bmatrix} = \frac{1}{\rho} \begin{bmatrix} \Gamma'_v & \rho M_v \\ \Gamma'_w & \rho M_w \end{bmatrix} \tag{2.26}$$

With $\rho(\theta) = \Gamma'_v(\theta)^2 + \Gamma'_w(\theta)^2$. It can be checked that $\dot{\theta} = \Omega$. For $\varepsilon \neq 0$ v evolves with the $X(t)$ term so $v = S - w - w_0 + I + \varepsilon X(t)$ and $\dot{w} \to \dot{w} + \varepsilon X(t)$ which then means $\dot{v} \to -\varepsilon X(t)$. Thus

$$\frac{\mathrm{d}\theta}{\mathrm{dt}} = \Omega + \varepsilon R(\theta) X(t).$$

Where $R(\theta)$ is the response function and is given by

$$\begin{aligned} R(\theta) &= \frac{1}{\rho(\theta)} \frac{\mathrm{d}}{\mathrm{d}\theta} [\Gamma_w(\theta) - \Gamma_v(\theta)], \\ &= \Omega \left[\frac{1}{G(\theta; S)} + \kappa(0)\delta(\theta) + \kappa(\theta_T)\delta(\theta - \theta_T) \right]. \end{aligned}$$

Using the notation $G(\theta; S) = G(\Gamma_w(\theta); S)$ and $\theta_T = T_1/T$. The κ's can be calculated by the stipulation that $\theta(t)$ must evolve smoothly when S changes from 0 to 1 and 1 to 0. This can be assured by choosing

$$\begin{aligned} \kappa(0) &= \left[\frac{1}{G(0;0)} - \frac{1}{G(1;1)} \right], \\ \kappa(\theta_t) &= \left[\frac{1}{G(\theta_T;0)} - \frac{1}{G(\theta_T;1)} \right]. \end{aligned}$$

From the periodic solution (2.22), $\Gamma_w = w(\theta T)$ so we have

$$G(\theta; S) = \begin{cases} e^{-\beta\theta_T}[A - \beta w_2] & S = 0; \\ e^{-\beta T(\theta - \theta_T)}[A + 1 - \beta w_1] & S = 1. \end{cases} \tag{2.27}$$

So we have that $S = 0$ for $\theta \in [0, \theta_T)$ and $S = 1$ if $\theta \in (\theta_T, 1)$.

The response function of the McKean model shown in figure (2.4.5)

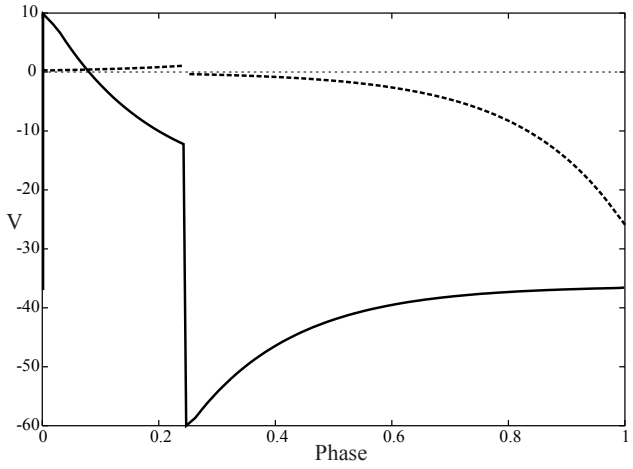

Figure 2.4.5: The exact PRC of the McKean model in the singular limit $\mu \ll 1$ with a spike superimposed onto the diagram.

The PRC of the non singular limit can be seen in figure (2.4.6) and the differences between the response function in the singular and non-singular limit are clearly visible.

It can be seen that whilst the PRC of the McKean model has a very different form than both the Hodgkin-Huxley and FitzHugh-Nagumo models, all models are positive for the beginning part of the spike and are negative after the spike. This is one more example that shows that even though the spikes of the Hodgkin-Huxley,

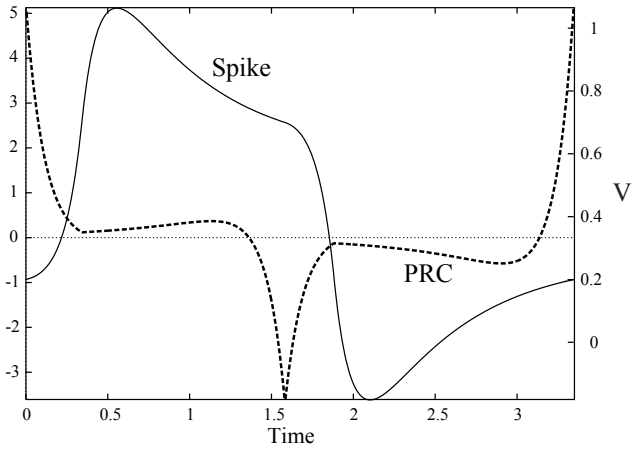

Figure 2.4.6: The numerically calculated PRC of the McKean model away from the singular limit. The corresponding spike is superimposed onto the diagram. Here $\mu = 0.2$ and $I = 0.8$.

FitzHugh-Nagumo and McKean models look different their PRCs all behave in qualitatively the same way.

2.5 Periodic Forcing

In the previous sections of this chapter we looked at the systems with a general input $I(t)$. However the pictures produced were all with constant input. Looking to next chapters work on networks it is worth focussing on the subset of periodic inputs of the form $I(t) = I(t + \Delta)$ for some constant Δ.

2.5.1 Simple Example

Consider an limit cycle oscillator of the periodic form

$$\frac{\mathrm{d}\phi}{\mathrm{dt}} = \Omega + \epsilon R(\phi) I(t),$$

where Ω is the uncoupled ($\epsilon = 0$) period of oscillations. Consider the instantaneous input $I(t)$ to have the form

$$I(t) = b \sum_n \delta(t - n\Delta).$$

The resulting new phase on the limit cycle is a function of the phase at the time ($\phi(T_n)$), and magnitude (b) of, the perturbation. This is illustrated in figure (2.5.1) So we have a function f that gives the change in phase between just before ($\phi(T_n)$)

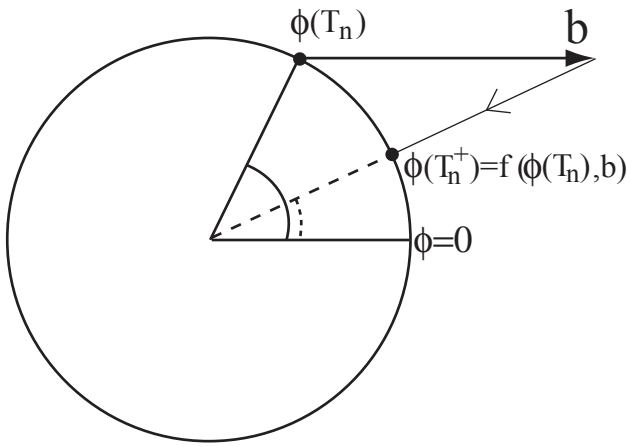

Figure 2.5.1: An illustration of the effect an instantaneous input with magnitude b has on a limit cycle oscillator.

and just after ($\phi(T_n^+)$) the instantaneous periodic input, it is the response function

of the system. We can write

$$\phi(T_n^+) = f(\phi(T_n), b),$$

and because between inputs there are no other inputs (i.e. the systems evolves as if $\epsilon = 0$) we have that

$$\phi(T_{n+1}) = \phi(T_n^+) + \Omega\Delta.$$

We therefore have a map of the form

$$\phi_{n+1} = f(\phi_n, b) + \Omega\Delta \equiv g(\phi_n, b),$$

For illustration consider the simple case of the Poincaré section of the flow on a Torus where the function $g(\phi_n, b)$ is given by

$$g(\phi, b) = \phi + b \sin 2\pi\phi$$

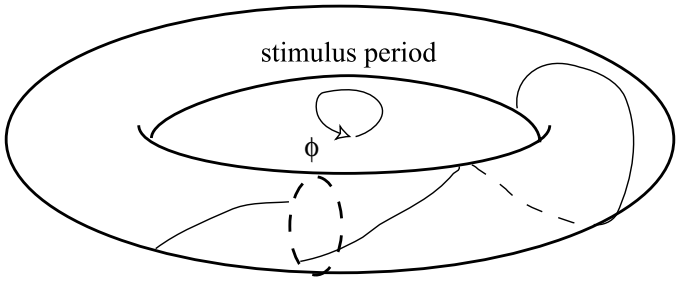

Figure 2.5.2: Illustration showing flow on torus

Obviously for $b < 1/2\pi$ the map is invertible and it can be seen that even in this simple example Arnol'd tongues exist in the (Δ, b). Inside the $N : M$ Arnol'd tongue all orbits asymptotically approach a stable $N : M$ mode-locking pattern.

For each such orbit there is a rotation number:

$$\rho = \lim_{N\to\infty} \frac{1}{N} \sum_{n=1}^{N} \phi_{n+1} - \phi_n$$

which measures the average rotation between stimuli. The stability of fixed point ϕ^* can be calculated from

$$\left\{ \left. \frac{\partial \phi_{n+1}}{\partial \phi_n} \right|_{\phi^*} \right\}. \tag{2.28}$$

If equation (2.28) is ± 1 we have a stability border (1 gives tangent bifurcation and -1 gives a period doubling bifurcation). The construction of the Arnol'd tongues [43], is given by $\rho = 1$ (so that $\phi_{n+1} - \phi_n = 1$). This gives

$$1 + \phi^* = g(\theta^*, b) + \Delta, \quad \text{or} \quad \frac{1 - \Delta}{b} = \sin(2\pi\phi^*)$$

Substituting this into the border conditions (tangent bifurcation: $\cos 2\pi\phi = 0$ or $\sqrt{1 - \sin^2 2\pi\phi} = 0$ so $\sin 2\pi\phi = \pm 1$, doubling bifurcation: $1 - \sin^2 2\pi\phi = \pi^{-2} b^{-2}$) to give

$$b = \pm(\Delta - 1), \qquad b^2 = \pi^{-2} + (\Delta - 1)^2$$

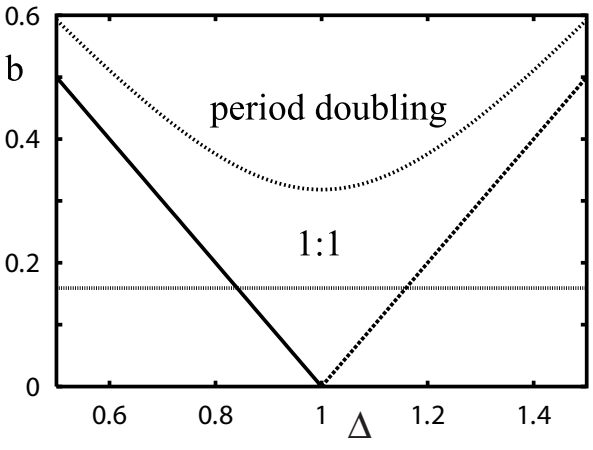

Figure 2.5.3: Arnol'd tongue structure for 1:1 mode-locking.

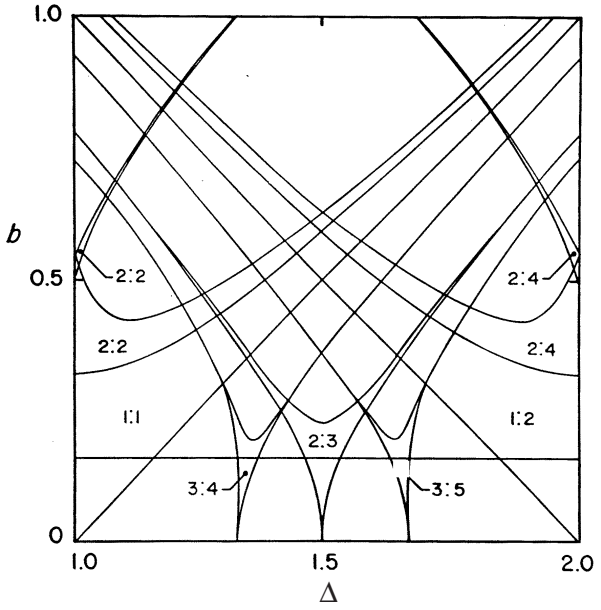

Figure 2.5.4: Full Arnol'd tongue structure for other $N : M$ orbits. Note the existence of $N + N' : M + M'$ orbits between orbits of type $N : M$ and $N' : M'$.

2.5.2 1:1 mode-locking of the periodically forced IF neuron

Consider an IF neuron as in section (2.3) with threshold at 1 and reset level set to 0 being driven by a Δ periodic signal $I(t) = I(t+\Delta)$:

$$\dot{v} = -\frac{v}{\tau} + I(t), \qquad T_n < t < T_{n+1}$$

As before an implicit map of the firing times may be obtained by integrating between reset and threshold,

$$\begin{aligned} \mathrm{e}^{T_{n+1}/\tau} &= \int_{T_n}^{T_{n+1}} I(s)\mathrm{e}^{s/\tau}\mathrm{d}s, \\ &= \int_{-\infty}^{T_{n+1}} I(s)\mathrm{e}^{s/\tau}\mathrm{d}s - \int_{-\infty}^{T_n} I(s)\mathrm{e}^{s/\tau}\mathrm{d}s. \end{aligned} \tag{2.29}$$

Introducing the function

$$G(t) = \int_{-\infty}^{0} \mathrm{e}^{s/\tau} I(t+s)\mathrm{d}s, \qquad \text{with} \qquad G(t) = G(t+\Delta),$$

gives from (2.29)

$$\mathrm{e}^{T_{n+1}/\tau}[G(T_{n+1}) - 1] = \mathrm{e}^{T_n/\tau} G(T_n). \tag{2.30}$$

Defining the function

$$F(t) = \mathrm{e}^{t/\tau}[G(t) - 1],$$

we obtain from (2.30)

$$F(T_{n+1}) = F(T_n) + \mathrm{e}^{T_n/\tau}.$$

If F is invertible ($F'(t) \neq 0$ for all t) and F^{-1} is defined on the range of $F(t) + \mathrm{e}^{t/\tau}$ then we have an explicit map of the form

$$T_{n+1} = \Psi(T_n), \qquad \Psi(t) = F^{-1}[F(t) + \mathrm{e}^{t/\tau}].$$

Since

$$G'(t) = I(t) - \frac{G}{\tau}, \qquad \text{then} \qquad F'(t) = \mathrm{e}^{t/\tau}[I(t) - 1/\tau],$$

so that $F'(t) \neq 0$ if $A(t) \neq 1/\tau$. A 1:1 mode-locked solution is defined by $T_n = (n+\phi)\Delta$, giving a fixed point equation

$$G(\phi\Delta) = \frac{1}{1-\mathrm{e}^{-\Delta/\tau}}.$$

Stability is examined by considering perturbations of the form $T_n \to T_n + \delta_n$, giving

$$F(T_{n+1}) + F'(T_{n+1})\delta_{n+1} = F(T_n) + F'(T_n)\delta_n + \mathrm{e}^{T_n/\tau}[1+\delta_n/\tau].$$

When $F'(T_{n+1}) \neq 0$ (i.e. the firing map is explicit)

$$\delta_{n+1} = \kappa(\phi)\delta_n.$$

So we have

$$\kappa(\phi) = \left.\frac{F'(T_n) + \mathrm{e}^{T_n/\tau}/\tau}{F'(T_{n+1})}\right|_{T_n=(n+\phi)\Delta} = \mathrm{e}^{-\Delta/\tau}\frac{I(\phi\Delta)}{I(\phi\Delta)-1/\tau}.$$

Solutions are stable if

$$|\kappa(\phi)| < 1.$$

The borders of the regions where 1:1 solutions become unstable are defined by $\kappa(\phi) = 1$ (tangent bifurcation) and $\kappa(\phi) = -1$ (period doubling bifurcation).

When the firing map is only available implicitly solutions may lose stability in a non-smooth fashion. (a) There is a tangential intersection of the trajectory with the threshold value such that upon variation of the bifurcation parameter the local maxima of the IF trajectory passes through threshold from above. They are defined by $\dot{v} = -v/\tau + I = 0$, so that $I(T_n) = 1/\tau$ or equivalently $F'(T_n) = 0$. (b) A sub-threshold local maxima increases through threshold leading to the creation of a new firing event at some earlier time than usual. They are defined by $F(T^*) = F(T_n) + \mathrm{e}^{T_n/\tau}$ and $F'(T^*) = 0$ with $T^* < T_{n+1}$ and T_{n+1} is the solution to $F(T_{n+1}) = F(T_n) + \mathrm{e}^{T_n/\tau}$.

As an example consider the case

$$I(t) = I + \begin{cases} +\epsilon & 0 \leq t < \Delta/2, \\ -\epsilon & \Delta/2 < t < \Delta. \end{cases}$$

The firing map is explicit when $I(t) \neq 1/\tau$, which is guaranteed upon choosing $I(t) > 1/\tau$, ie $I - \epsilon > 1/\tau$. Conveniently the border condition $|\kappa(\phi)| = 1$ becomes independent of ϕ, since $A(\phi) = I \pm \epsilon$. A tangent bifurcation occurs when the map is explicit and $\kappa = 1$:

$$\pm\epsilon = -I + \frac{1/\tau}{1 - \mathrm{e}^{-\Delta/\tau}}, \qquad \epsilon < I - 1/\tau.$$

The boundaries calculated can be seen in figure (2.5.5).

It can be seen from the tongue structure in figure (2.5.5) that the 1:1 solution is

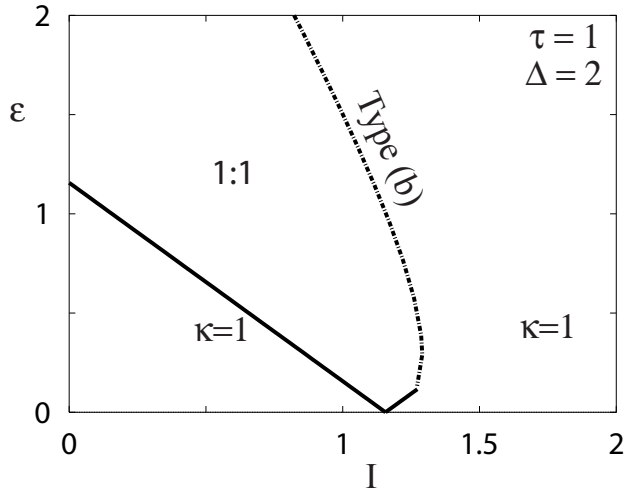

Figure 2.5.5: A close up of the 1:1 Arnol'd tongue solution of the integrate and fire model. It can be seen that the larger the coupling the wider the window of the 1:1 solution.

enhanced with increasing coupling. Although the IF model is not as sophisticated as the HH model, we shall show in the next section that the same mode-locking

trends are seen for the HH and McKean models. Further discussion to be found in the papers of Coombes [44, 45, 46, **?**]

2.5.3 Simulations of periodic forcing

For the more complex models it is not generally possible to calculate the Arnol'd tongues analytically. However the behaviour exhibited by the simple examples can be seen in simulations of more complex models. Figures (2.5.6) and (2.5.7) are examples of 1 to 1 solutions, the periodic forcing (in this case sinusoidal) has the same period as the period of the oscillations. As predicted by the theory, the 1 to 1 solution exists over a progressively larger window as the amplitude of the forcing increases.

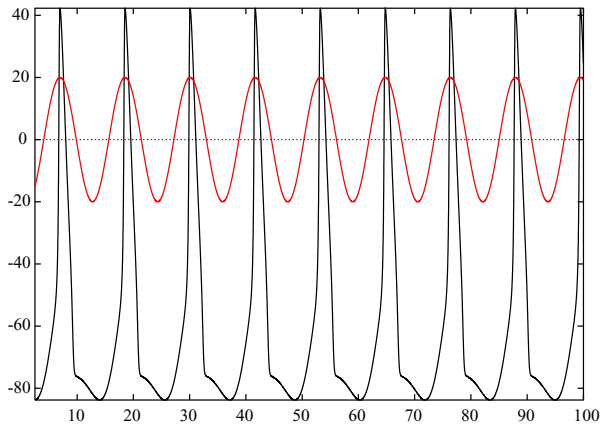

Figure 2.5.6: A illustration showing periodic sinusoidal forcing of the HH model overlaid with the resulting spikes. This is an example of a $1:1$ solution.

The observed behaviour of these two models to periodic inputs is also consistent with what is seen in figure (2.5.5). However unlike for the Hodgkin-Huxley and

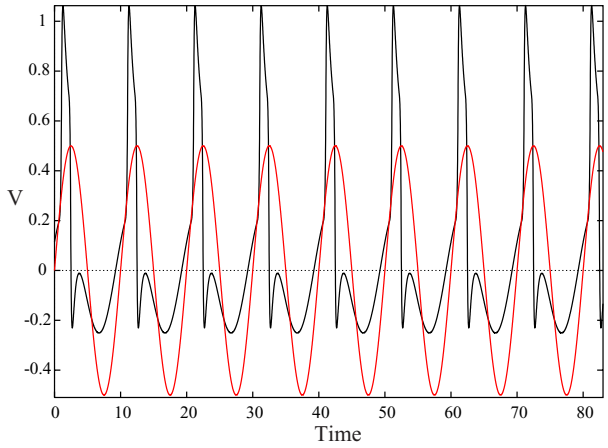

Figure 2.5.7: A illustration showing periodic sinusoidal forcing of the McKean model overlaid with the resulting spikes. This is an example of a $1:1$ solution.

McKean models, the theory of mode-locking for the Integrate and Fire model is fully developed in [48].

2.6 Conclusions

In this chapter we have shown that there is a lot of diversity in the oscillatory subset of neuron models. As it was constructed to, the Hodgkin-Huxley model gives biologically realistic action potentials. However we showed that there are a few other more simple models that capture this oscillatory nature. Of particular interest is the McKean model as it is the simplest model that can generate action potentials. The similar nature of these models poses the question, do the models still act like the Hodgkin-Huxley model in different situations such as in a synaptically interacting network. The results obtained with periodic forcing suggest that we might expect to see synchrony in a network of neurons. Exploring the properties

of small weakly coupled networks is the focus of the next chapter.

Chapter 3

Small Discrete Networks

In the previous chapter, single neuron models were examined. It can be seen that under constant input, these models produce oscillatory or fixed point behaviour depending on the magnitude of the constant input. It was also shown that this behaviour persisted even when the input was periodic. Such a periodic signal can be thought of as the input from other neurons in a network. To model the input from other neurons one must understand the method of neural signal transference, which is illustrated in figure (3.0.1). When a neuron 'fires' a voltage spike is generated at the axon hillock and propagates along the axon to the synapse where the voltage displaces neuro-transmitters. These neuro-transmitters diffuse across the synaptic cleft and bind to the dendritic tree of another neuron. This accumulation neuro-transmitters induces a voltage in the post-synaptic dendritic tree and the voltage 'signal' is either passively or actively transported to the soma of the post-synaptic neuron. There are a few things that effect the signal when it travels between the soma of one neuron to that of another. Firstly there can be a delay because the signal travels down the axon of the neuron at a finite speed. The magnitude of this delay is simply a function of the length of the axon. The lengths of axons can range in length from much less than a millimeter to several hundred

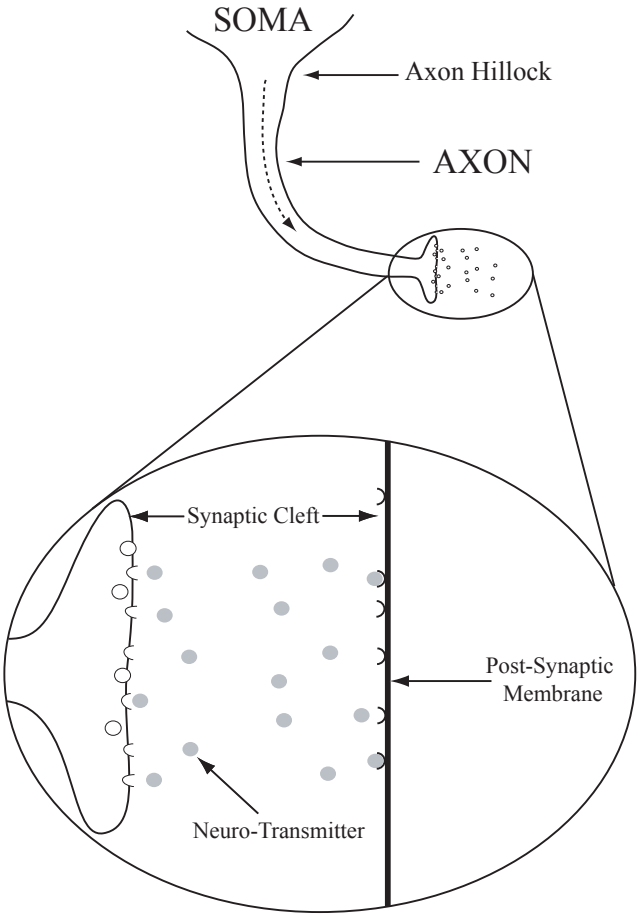

Figure 3.0.1: Caricature neural signal transference.

millimeters and is dependent on the type and location of the neuron. Secondly the transfer of the signal via neuro-transmitters causes the signal to become 'smoothed out' and depending on the size of the synaptic cleft and the neuro-transmitters involved, the relative amplitudes and durations of signals can be substantially different relative to the incoming action potential. We shall term this a distributed 'delay'. Finally, the dendritic tree is a complicated structure in its own right and can contribute a delay of its own. However we reserve discussion of this to the next chapter. Ignoring the dendritic structure for the moment progress can be made modelling the synaptic effects with the use of a synaptic kernel. Simple discrete delays can also be introduced to model axonal delays. The first problem is how to model networks of neurons. In biological neural networks the number of neurons can be up to the order of 10^{10}. These systems can only be studied analytically in slightly more abstract ways, looking at neural field models of populations of neurons and average firing times [49, 50] [51, 52] [53] [54]. In contrast understanding the dynamics of small oscillatory networks can give insight into systems such as the stomatogastric ganglion circuit [55]. The coupled equations for small networks can often be solved however when restricting attention to weak coupling. In this case the powerful tool of averaging can be brought to bear [56] [57]. That is the focus of this chapter.

3.1 General Theory Of Coupled Oscillators

Before moving on to the specific coupled oscillator networks it is useful looking at the general case (discussed in [41] and [56]).

Consider a set of N first order non-linear differential equations

$$\dot{X}_k = F_k(X), \qquad X \in \mathbb{R}^m, \qquad k = 0, 1, ..., N.$$

Let there be a periodic solution such that

$$\dot{X}_k = U_k(t); \qquad U_k(t+T) = U_k(t), \qquad k = 0, 1, ..., N.$$

Where T is the period of the periodic solution. The above N equations give a periodic orbit in Nm dimensions. Now assume there is some form communication between the N systems :

$$\dot{X}_k = F_k(X) + \epsilon \sum_j G_k(X_k, X_j), \qquad k \neq j, \tag{3.1}$$

and assume that ϵ is sufficiently small so that the limit cycles persist. For this system of coupled oscillators it is possible to perform a change of variables into a phase variable and $\theta \in \mathbb{S}$ and a set of of variables normal to the limit cycle $b \in \mathbb{R}^{m-1}$, as follows

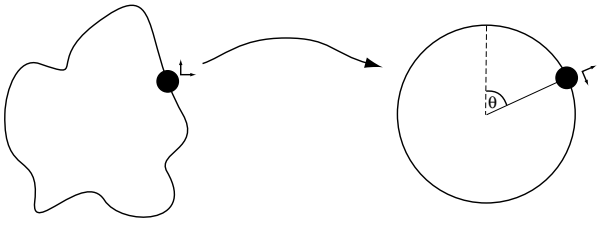

Figure 3.1.1: Illustration of principle in 2-d.

Using the coordinate transform $X \to (\theta, b)$. We may write

$$X_k(t) = U_k(\theta_k(t)) + M_k(\theta_k(t))b_k + O(|b_k|^2).$$

Here $M \in \mathbb{R}^{m-1}$ and satisfies

$$M_k(\theta)^T M_k(\theta) = 1, \tag{3.2}$$

$$U_k'(\theta)^T M_k(\theta) = 0, \tag{3.3}$$

where $' \equiv \frac{\mathrm{d}}{\mathrm{d}\theta}$. It is clear that the lower the dimension of the normal coordinates, the more complex the calculations become. When $b = 0$, J_k is simply an orthogonal matrix and its inverse is a simple calculation. The Jacobian J of this transformation is

$$J_k(\theta_k, b_k) = (U_k'(\theta_k) + M_k'(\theta_k)b_k, M_k(\theta_k)) + O(|b_k|^2).$$

If a matrix B is small, the inverse of $(A + B)$ is $(I - A^{-1}B)A^{-1}$. Assuming that b is small, J can be inverted using this identity.

$$(I - J_{k0}^{-1}[M_k'b_k, 0])J_{k0}^{-1} + O(|b_k|^2) = \begin{bmatrix} (1 - (U_k')^T M_k'b_k/\rho_k)(U_k')^T/\rho_k \\ -(M_k)^T M_k'b_k(U_k')^T/\rho_k + (M_k')^T. \end{bmatrix} + O(|b_k|^2).$$

Where $J_{k0} = J_k(\theta_k, 0)$ and

$$J_{k0}^{-1} = \begin{bmatrix} (U_k')^T\rho_k \\ (M_k)^T \end{bmatrix}, \qquad \rho_k = |U_k'|^2.$$

Also note that

$$\begin{aligned} F_k(U_k + M_kb_k) &= F_k(U_k) + D_kM_kb_k + O(|b_k|^2), \\ &= U_k' + D_kM_kb_k + O(|b_k|^2), \end{aligned}$$

where D_k is the Jacobian of F_k at U_k, to lowest order M_k, D_k and U_k' are periodic in θ and also independent of b_k to lowest order.
Differentiating (3.2) w.r.t. θ and using the fact that $U_k'' = D_kU_k'$, gives

$$\begin{aligned} &U_k'(\theta)^T M_k'(\theta) + U_k''(\theta)^T M_k(\theta), \\ =&U_k'(\theta)^T M_k'(\theta) + (U_k')^T(D_k)^T M_k = 0. \end{aligned}$$

Re-arranging the above gives

$$(U_k')^T(D_k)^T M_k = -(U_k')^T M_k',$$

and similarly from differentiating (3.2) we have that

$$-(M_k)^T M_k' = (M_k')^T M_k.$$

In the last chapter these expression were calculated for the McKean model (in that case $N = 2$). Substituting the above equations into (3.1) gives

$$\frac{\mathrm{d}\theta_k}{\mathrm{dt}} = \frac{1}{T} + \frac{(U_k')^2}{\rho_k}[(D_k + (D_k)^T)M_k b_k G_k], \tag{3.4}$$

$$\frac{\mathrm{d}b_k}{\mathrm{dt}} = ((M_k')^T D_k M_k + (M_k')^T M_k)b_k + (M_k)^T G_k. \tag{3.5}$$

In the limit $b \to 0$, which is equivalent to "infinite attraction" to the limit cycle, we can ignore the dynamics of b_k and so simply have that

$$\frac{\mathrm{d}\theta_k}{\mathrm{dt}} = 1 + \epsilon \sum_j h_k(\theta_k, \theta_j), \tag{3.6}$$

with

$$h_k(\theta_k, \theta_j) = \frac{1}{\rho_k(\theta_k)}(U_k')^T(\theta_k) G_k(U_k(\theta_k), U_j(\theta_j)),$$

which is clearly of lower dimension than (3.1).

So far the theory is valid for all limit cycle oscillators. In the case where neural systems are the focus further progress can be made. Motivated by the notion of the response function in chapter 2, and other work on coupled neurons [58],[59], we consider the function h_k to have the structure

$$h_k(\theta_j, \theta_k) = W_{jk} R(\theta_j) P(\theta_k T),$$

where W_{jk} is some 'weight' or 'connection' matrix between two neurons j and k. Consider $P(\theta)$ as a periodic function such that $P(t + T) = P(t)$. As in chapter 2 we consider $R(\theta)$ as the response function, which is therefore also periodic such that $R(\theta + 1) = R(\theta)$.

For the weakly coupled case $0 < \epsilon \ll 1$, [56] shows that a method of averaging can be used on system of the form (3.6), and there exists a change of variables $\theta_j = t/T + \phi_j + \epsilon g(\phi_j, t, \epsilon)$ (see [60] for a discussion of coupled oscillators without averaging). Applying this theorem gives

$$\frac{\mathrm{d}\phi_j}{\mathrm{dt}} = \epsilon \sum_k W_{jk} H(\phi_k - \phi_j) + O(\epsilon^2), \tag{3.7}$$

where $H(\phi)$ is known as the interaction function and has the form

$$H(\phi) = \frac{1}{T} \int_0^T R(t/T) P(t + \phi T) \mathrm{d}t. \tag{3.8}$$

The error between the true solution and the solution obtained from the averaging theorem is of order ϵ for a time scale $t \sim 1/\epsilon$.

Phase Locked States

A major feature of coupled oscillatory systems is their ability to phase lock. For a network of N oscillators we can define 1:1 phase locked solutions of (3.6) to be of the form $\theta_j(t) = \phi_j + t/\Delta$, where ϕ_j is a constant phase and Δ is the collective period of the phase locked state. Substituting this into (3.7) and working to $O(\epsilon)$ gives

$$\frac{1}{\Delta} = \frac{1}{T} + \sum_k W_{jk} H(\phi_k - \phi_j) \qquad \forall j. \tag{3.9}$$

Choosing a reference oscillator, the N equations of (3.9) determine the collective period Δ and $N - 1$ relative phases. To analyse the local stability of a phase locked solution $\Phi = (\phi_1, \ldots, \phi_N)$, we linearise (3.9) by setting $\theta_j(t) = \phi_j + t/T + \tilde{\theta}_j(t)$ and expand to first order in $\tilde{\theta}_j$ to obtain

$$\frac{\mathrm{d}\tilde{\theta}_j}{\mathrm{dt}} = \epsilon \sum_k \widehat{H}_{jk}(\Phi) \tilde{\theta}_j, \tag{3.10}$$

where

$$\widehat{H}_{jk}(\Phi) = W_{jk}H'(\phi_k - \phi_j) - \delta_{j,k}\sum_m W_{jm}H'(\phi_m - \phi_j),$$

and $H'(\phi) = \mathrm{d}H(\phi)/\mathrm{d}\phi$. One of the eigenvalues of the Jacobian $\widehat{H}$ is always zero, and the corresponding eigenvector points in the direction of the flow, that is $(1, 1, \ldots, 1)$. The phase locked solution will be stable provided all other eigenvalues have negative real parts. In any network a common phase locked solution is synchrony, where there is no phase difference between phase locked oscillators. Another solution we might expect to see is the 'splay' solution, where the phase locked oscillators have the same phase difference between each one. For N oscillators we have the condition for a splay state

$$\phi_n = \phi_1 + n/N \qquad n = 1, ..., N.$$

This principle is illustrated in figure (3.1.2).

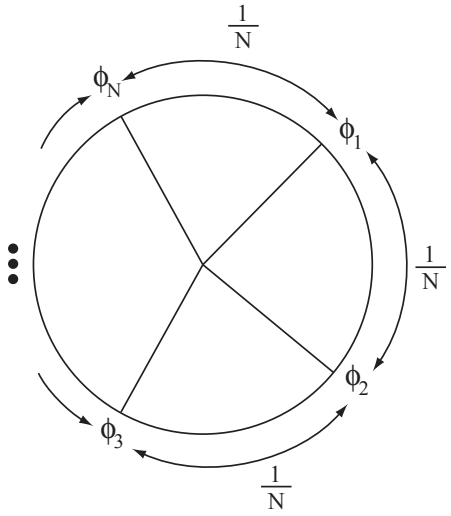

Figure 3.1.2: Illustration of the principle of splay state phase locked solution.

Take an example of two oscillators ($N = 2$) and choose the relative weighting between the neurons to be simply $W_{12} = W_{21} = 1$.

$$\dot{\theta_1} = 1/T + \epsilon H(\theta_2 - \theta_1),$$
$$\dot{\theta_2} = 1/T + \epsilon H(\theta_1 - \theta_2).$$

Define $\phi = \theta_2 - \theta_1$ and construct the equation

$$\dot{\phi} = \dot{\theta_2} - \dot{\theta_1} = \epsilon \left[H(\phi) - H(-\phi) \right]. \tag{3.11}$$

A constant phase difference of the phase locked solution is a zero of the function $K(\phi) = H(\phi) - H(-\phi)$. A given phase locked state is stable provided

$$\epsilon \frac{\mathrm{d}K(\phi)}{\mathrm{d}\phi} > 0.$$

By the symmetry of the equations, there will be guaranteed solutions at $\phi = 0$ (the synchronous solution) and at $\phi = 0.5$ (the anti-synchronous solution).

Using this same idea, the equations for three oscillators ($N = 3$) can be constructed

$$\dot{\phi_1} = \epsilon \left[H(-\phi_1) + H(\phi_2 - \phi_1) - H(\phi_1) - H(\phi_2) \right] \tag{3.12}$$
$$\dot{\phi_2} = \epsilon \left[H(\phi_1 - \phi_2) + H(-\phi_2) - H(\phi_1) - H(\phi_2) \right] \tag{3.13}$$

where $\phi_1 = \theta_2 - \theta_1$ and $\theta_3 - \theta_1$. By symmetry we expect a splay solution of the form $\phi_1 = 1/3$, $\phi_2 = 2/3$ as well as the synchronous solution $\phi_1 = \phi_2 = 0$.

Focus On Synaptic Coupling

In neural systems $P(\theta_k T)$ can be considered to be the signal from neuron k which we may write as $P(\theta_k) = P(t + \phi_k T)$. This can be modelled by a series of signals convoluted with some form of synaptic kernel. The synaptic kernel represents synaptic processing and can be thought of as the convolution of a temporal kernel

with an incoming action potential. Consider the form for the output $P(t)$ from any neuron

$$P(t) = \sum_m \eta(t - mT), \tag{3.14}$$

3.2 Fourier Representations

For a general neuron model and hence a general response function $R(\theta)$ and a general synaptic kernel $P(t)$ we need to be able to calculate the interaction $H(\phi)$. This can be difficult depending on the form of these functions. However if we are in the weak coupling regime we know that the functions are periodic and have the same period. This suggests that using the Fourier transformation of these functions may allow progress for the general case.

3.2.1 Solution Of General Network Equations Using Fourier Transforms

Perhaps the most versatile forms for the functions $R(t)$ and $P(t)$ is their Fourier representations. For any model the response function can either be calculated analytically or numerically and under Fourier transformation

$$R(t/T) = \sum_{k=-\infty}^{\infty} R_k \mathrm{e}^{2\pi i k t/T}.$$

Define $w_k = 2\pi k/T$, then the Fourier coefficients R_k are given by

$$R_k = \frac{1}{T}\int_0^T R(t/T)\mathrm{e}^{-iw_k t}\mathrm{d}t. \tag{3.15}$$

The function $P(t)$ can be calculated similarly

$$P(t) = \sum_{k=-\infty}^{\infty} P_k \mathrm{e}^{i2\pi kt/T}.$$

where

$$P_k = \frac{1}{T}\int_0^T P(t)\mathrm{e}^{-iw_k t}\mathrm{d}t. \tag{3.16}$$

For $P(t)$ given by (3.14) we have

$$P_k = \frac{1}{T}\sum_{j\in\mathbb{Z}}\int_0^T \eta(t-jT)\mathrm{e}^{-iw_k t}\mathrm{d}t. \tag{3.17}$$

Shifting the time variable $t = t - jT$ we get

$$\begin{aligned} P_k &= \frac{1}{T}\sum_{j=0}^{-\infty}\int_{-jT}^{T(1-j)} \eta(t)\mathrm{e}^{-iw_k t}\mathrm{e}^{-iw_k jT}\mathrm{d}t \\ &= \frac{1}{T}\widehat{\eta}(w_k) \end{aligned}$$

where $\widehat{\eta}(w) = \int_0^\infty \eta(t)\mathrm{e}^{-iwt}\mathrm{d}t$ and we have the fact that $\mathrm{e}^{iw_k jT} = \mathrm{e}^{i2\pi kj} = 1$.
This enables the calculation of the function $H(t)$ from (3.8) as

$$\begin{aligned} H(\phi) &= \frac{1}{T}\int_0^T \sum_{k=-\infty}^{\infty} R_k \mathrm{e}^{iw_k t} \sum_{j=-\infty}^{\infty}\int_0^\infty P_j \mathrm{e}^{iw_j(t+\phi T)}\mathrm{d}t \\ &= \sum_{k=-\infty}^{\infty} R_k P_{-k}\mathrm{e}^{iw_k t\phi T} \end{aligned} \tag{3.18}$$

using the identity $1/T\int_0^T \mathrm{e}^{it[w_k+w_j]}\mathrm{d}t = \delta(w_k + w_j)$.

We have from (3.18) the structure of the fourier expression

$$H(\phi) = \sum_{k=-\infty}^{\infty} H_k \mathrm{e}^{iw_k phi}$$

where

$$H_k = R_k P_{-k} = \frac{R_k}{T} \widehat{\eta}_{w_{-k}}$$

3.2.2 Alpha Function Coupling

A common choice for a synaptic kernel is the alpha function, it has a good resemblance to experimental observations of post synaptic response but has a simple form

$$\alpha(\tau) = \alpha^2 \tau e^{-\alpha\tau} \Theta(\tau), \tag{3.19}$$

where $\Theta(\tau)$ is the step function and α is some constant.
An illustration of the post synaptic response shapes the alpha function produces for two different values of alpha is shown in figure (3.2.1)

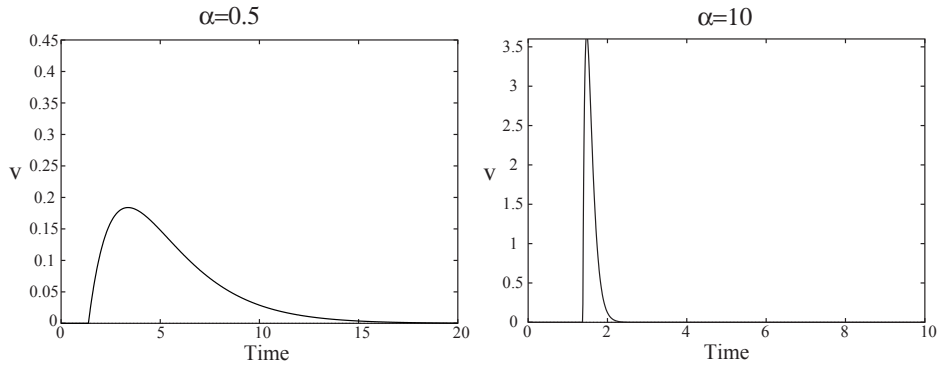

Figure 3.2.1: The post synaptic response shapes produced by the alpha function for two different values of alpha, $\alpha = 0.5$ (left) and $\alpha = 10$ (right).

The Fourier form of this kernel is

$$\begin{aligned}
P_k &= \frac{1}{T}\int_0^\infty \alpha^2 t\mathrm{e}^{-\alpha t}\mathrm{e}^{-iw_k t}\mathrm{d}t, \\
&= \frac{\alpha^2}{T}\int_0^\infty t\mathrm{e}^{-t(\alpha+iw_k)}\mathrm{d}t, \\
&= \frac{\alpha^2}{T(\alpha+iw_k)}\left(\left[-t\mathrm{e}^{-t(\alpha+iw_k)}\right]_0^\infty + \int_0^\infty \mathrm{e}^{-t(\alpha+iw_k)}\mathrm{d}t\right), \\
&= \frac{\alpha^2}{T(\alpha+iw_k)}\left(0 - \frac{1}{\alpha+iw_k}\left[\mathrm{e}^{(\alpha+iw_k)}\right]_0^\infty\right), \\
&= \frac{-\alpha^2(0-1)}{T(\alpha+iw_k)^2} = \frac{\alpha^2}{T(\alpha+iw_k)^2}.
\end{aligned}$$

So that in this case the Fourier representation for $P(t)$ is

$$P(t) = \sum_{k=-\infty}^{\infty} \frac{\alpha^2 \mathrm{e}^{iw_k t}}{T(\alpha+iw_k)^2}. \tag{3.20}$$

3.2.3 Small Hodgkin-Huxley Network

In the last chapter it was mentioned that it was possible to numerically calculate the response function for the Hodgkin-Huxley model. Using this response function in Fourier form it is therefore possible (using the methods above) to construct a Fourier expression for the interaction function. It is therefore possible to simulate a network of weakly coupled HH neurons. From the theory of phase-locked states presented in section (3.1), it is also possible to construct bifurcation diagrams for the HH model without resorting to brute force numerical simulations. A simple example is two identical neurons coupled with alpha function coupling. We have two equations as in (3.11).

Plotting phase locked states where $\dot{\phi} = 0$ with varying alpha gives a bifurcation diagram, shown in figure (3.2.2) The HH function can be considered the progenitor of the other neuron models seen in the last chapter. Using the same network construction with different neuron models should give a way of comparing the different models.

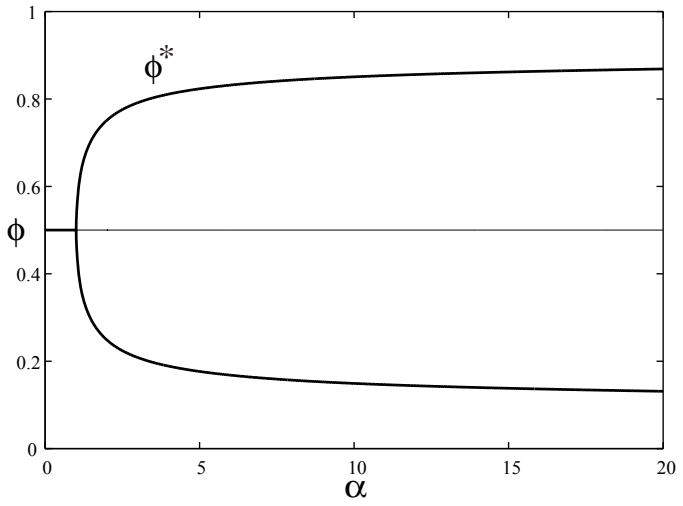

Figure 3.2.2: A bifurcation diagram of varying α for a HH network, the system undergoes a pitchfork bifurcation as the system goes from 2 (ϕ=0,0.5) to 4 (ϕ=0,0.5,ϕ^*,$1-\phi^*$) solutions. Thick (thin) lines are stable (unstable).

3.2.4 Simple Response Functions

Motivated by the piecewise exponential shaped response functions of the McKean and the integrate and fire models, we can take a generic form for a response function,

$$R(t/T) = \sum_{j=1}^{N} C_j \mathrm{e}^{b_j t}, \in (a_{j-1}, a_j) \qquad t \in (0, T), \tag{3.21}$$

where there are $N-1$ discontinuities in $R(t/T)$ and $a_0 = 0$ and $a_N = T$. The a_j in between are determined by the value of t/T at the discontinuities of $R(t/T)$.

This makes the calculation of the interaction function more simple. Using equa-

tions (3.8),(3.20) and (3.21),

$$\begin{aligned}
H(\phi) &= \frac{1}{T}\int_0^T \sum_{j=1}^{N} C_j \mathrm{e}^{b_j t} \sum_{k=-\infty}^{\infty} P_k \mathrm{e}^{iw_k(t+\phi T)} \mathrm{d}t, \\
&= \frac{1}{T}\sum_{j=1}^{N} C_j \int_{a_{j-1}}^{a_j} \mathrm{e}^{b_j t} \left(P_0 + \sum_{k\neq 0} P_k \mathrm{e}^{iw_k(t+\phi T)} \right) \mathrm{d}t, \\
&= \frac{1}{T}\sum_{j=1}^{N} \left[C_j P_0 \int_{a_{j-1}}^{a_j} \mathrm{e}^{b_j t} \mathrm{d}t + C_j \sum_{k\neq 0} P_k \mathrm{e}^{iw_k \phi T} \int_{a_{j-1}}^{a_j} \mathrm{e}^{(b_j+iw_k)t} \mathrm{d}t \right], \\
&= \frac{1}{T}\sum_{j=1}^{N} C_j \left[\frac{P_0}{b_j} \left(\mathrm{e}^{b_j a_j} - \mathrm{e}^{b_j a_{j-1}} \right) + \sum_{k\neq 0} \frac{P_k}{b_j + iw_k} \left(\mathrm{e}^{b_j a_j} \mathrm{e}^{iw_k(a_j+\phi T)} - \mathrm{e}^{b_j a_{j-1}} \mathrm{e}^{iw_k(a_{j-1}+\phi T)} \right) \right].
\end{aligned}$$

The McKean Model is a model that can be written in this form with

$$N = 2, \quad C_1 = BR_1, \quad C_2 = R_1 \mathrm{e}^{-\beta(1-\theta_T)T},$$
$$b_{1,2} = \beta, \quad a_0 = 0, \quad a_1 = (1-\theta_T)T, \quad a_2 = T,$$

where

$$R_1 = \Omega/(A - \beta w_2),$$
$$B = (A - \beta w_2)/(A + 1 - \beta w_1).$$

The integrate and fire model is another that can be written in this form,

$$N = 1, \quad C_1 = 1, \quad b_1 = T/\tau, \quad a_0 = 0, \quad a_1 = T.$$

In chapter 5 a model using a three piece phase response curve will be defined. This method can be used for that case as well.

3.3 Networks

Although the use of Fourier transforms is a powerful method calculating the interaction function, it is not always necessary. For certain choices of model and

synaptic kernel it is possible to calculate the interaction function explicitly.

3.3.1 Explicit Alpha Function Solution

It is possible to calculate synaptic function $P(t)$ explicitly for certain choices of synaptic kernel. This has the advantage of not having to its fourier transforms. The alpha function is one such synaptic kernel which can be solved explicitly

$$P(t) = \sum_m \alpha(t - mT) \quad ; \quad P(t+T) = P(t),$$

so we have

$$P(t) = \sum_{m=\infty}^{-\infty} \alpha^2 (t - mT) e^{-\alpha(t-mT)} \Theta(t - mT),$$

which can be written as

$$P(t) = \sum_{m=0}^{\infty} \alpha^2 (t + mT) e^{-\alpha(t+mT)},$$

because the step function causes the summation limits to be restricted.

$$\begin{aligned}
P(t) &= \alpha^2 e^{-\alpha t} \sum_{m=0}^{\infty} \left[t e^{-\alpha m T} - m e^{-\alpha m T} \right], \\
&= \alpha^2 e^{-\alpha t} \left[\frac{t}{1 - e^{-\alpha T}} - \sum_{m=0}^{\infty} m e^{-\alpha m T} \right], \\
&= \alpha^2 e^{-\alpha t} \left[\frac{t}{1 - e^{-\alpha T}} - \sum_{m=0}^{\infty} \frac{\mathrm{d}}{\mathrm{d}(\alpha \mathrm{T})} \left(-e^{-\alpha m T} \right) \right], \\
&= \alpha^2 e^{-\alpha t} \left[\frac{t}{1 - e^{-\alpha T}} + \frac{\mathrm{d}}{\mathrm{d}(\alpha \mathrm{T})} \left(\frac{1}{1 - e^{-\alpha T}} \right) \right], \\
&= \alpha^2 e^{-\alpha t} \left[\frac{t}{1 - e^{-\alpha T}} + \frac{e^{-\alpha T}}{(1 - e^{-\alpha T})^2} \right].
\end{aligned}$$

So we have

$$P(t) = \frac{\alpha^2 e^{-\alpha t}}{1 - e^{-\alpha T}} \left[t + \frac{e^{-\alpha T}}{1 - e^{-\alpha T}} \right], \quad 0 < t/T + \phi < 1. \tag{3.22}$$

For this special case we have an explicit solution and there is no need to use Fourier transformations. This is an advantage because for practicality there will be a truncation error using a Fourier series.

3.3.2 Integrate and Fire Network

A network of integrate and fire neurons has been widely investigated [61, 62, 63] [64, 65]. As described in the general theory at the beginning of this chapter we can explicitly calculate the interaction function for the case of alpha function synapses. Suppose there is a network of N identical coupled linear integrate and fire neurons. From (3.22) we have the explicit form of the function $P(t)$ for an alpha function and using the a simple response function $R(t/T) = e^t$ from chapter 2 we can calculate the interaction function,

$$\begin{aligned} H(\phi) &= \frac{1}{T}\int_0^T \mathrm{e}^t \frac{\alpha^2 T \mathrm{e}^{-\alpha t+\phi T}}{1-\mathrm{e}^{-\alpha T}}\left[t+\phi+\frac{\mathrm{e}^{-\alpha T}}{1-\mathrm{e}^{-\alpha T}}\right]\mathrm{d}t, \\ &= \kappa(\phi)\int_0^T \left[\frac{T\mathrm{e}^{-\alpha T}}{1-\mathrm{e}^{-\alpha T}}+\phi T+t\right]\mathrm{e}^{t(1-\alpha)}\mathrm{d}t, \end{aligned}$$

where

$$\kappa(\phi) = \frac{\alpha^2 \mathrm{e}^{-\alpha\phi T}}{T(1-\mathrm{e}^{-\alpha T})},$$

and note that there is a discontinuity on the interval $[0, T)$ when the neuron fires and resets so we have to split the integral over this discontinuity

$$\begin{aligned} H(\phi) = \kappa(\phi)&\int_0^{T(1-\phi)} \left[\frac{Te^{-\alpha T}}{1-e^{-\alpha T}}+\phi T+t\right]e^{t(1-\alpha)}\mathrm{d}t \\ &+\kappa(\phi-1)\int_{T(1-\phi)}^{T} \left[\frac{Te^{-\alpha T}}{1-e^{-\alpha T}}+(\phi-1)T+t\right]e^{t(1-\alpha)}\mathrm{d}t. \end{aligned}$$

Using

$$\int_a^b \mathrm{e}^{t(1-\alpha)}\mathrm{d}t = \frac{1}{1-\alpha}\left[\mathrm{e}^{b(1-\alpha)}-\mathrm{e}^{a(1-\alpha)}\right],$$

and

$$\int_a^b t\mathrm{e}^{t(1-\alpha)}dt = \frac{1}{1-\alpha}\left[\mathrm{e}^{b(1-\alpha)}\left(b-\frac{1}{1-\alpha}\right)-\mathrm{e}^{a(1-\alpha)}\left(a-\frac{1}{1-\alpha}\right)\right],$$

and defining

$$\begin{aligned}\gamma(\phi) &= \phi T + \frac{T\mathrm{e}^{-\alpha T}}{1-\mathrm{e}^{-\alpha T}},\\ \eta(\phi) &= T(1-\phi)(1-\alpha),\\ \beta(\phi) &= \mathrm{e}^{\eta(\phi)}\left(T(1-\phi)-\frac{1}{1-\alpha}\right),\end{aligned}$$

gives

$$\begin{aligned}H(\phi) = &\frac{\kappa(\phi)}{1-\alpha}\left[\gamma(\phi)\left(\mathrm{e}^{\eta(\phi)}-1\right)+\beta(\phi)+\frac{1}{1-\alpha}\right]\\ &+\frac{\kappa(\phi-1)}{1-\alpha}\left[\gamma(\phi-1)\left(\mathrm{e}^{T(1-\alpha)}-\mathrm{e}^{\eta(\phi)}\right)+\mathrm{e}^{T(1-\alpha)}\left(T-\frac{1}{1-\alpha}\right)-\beta(\phi)\right]. \quad (3.23)\end{aligned}$$

This is the explicit interaction function of the integrate and fire model with alpha function coupling. Using this it is possible to look at phase locked behaviour of a network of IF neurons. Phase locked states can be found simply by the zeros of the interaction function and their stability is simply the sign of the derivative at these zeros, stable when negative and unstable when positive as discussed earlier.

Using the 2 oscillator network equations as set out earlier in (3.11) we can examine the interaction function by plotting it for different values of α. This can be seen in figures (3.3.1) and (3.3.2), and it is clear that the system has undergone a bifurcation as the number of solution changes from 2 to 4.

Plotting a bifurcation diagram is of interest to see the nature of the evolution of solutions with varying α. This can be seen in figure (3.3.3).

Using (3.12) and (3.13) it is possible to to look at a network of three identical IF neurons. This can be seen in figure (3.3.4). The stable splay state solutions (labelled 2) lose their stability via super critical Hopf bifurcation at $\alpha \approx 8$ where a stable limit

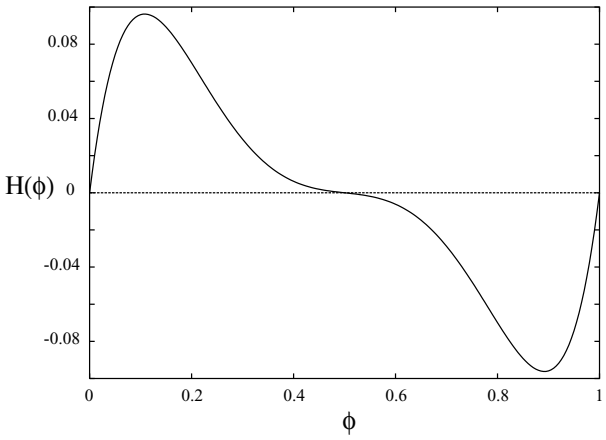

Figure 3.3.1: The interaction function of the IF model with $\alpha = 4.5$, there is an unstable solution at $\phi = 0$, and a stable solution at $\phi = 0.5$.

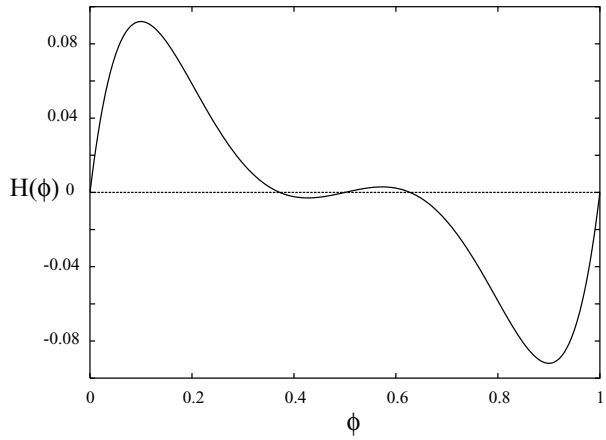

Figure 3.3.2: The interaction function of the IF model with $\alpha = 5.7$, there are two unstable solutions at $\phi = 0$ and $\phi = 0.5$, and two stable solutions now exist a on either of $\phi = 0.5$.

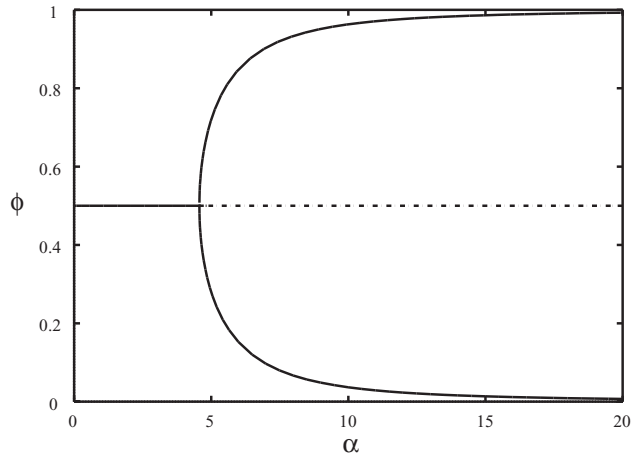

Figure 3.3.3: This shows a pitchfork bifurcation generated by the IF model, the anti-phase solution changes stability from stable to unstable at the bifurcation point and creates two new stable solutions. Solid (dashed) lines are stable (unstable).

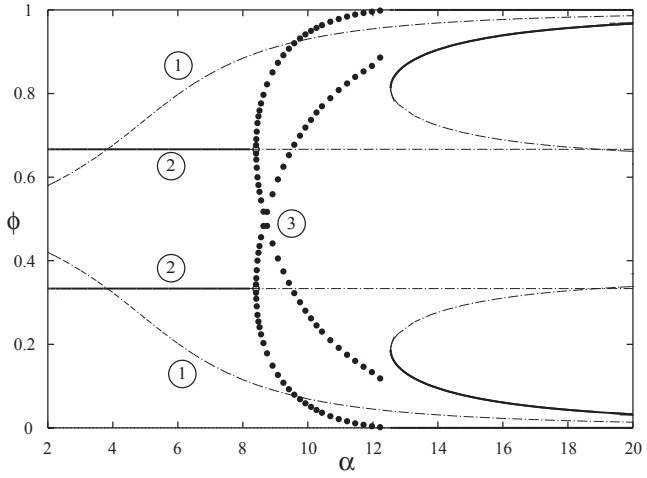

Figure 3.3.4: Bifurcation Diagram for $\Phi = \phi_1$ and ϕ_2 showing Hopf bifurcations and saddle node bifurcations for the three neuron network. Solid (dashed) lines are stable (unstable).

cycle is created (labelled 3). The amplitude of these limit cycles grow until they are destroyed in a global heteroclinic bifurcation (due to a collision with invariant manifolds associated with the 2-in-phase solutions (labelled 1)). At the same point as the heteroclinic bifurcation, two saddle node bifurcations are created.

3.3.3 McKean Network

The McKean model is another model that has been widely studied [66]. It is also possible to calculate the explicit interaction function for this model. The form of the interaction function has to be slightly altered from before,

$$H(\phi) = \frac{1}{T}\int_0^T R(t/T + \theta_T)P(t + \phi T)\mathrm{d}t, \tag{3.24}$$

where θ_T is a phase shift to account for the fact that the response function is not defined with its origin at the jump between $S = 0$ and $S = 1$ (i.e. the start of the action potential). If we choose $P(t)$ as (3.22) it is possible to obtain an explicit form for $H(\phi)$.

The response function as calculated before (for $\theta \neq 0$, θ_T) has the form

$$R(t/T) \equiv \begin{cases} R_1(t) & = \Omega \mathrm{e}^{\beta t}/(A - \beta w_2), \quad t/T \bmod 1 \in [0, \theta_\mathrm{T}), \\ R_2(t) & = B\mathrm{e}^{-\beta\theta_T T}R_1(t), \quad t/T \bmod 1 \in (\theta_\mathrm{T}, 1), \end{cases}$$

Where $B = (A - \beta w_2)/(A + 1 - \beta w_1)$. Using the periodicity properties of $P(t)$ and $R(t)$ it is possible to write

$$H(\phi) - \widehat{H}(\phi) = \begin{cases} BF(\phi; 0, 1 - \phi, 0) + BF(\phi; 1 - \phi, 1 - \theta_T, -1) \\ \qquad + \mathrm{e}^{\beta(\theta_T - 1)T}F(\phi; 1 - \theta_T, 1, -1), \phi > \theta_T; \\ BF(\phi; 0, 1 - \theta_T, 0) + \mathrm{e}^{\beta(\theta_T - 1)T}F(\phi; 1 - \theta_T, 1 - \phi, 0) \\ \qquad + \mathrm{e}^{\beta(\theta_T - 1)T}F(\phi; 1 - \phi, 1, -1), \phi < \theta_T; \end{cases} \tag{3.25}$$

where

$$F(\phi; a, b, c) = \frac{1}{T}\int_a^b R_1(t)P(t + \phi T + cT)\mathrm{d}t, \tag{3.26}$$

and

$$\widehat{H}(\phi) = \Omega^2[\kappa(0)P((\phi - \theta_T)T) + \kappa(\theta_T)P(\phi T)].$$

Note that $\widehat{H}(\phi)$ is a discontinuous function at $\phi = 0$ and $\phi = \theta_t$, since $P(0) \neq P(T)$.

Choosing the alpha function synaptic as before, so using the form (3.22) the calculation of the interaction function is straightforward. Using this, the calculation of (3.26) is again straight forward

$$F(\phi; a, b, c) = \frac{\alpha^2 \mathrm{e}^{-\alpha(\phi+c)T}}{T^2(1 - \mathrm{e}^{-\alpha T})(\beta - \alpha)(A - \beta w_2)} M(\phi; aT, bT, c), \tag{3.27}$$

with

$$\begin{aligned} M(\phi; a, b, c) = &\left[(\phi + c)T + \frac{T\mathrm{e}^{-\alpha T}}{(1 - \mathrm{e}^{-\alpha T})} - \frac{1}{(\beta - \alpha)}\right]\left(\mathrm{e}^{b(\beta-\alpha)} - \mathrm{e}^{a(\beta-\alpha)}\right) \\ &+ \left(b\mathrm{e}^{b(\beta-\alpha)} - a\mathrm{e}^{a(\beta-\alpha)}\right). \end{aligned} \tag{3.28}$$

Two McKean Neuron Networks

In a system of two neurons we have the coupled equations as in (3.11). As with the integrate and fire model we can look at the bifurcation diagram Varying alpha simulates having fast or slow spikes for synaptic communication as seen in experiments.

In figure (3.3.5) there are two different bifurcation diagrams for the McKean model with $a = 0.25$ and $a = 0.32$. It shows that the changing of this parameter changes solutions one finds. Although the solutions obtained with $a = 0.32$ are consistent with those seen in the Hodgkin-Huxley model, $a = 0.25$ is the standard parameter value and it is interesting to investigate this solution. It can be seen that for small

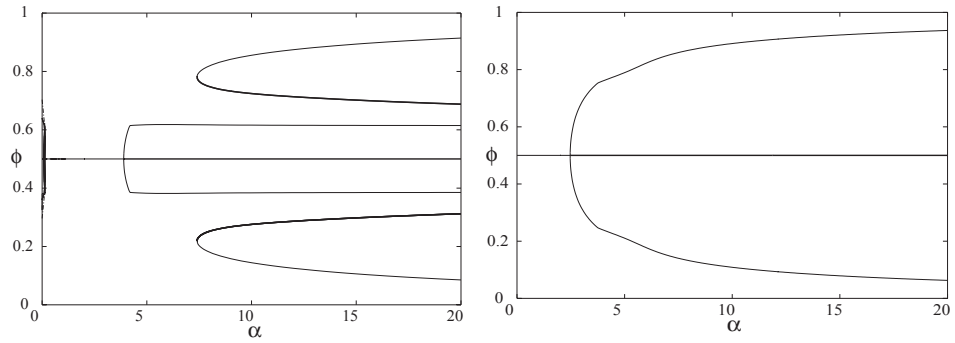

Figure 3.3.5: Bifurcation diagram showing how solutions for 2 neurons change with α for the McKean model with $a = 0.25$ (left) and $a = 0.32$ (right).

α there are just two solutions the synchronous and anti-synchronous solution. The anti-synchronous solution is unstable, as α increases there is a pitchfork bifurcation and also for slightly higher α there are saddle node bifurcations as well. This shows that as α is increased the system exhibits more solutions and there are several stable solutions which persist for a significant range of α. This shows that this model of the neuron can have different solution than some of the other models such as the integrate and fire model.

Delays

Axonal delays introduce a discrete form of delay, which manifests itself as a phase shift in the interaction function. To see whether this would have an effect on the fixed points of the system, it is of interest to simulate this delay. For 2 neurons in place of (3.11) we have

$$\epsilon\,[H(\phi - \tau/T) - H(1 - \phi - \tau/T)] \tag{3.29}$$

Where τ is the delay of communication Using this simple simulation of a delay in

communication, gives a feel of how a delay effects the system. In figure (3.3.6) a small delay is introduced, it shows the difference it can make to the solutions of the system, there is now a new solution appearing for $\phi \approx 1$.

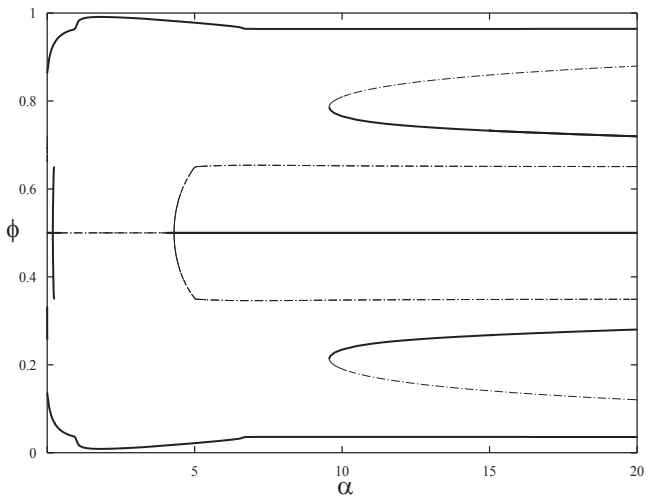

Figure 3.3.6: Bifurcation diagram for the McKean model with changing α and a delay of $\tau = 0.1$ (2 neurons)

Increasing the delay in figure (3.3.7) shows that the delay is beginning to effect the saddle node bifurcations.

In figure (3.3.8) the delay increases in magnitude and the new solution begins to restrict the saddle nodes, and begins to deform the shape of the pitchfork.

In figure (3.3.9) the delay is increased more, it has destroyed the saddle nodes and has restricted the pitchfork even more.

It is clear that having a delay changes the phase locked states. Another way to examine the changes the delays can cause is to vary τ for a constant α

In figure (3.3.10) the bifurcation in τ for small $\alpha = 0.75$ shows there are just the anti-synchronous and synchronous solutions, and as τ increases the synchronous

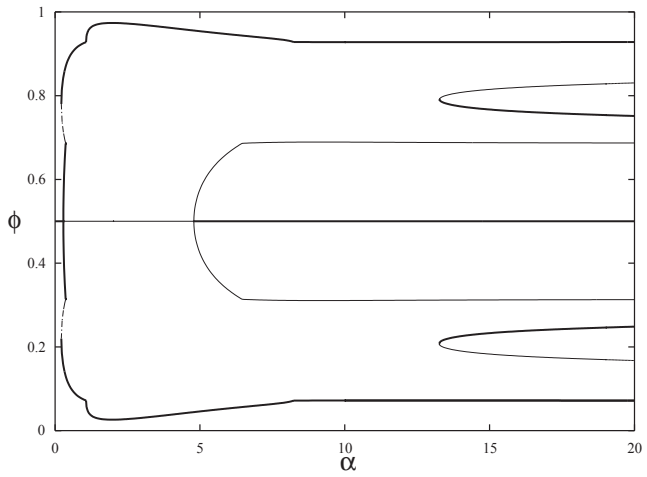

Figure 3.3.7: Bifurcation diagram for the McKean model with changing α and a delay of $\tau = 0.2$ (2 neurons)

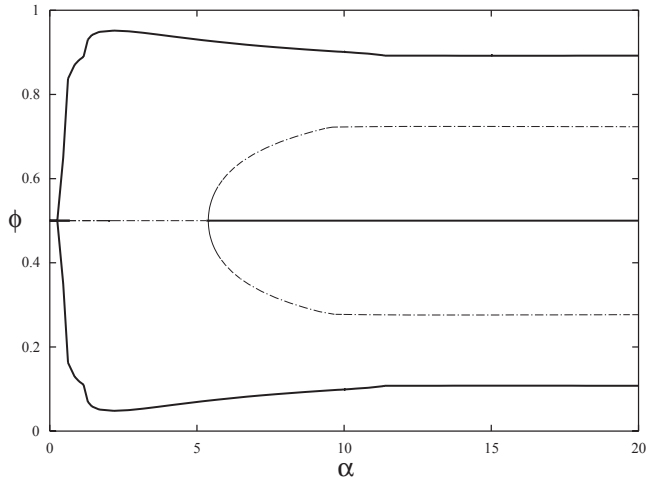

Figure 3.3.8: Bifurcation diagram for the McKean model with changing α and a delay of $\tau = 0.3$ (2 neurons)

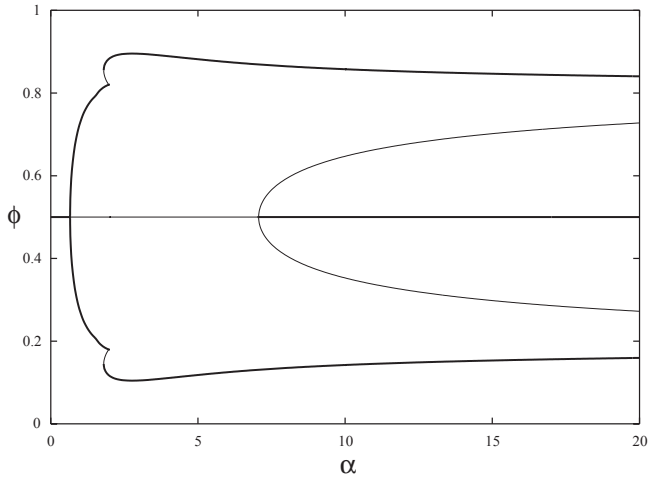

Figure 3.3.9: Bifurcation diagram for the McKean model with changing α and a delay of $\tau = 0.5$ (2 neurons)

solution collides with the anti-synchronous solution.

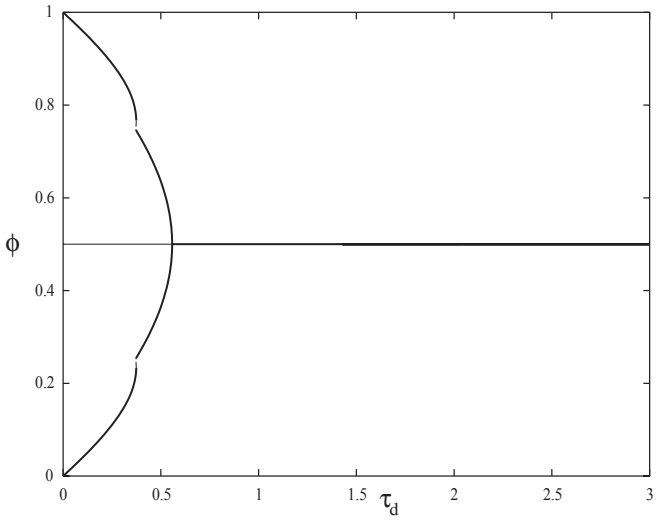

Figure 3.3.10: Bifurcation diagram for the McKean model with changing delay τ for $\alpha = 0.75$

In figure (3.3.11) the bifurcation in τ for $\alpha = 10$ shows the the anti-synchronous and

synchronous solution colliding, the pitchfork solution is now visible also, it too is destroyed as τ is increased

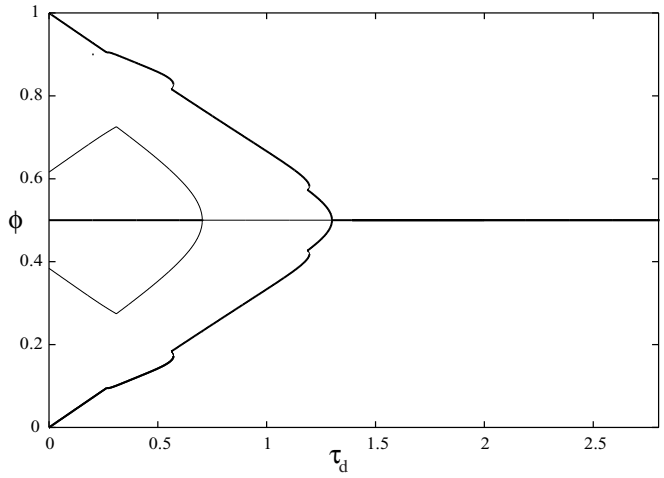

Figure 3.3.11: Bifurcation diagram for the McKean model with changing delay τ for $\alpha = 10$

In figure (3.3.12) the bifurcations are the same as for smaller α except that the saddle nodes are now solutions as well. As with the other solutions the saddle nodes are destroyed as the delay is increased

Conclusions For Two McKean Neuron Networks

It is clear from the various diagrams that there are many phase locked solutions which persist through both varying α and τ, this shows that these solutions are fairly robust. The saddle node solutions are quickly effected by the onset of a delay and are eventually destroyed as the delay increases. In fact all solutions except the anti-synchronous and synchronous solutions (which are guaranteed by the symmetry of the network equations) are destroyed for large delays. This is important to note, all biologically realistic systems have some intrinsic delay in

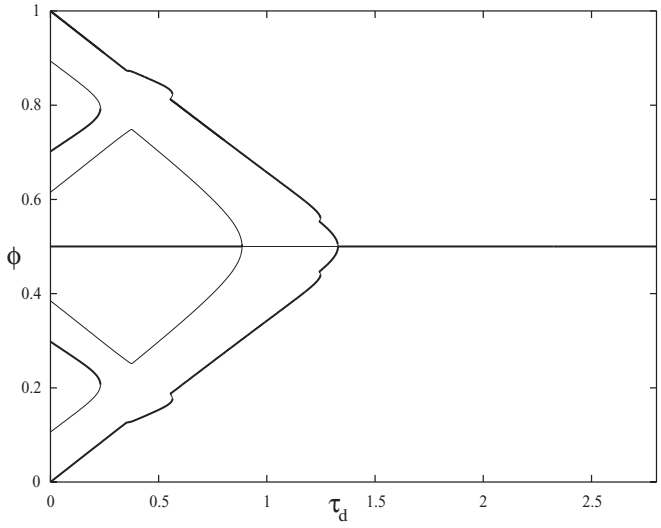

Figure 3.3.12: Bifurcation diagram for the McKean model with changing delay τ for $\alpha = 15$

them, so the magnitude of any delay would have a significant effect on the number and nature of solutions.

3.3.4 Three McKean Neurons

To examine the behaviour of three neurons we can use the set of equations as seen earlier (3.12) and (3.13)

A bifurcation diagram can be made of the network results, however the bifurcation diagram has two parts as the variables are defined in terms of each other

The numbers represent the corresponding solutions for figures (3.3.4) and (3.3.14), ie the 1's are the splay solution. The main solutions to note in these very complex diagrams are

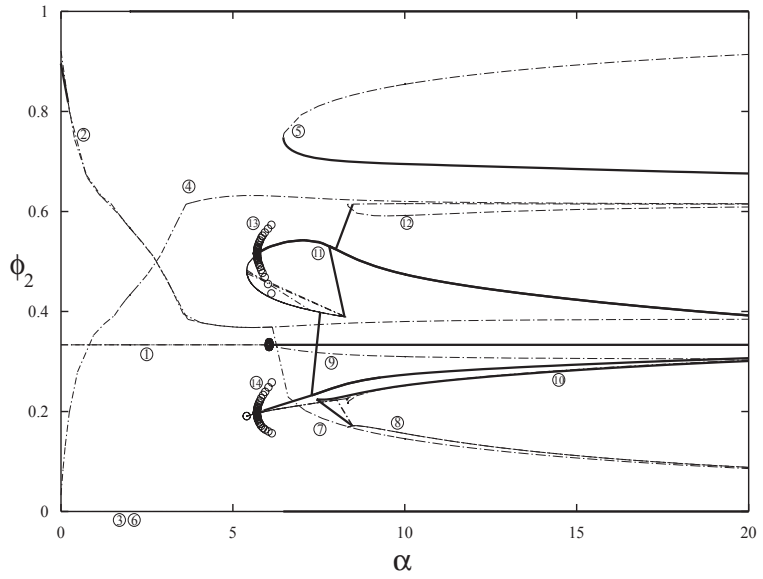

Figure 3.3.13: Bifurcation diagram of ϕ_2 showing the solutions for a 3 McKean neuron network.

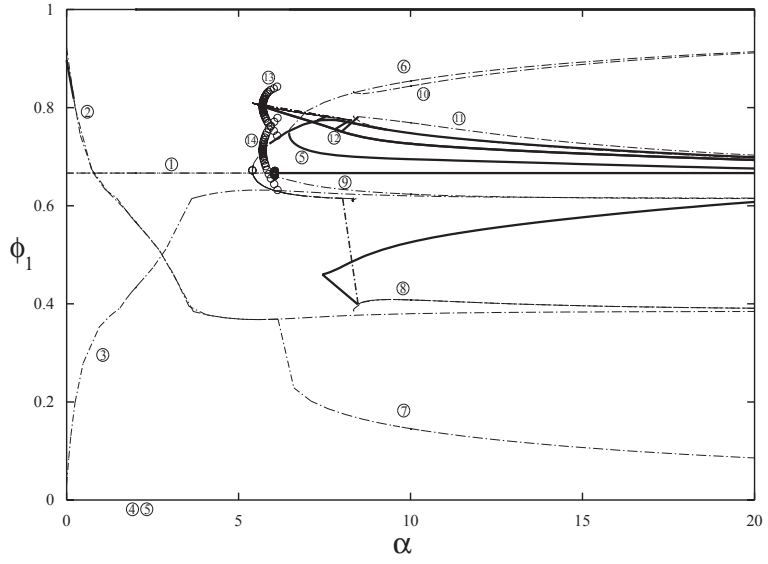

Figure 3.3.14: Bifurcation diagram of ϕ_1 showing the solutions for a 3 McKean neuron network.

1 The splay solution, which is at $\phi_1 = 2/3, \phi_2 = 1/3$

2 A solution where $\phi_1 = \phi_2$

5 A saddle node where $\phi_1 = \phi_2$

13 A Hopf Bifurcation with limit cycles persisting for a significant duration

14 A Hopf Bifurcation with limit cycles persisting for a significant duration

The splay solution undergoes a Hopf bifurcation, but the limit cycles do not persist for increasing α. The Hopf's created limit cycles marked as (13) and (14) do persist for increasing alpha, and these are shown in figure (3.3.15).

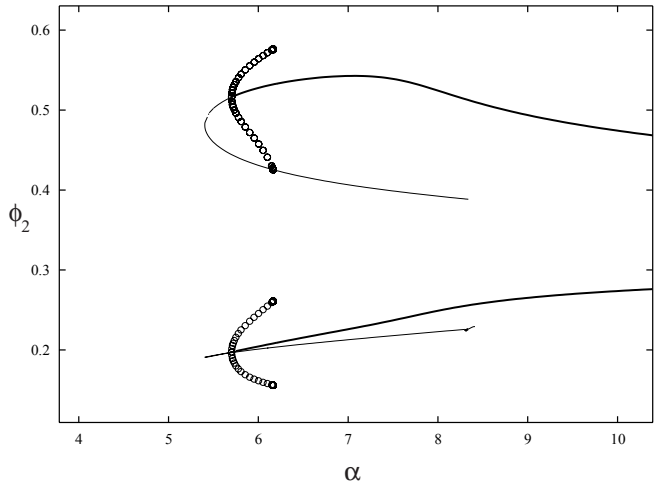

Figure 3.3.15: Both Hopfs for ϕ_2 for the McKean model.

It is clear to see in figures (3.3.16) and (3.3.17) that the limit cycles are destroyed. The cause of the destruction of the limit cycles is the collision with the same branch structure. As these limit cycles seem to be destroyed by the same structure they originate from, this suggests a homoclinic bifurcation.

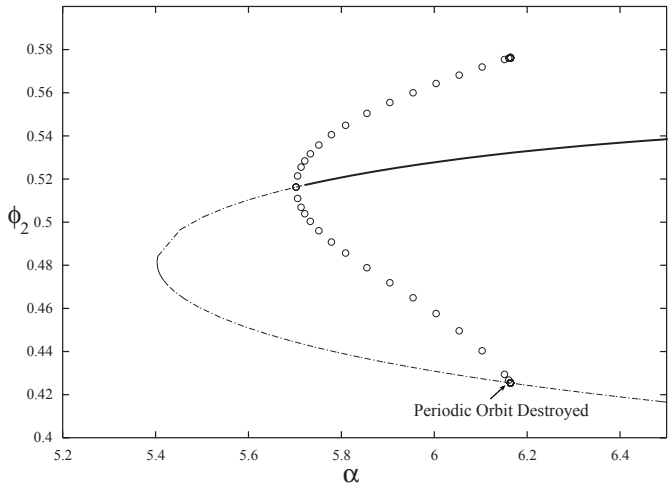

Figure 3.3.16: The destruction of the limit cycles (13) in ϕ_2 for the McKean model.

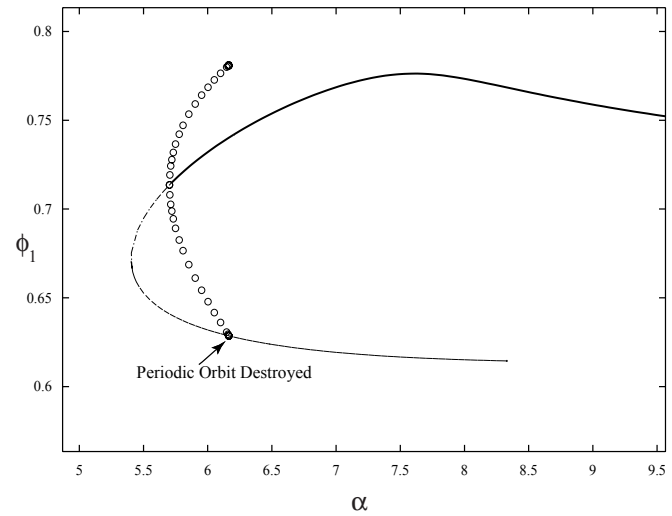

Figure 3.3.17: The destruction of the limit cycles (14) in ϕ_1 for the McKean model.

The period of the Hopf is shown in figure (3.3.18) it shows how the period of the limit cycles behave as α increases.

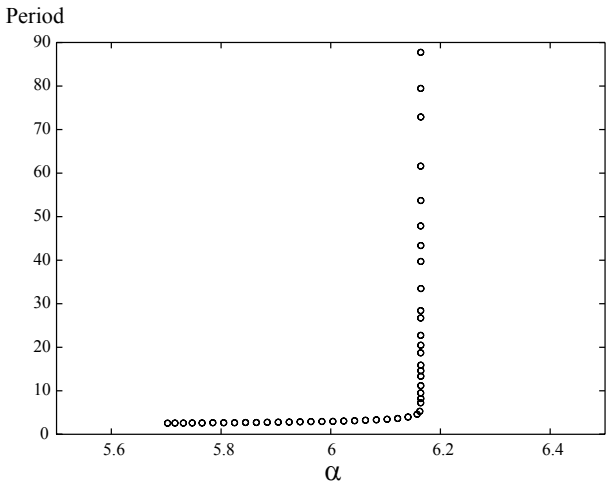

Figure 3.3.18: The change in limit cycle (13) period with α for the McKean model.

Though not shown, an almost identical picture exists for the other Hopf.

Both limit cycles have a period which shoots off to infinity as α increases, this implies both are homoclinic bifurcations.

3.4 Conclusions

In this chapter it was shown that the dynamics of weakly interacting McKean relaxation oscillators captured the types of phase-locked behaviour found in similar Hodgkin-Huxley networks.

However, one should note the major assumptions of strong relaxation and weak coupling. However this restriction still leads to a useful caricature of the far more

complicated Hodgkin-Huxley model. Moreover, by the Fenichel persistence theorem [67], results obtained in the singular limit ($\mu = 0$) are expected to extend to the non-singular limit (μ small). The assumption of weak coupling has further allowed us to bring to bear the powerful machinery of coupled oscillator theory. In strongly coupled networks however phase-locked states are known to give rise to phenomena such as frequency plateaus, oscillator death and pattern formation (see [68] for further discussion). Thus, insight into the dynamics of strongly coupled spiking biophysical neural models may gain significantly from a study of more tractable McKean networks. The development of such a theory is an open challenge, although some initial progress has already been made for the case of instantaneous synapses [58]. This challenge could be addressed in future work using recent techniques developed for the numerical bifurcation study of synaptically interacting Hodgkin-Huxley neurons [69].

In terms of solutions observed, simply increasing the network size by one neuron gives different results than for 2 neurons. However some results do seem to persist namely the splay state (anti-synchronous for 2 neurons), this is due to the symmetries in the network equations. Between a network of 2 and 3 neurons there is an increase in the number of solution and the types of solution seen. This change in the number and type of solutions poses the question of how the solutions alter as network size increases further, as for even just a small increase the changes are non-trivial (for example Hopf bifurcations appear).

One issue that was not fully explored was the connectivity between neurons, for two neurons the choices of connectivity are limited but in larger networks the notion of organisation of connections is an open question. Using the theory outlined it would be possible to examine increasingly larger networks and examine what other phase locked states exist. However solving large numbers of equations becomes analytically more challenging and computationally impractical because to

define a generic phase-locked state in a network of N oscillators requires the simultaneous solution of N algebraic equations. Clearly for large N this is practically unfavourable and so will not be focused on here. However it is worth looking at the limit of increasing network size, i.e. a continuum of neurons. This will allow the ability to focus on the large network properties without having to solve an impractical number of equations. A continuum description of neural tissue is the focus of the next chapter.

Chapter 4

Continuum Networks And Dendrites

In the last chapter it was mentioned that large populations were difficult to analyse in a practical way. This is because as the network size increases, so does the number of equations that need to be solved. It is however possible to make progress by considering a large dense network to be in fact a continuum. The study of a continuum network is a logical extension of the discrete network work and it is the focus of this chapter.

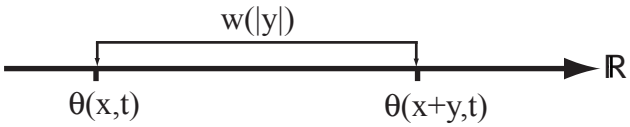

Figure 4.0.1: Illustration of the construction of a continuum network, two points x and $x + y$ are connected with the spatial weight function $w(y)$.

Figure (4) shows the principle of the continuum network. Two densities of neurons at x and $x + y$ have distance y between them, the nature of the connection is

determined by $w(y)$. The function $w(y)$ is a spatial weight function that gives the connection distribution along the continuum of neurons. It can be thought of as the analogue of the weight matrix w_{ij} for discrete networks. In particular the notion of synchrony and splay states from discrete networks carry over to the continuum case. In a continuum of oscillators one can expect to find phase wave solutions (which can be thought of as analogous to the splay state) and these are seen when simulating 1D and 2D neuronal oscillator networks [70]. The nature of the connections in these systems widely effects the synchronous and phase wave solutions. Indeed a continuum model of weakly interacting phase oscillators has recently been used to explain the seemingly contradictory result in which synchrony is stable for localised excitatory coupling, but long range excitatory coupling leads to an unstable synchronous state [71, 72]. However the work by Crook $et\ al$ ignores the effects of any form of synaptic or dendritic processing.

Extending the Fourier constructions of the previous chapter allows us to pursue a similar analysis, paying close attention to the contributions from distributed delays. Following [72] we allow for the finite propagation speed of signals (action potentials) between neurons and introduce a space dependent delay into the model.

4.1 Continuous Networks

4.1.1 Space Dependent Delays

Taking the continuum limit of the discrete network equations seen in the last chapter gives

$$\frac{\partial\theta(x,t)}{\partial t} = \frac{1}{T} + \epsilon\int_{-\infty}^{\infty} w(y)H(\theta(x+y,t) - \theta(x,t) - D(y))\mathrm{d}y. \tag{4.1}$$

This is an integral equation for the evolution of phase $\theta(x,t)$, with some space dependant delay $D(y)$ (over a distance y). The space dependant delay function $D(y)$ represents the delay caused by a signal travelling along the network and as such is a function of the separation distance y. This delay function can have many forms to encompass different forms of delay. For reasons of simplicity we will choose $D(y) = |y|/v$, where v represents the signal velocity relative to the natural frequency of oscillation. This gives a simple form of axonal delay which increases linearly with the separation between neurons.

In this case equation (4.1) becomes

$$\frac{\partial\theta(x,t)}{\partial t} = \frac{1}{T} + \epsilon\int_{-\infty}^{\infty} w(y)H(\theta(x+y,t) - \theta(x,t) - |y|/v)\mathrm{d}y.$$

For travelling wave solutions of the form

$$\theta(x,t) = \Omega t + \beta x, \qquad (\text{mod } 1), \tag{4.2}$$

we obtain the dispersion relation $\Omega = \Omega(\beta)$ where

$$\Omega(\beta) = \frac{1}{T} + \epsilon\int_{-\infty}^{\infty} w(y)H(\beta y - |y|/v)\mathrm{d}y.$$

4.1.2 Stability Of Solutions

Assuming a solution exists we establish the stability of the solution by adding a small perturbation $\phi \ll 1$, to the system and write

$$\theta(x,t) = \Omega t + \beta x + \phi(x,t).$$

Substitution into (4.1) gives

$$\Omega + \frac{\partial\phi}{\partial t} = \frac{1}{T} + \epsilon\int_{-\infty}^{\infty} w(y)H(\beta y - |y|/v + \phi(x+y,t) - \phi(x,t))\mathrm{d}y.$$

If we expand the interaction function as a Taylor series we have

$$H(\theta(x+y,t)-\theta(x,t)-|y|/v) \approx H(\beta y-|y|/v)+H'(\beta y-|y|/v)[\phi(x+y,t)-\phi(x,t)]$$

yielding

$$\frac{\partial \phi(x,t)}{\partial t} = \epsilon \int_{-\infty}^{\infty} w(y) H'(\beta y-|y|/v)[\phi(x+y,t)-\phi(x,t)]\mathrm{d}y. \tag{4.3}$$

We take ϕ to be separable, periodic in space, and of the form

$$\phi(x,t) = \mathrm{e}^{ipx}\mathrm{e}^{\lambda t}, \qquad \text{so that} \qquad \frac{\partial \phi(x,t)}{\partial t} = \lambda \mathrm{e}^{ipx}\mathrm{e}^{\lambda t} = \lambda(\phi(x,t)).$$

This generates the eigenvalue equation

$$\lambda(p) = \epsilon \int_{-\infty}^{\infty} w(y) H'(\beta y-|y|/v)[\mathrm{e}^{ipy}-1]\mathrm{d}y. \tag{4.4}$$

Solutions are stable if

$$\mathrm{Re}(\lambda(p)) < 0 \qquad \forall p \neq 0.$$

Note that translation invariance guarantees the eigenvalue $\lambda(0) = 0$.

4.1.3 Fourier H Function

As seen in the previous chapter we can write the H function as a Fourier series,

$$H(\phi) = \sum_k H_k \mathrm{e}^{i2\pi k\phi},$$

so we get

$$H'(\phi) = \sum_k i2\pi k H_k \mathrm{e}^{i2\pi k\phi} \equiv \sum_k H'_k \mathrm{e}^{i2\pi k\phi}.$$

From (4.4) we have the alternative representation

$$\lambda(p) = \epsilon \int_{-\infty}^{\infty} w(y) \sum_k H'_k \mathrm{e}^{i2\pi k[\beta y-|y|/v]} \left(\mathrm{e}^{ipy}-1\right) \mathrm{d}y.$$

For even synaptic footprint kernels $w(y) = w(|y|)$, we also have that

$$\lambda(p) = \epsilon \sum_k H'_k \int_0^\infty w(y) \mathrm{e}^{-i2\pi k|y|/v} \left\{ \mathrm{e}^{i2\pi k\beta y}(\mathrm{e}^{ipy} - 1) + \mathrm{e}^{-i2\pi k\beta y}(\mathrm{e}^{-ipy} - 1) \right\} \mathrm{d}y. \quad (4.5)$$

Introducing the half Fourier transform

$$\widetilde{w}(p) = \int_0^\infty w(y) \mathrm{e}^{-ipy} \mathrm{d}y, \quad (4.6)$$

allows us to write (4.5) in the form

$$\lambda(p) = \epsilon \sum_k H'_k Q_k(p).$$

where

$$\begin{aligned} Q_k(p) = \{ & \widetilde{w}(2\pi k(1/v - \beta) - p) - \widetilde{w}(2\pi k(1/v - \beta)) \\ & + \widetilde{w}(2\pi k(1/v + \beta) + p) - \widetilde{w}(2\pi k(1/v + \beta)) \}. \end{aligned} \quad (4.7)$$

This is a usefully compact representation.

4.1.4 Synaptic Footprint Functions

From the previous section it is necessary to calculate the Fourier form for the synaptic footprint kernel (4.6). Up to now the weight function has not been specified. For simplicity we shall restrict attention to the class of symmetric functions $w(y) = w(|y|)$. Two such examples are seen in figure (4.1.1).

These w functions are normalised so the area under them is 1. One advantage of these two weight functions is that their Fourier forms can be easily calculated.

For the exponential weight function $w(y) = \mathrm{e}^{-|y|/\sigma}/2\sigma$

$$\begin{aligned} \widetilde{w}(p) &= \frac{1}{2\sigma} \int_0^\infty \mathrm{e}^{-y[ip+1/\sigma]} \mathrm{d}y = \frac{1}{2\sigma[ip + 1/\sigma]}, \\ &= \frac{1 - ip\sigma}{2(1 + p^2\sigma^2)}. \end{aligned} \quad (4.8)$$

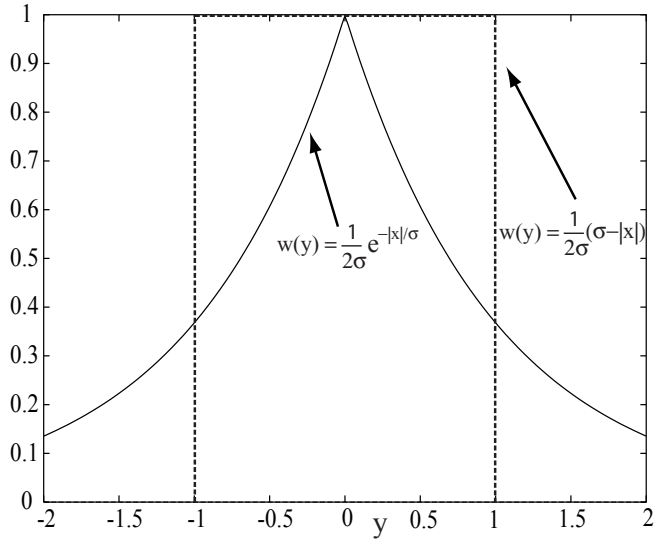

Figure 4.1.1: w functions, in this case $\sigma = 1$

For the square weight function $w(y) = \Theta(\sigma - |y|)/2\sigma$

$$\begin{aligned}\widetilde{w}(p) &= \frac{1}{2\sigma}\int_0^\sigma \mathrm{e}^{-ipy}\mathrm{d}y = \frac{1}{2\sigma}\left[\frac{\mathrm{e}^{-ip\sigma}}{-ip} - \frac{1}{-ip}\right], \\ &= \frac{i}{2p\sigma}\left[\mathrm{e}^{-ip\sigma} - 1\right]. \end{aligned} \tag{4.9}$$

The factor of 2σ in the above weight functions ensure the normalisation $\int_{\mathbb{R}} w(x)\mathrm{d}x = 1$.

4.1.5 Continuous McKean and Hodgkin-Huxley Networks

Using the method outlined above it is possible to construct travelling waves and analyse their stability. Having chosen the weight function, a Fourier form for an interaction function $H(\phi)$ is needed. In the last chapter these were calculated for the McKean and Hodgkin-Huxley models with alpha function coupling. This enables the comparison of the two models in a continuum network. There is the practical problem that the condition of stability ($\mathbb{R}\mathrm{e}\ \lambda(p) < 0$) of any point (x_0, y_0) has to be

checked for all values of p. To numerically check this stability some choice of step size (between points in the parameter plane of choice eg. (β, v)) and range of p must be made.

Simulations to establish the stability of solutions for the Hodgkin-Huxley and McKean models can be seen in figures (4.1.2) and (4.1.3) where we present the stability regions of the travelling wave solutions in the (β, v) parameter plane. For fast rise times, in the sense that $\alpha/\Omega \to \infty$, we find that for both models the synchronous state ($\beta = 0$) is unstable for small v and stable travelling waves appear.

The discrepancy between the value of v for which the synchronous solution changes stability in figures (4.1.2) and (4.1.3) for HH and McKean respectively can be attributed to the fact that the relative duration of action potentials between the two models is slightly different. Although the duration of the action potential in the McKean model can be adjusted by varying a, this is found not to lead to significant increased agreement. This is because, unlike the Hodgkin-Huxley model, we have restricted the McKean model to some singular limit ($\mu = 0$) where the rise and fall times of the action potential are instantaneous. Crook *et al*. [72] have suggested that the change in stability of the synchronous solution as the propagation delay grows is consistent with the oscillatory behaviour observed in both visual cortex, showing a tendency towards synchrony, and olfactory cortex, tending to produce travelling oscillatory waves; the latter has long-range connections and hence longer axonal delays.

The stability diagrams for much slower synapses are produced in figures (4.1.4) and (4.1.5).
Here, we see that both models once again give qualitatively similar predictions: namely that for slow synapses it is even easier to destabilise a synchronous solution in favour of a travelling wave, giving further weight to the suggestions of Crook *et al*.. We note that the value of v at which the synchronous solution changes

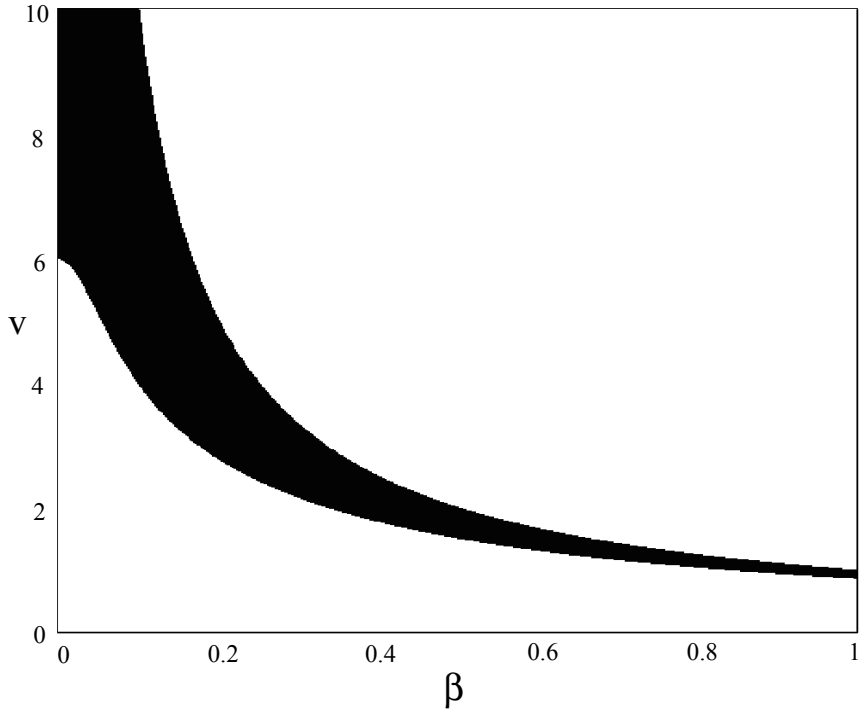

Figure 4.1.2: Region of stability (black) for the travelling wave solution in the (β, v) parameter plane for the continuum Hodgkin-Huxley model with an exponential synaptic footprint and an alpha function synaptic response with $\alpha = 20$. v is the velocity of an action potential and β is the phase gradient of a travelling wave: $\mathrm{d}\theta(x,t)/\mathrm{d}x = \beta$. For low v the synchronous solution ($\beta = 0$) is unstable and a stable travelling wave ($\beta \neq 0$) can be found. A grid of 250×250 points is used.

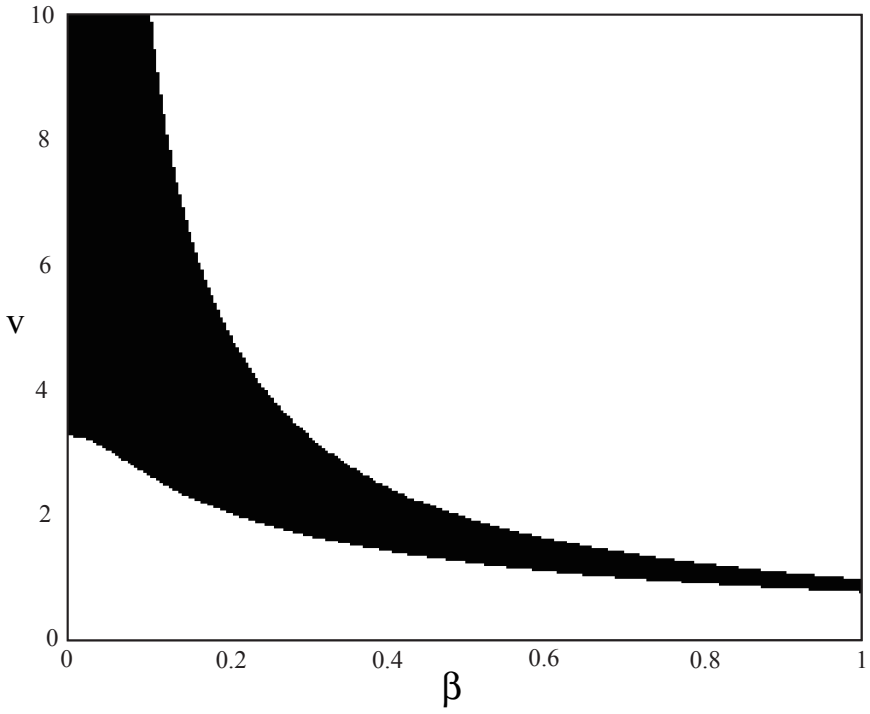

Figure 4.1.3: Region of stability (black) for the travelling wave solution in the (β, v) parameter plane for the continuum McKean model with an exponential synaptic footprint and an alpha function synaptic response with $\alpha = 20$. v is the velocity of an action potential and β is the phase gradient of a travelling wave: $\mathrm{d}\theta(x,t)/\mathrm{d}x = \beta$. For low v the synchronous solution ($\beta = 0$) is unstable and a stable travelling wave ($\beta \neq 0$) can be found. A grid of 250×250 points is used.

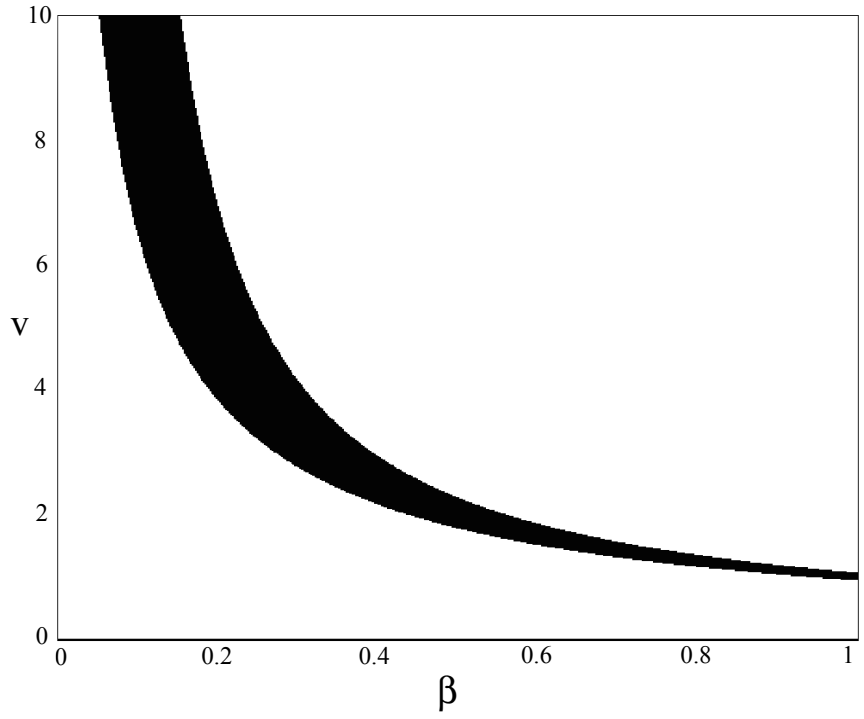

Figure 4.1.4: Region of stability (black) for the travelling wave solution in the (β, v) parameter plane for the continuum Hodgkin-Huxley model with an exponential synaptic footprint and an alpha function synaptic response with $\alpha = 1$. The value of v at which the synchronous solution changes from unstable to stable increases with decreasing α. A grid of 250×250 points is used.

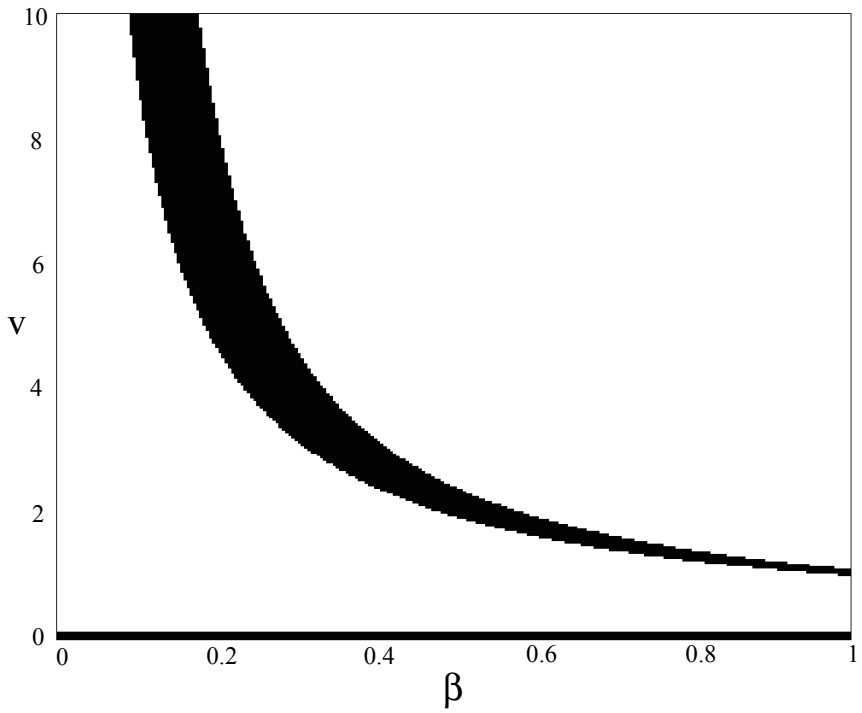

Figure 4.1.5: Region of stability (black) for the travelling wave solution in the (β, v) parameter plane for the continuum McKean model with an exponential synaptic footprint and an alpha function synaptic response with $\alpha = 1$. The value of v at which the synchronous solution changes from unstable to stable increases with decreasing α. A grid of 250×250 points is used.

from unstable to stable increases with decreasing α. For these results we are using an exponential weight function, results for square weight kernels have been produced and figure (4.1.6) shows the stability diagram for HH with $\alpha = 30$. The square weight function for the McKean model (not shown) also matches the exponential weight function results.

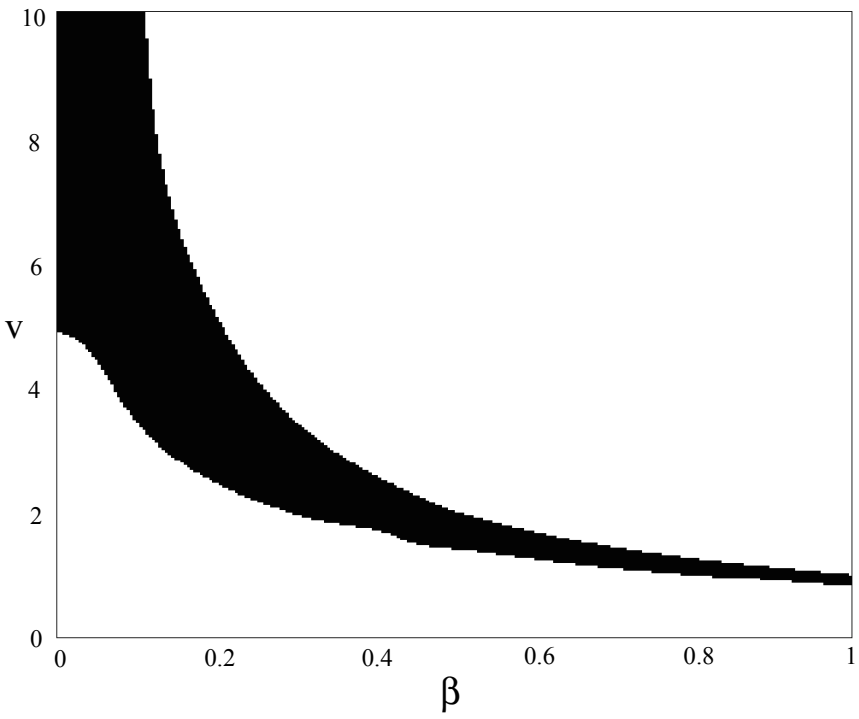

Figure 4.1.6: Region of stability (black) for the travelling wave solution in the (β, v) parameter plane for the continuum Hodgkin-Huxley model with a square synaptic footprint and an alpha function synaptic response with $\alpha = 20$. v is the velocity of an action potential and β is the phase gradient of a travelling wave: $\mathrm{d}\theta(x,t)/\mathrm{d}x = \beta$. For low v the synchronous solution ($\beta = 0$) is unstable and a stable travelling wave ($\beta \neq 0$) can be found. A grid of 250×250 points is used.

4.2 Dendrites

Up to now the network simulations have taken into account axonal effects (with space dependent delays) and the signal distortion associated synaptic effects (with the use of the alpha function synaptic kernel). However the dendritic tree has been ignored. The dendritic tree is a large branched spatio-temporal structure that historically has been associated with purely information gathering. The tree structure

can take up a large area relative to the other parts of the neuron, in many cases making up 99% of the surface area. With the advent of more high powered microscopy the detail of this structure has been examined more closely and there are thorn like projections called spines that can be seen whose function is unknown. It is also believed that the whole structure could also be excitable. However neither of these will be considered here. For further discussion see [73]

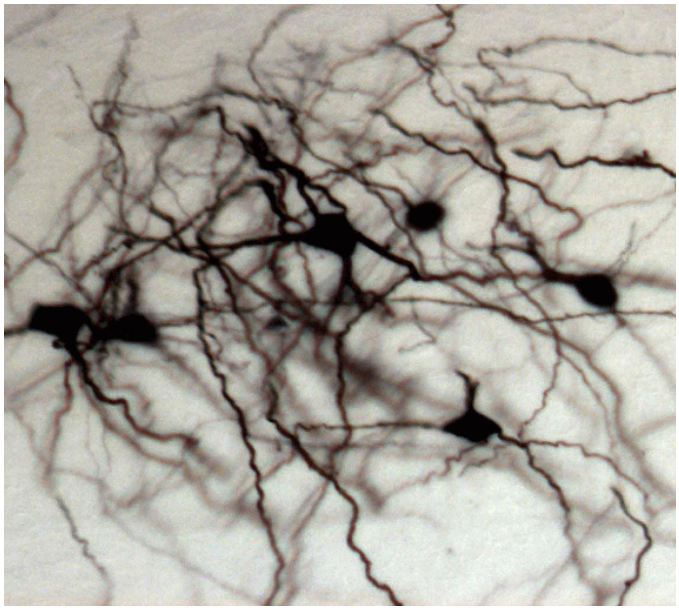

Figure 4.2.1: An actual image of some cortical neurons. The extensive structures of the dendritic trees are clearly visible.

Modelling such a large structure with the level of spatial complexity that would entail is not practical for network simulations, so some simplifications have to be made.

4.2.1 Cable Equation

The dendritic structure is often complicated (highly branched) and as such practically difficult to model. One simplification that can be made is to model the dendritic tree as a one dimensional spatial structure where the effect of the synapse location on the dendritic tree is decribed by a cable equation with just one variable ξ. The variable ξ can be considered as a dendritic coordinate, and the point ξ_0 as a point of synaptic input.

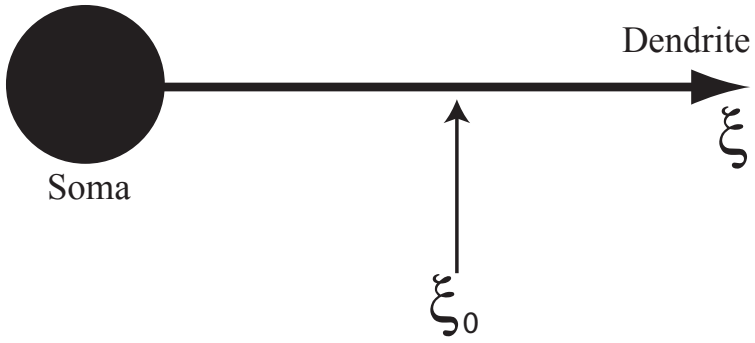

Figure 4.2.2: The idea of the idealised dendritic structure. The neuron receives signals at point ξ_0.

Starting from the fundamental cable equation

$$r_m c_m \frac{\partial V(\xi,t)}{\partial t} = -V(\xi,t) + \frac{r_m}{r_i}\frac{\partial^2 V(\xi,t)}{\partial \xi^2}, \qquad \xi \in \mathbb{R} \quad t \in \mathbb{R}^+. \tag{4.10}$$

Here $V(\xi,t)$ denotes the membrane potential at time t and position ξ along the cable relative to the resting potential of the membrane. Also r_m, r_i and c_m are membrane resistance, intracellular resistance and the membrane capacitance respectively.

4.2.2 Passive Dendrites

It is useful to reformulate (4.10) to incorporate the neurobiological parameters of space (λ) and time (τ), representing the space and time over which the membrane potential decays to 1/e of its original value. Setting $\tau = r_m c_m$, $\lambda = \sqrt{r_m/r_i}$, and $D = \lambda^2/\tau$ (Diffusion coefficient). We get

$$\frac{\partial V(\xi,t)}{\partial t} = -\frac{V(\xi,t)}{\tau} + D\frac{\partial^2 V(\xi,t)}{\partial \xi^2} + I_{EXT}(\xi,t), \tag{4.11}$$

where $I_{EXT}(\xi,t)$ is an external source term.

We can use Green's functions to help solve this as it is well suited for linear PDEs of this form. The Green's function of (4.11) satisfies

$$\frac{\partial G}{\partial t} + \frac{G}{\tau} - D\frac{\partial^2 G}{\partial \xi^2} = \delta(\xi)\delta(t). \tag{4.12}$$

The solution can be written in the form

$$V(\xi,t) = \int_0^t \int_0^\infty G(\xi-\xi',t-s) I_{EXT}(\xi',s)\mathrm{d}s\mathrm{d}\xi' + \int_0^\infty G(\xi-\xi',t)V(\xi',0)\mathrm{d}\xi'.$$

Taking the Fourier transform in space of (4.12) gives

$$\frac{\mathrm{d}\widetilde{G}}{\mathrm{dt}} + \widetilde{G}/\tau + Dk^2\widetilde{G} = \delta(t),$$

where

$$\widetilde{G}(k,t) = \int_{-\infty}^{\infty} \mathrm{e}^{-ikt} G(\xi,t)\mathrm{d}\xi.$$

Define $\lambda(k) = (1/\tau + Dk^2)$, this gives

$$\frac{\mathrm{d}\widetilde{G}}{\mathrm{dt}} - \lambda\widetilde{G} = \delta(t).$$

which implies

$$\widetilde{G}(k,t) = \mathrm{e}^{-\lambda(k)t}.$$

Taking the inverse transform

$$G(\xi,t)=\frac{1}{2\pi}\int_{-\infty}^{\infty}\mathrm{e}^{ik\xi}\mathrm{e}^{-\lambda(k)t}\mathrm{d}k=\frac{1}{2\pi}\int_{-\infty}^{\infty}\mathrm{e}^{-Dt(k-\frac{i\xi}{2Dt})^2}\mathrm{e}^{\frac{-\xi^2}{4Dt}}\mathrm{e}^{-t/\tau}\mathrm{d}k.$$

So the integral is now of the form

$$\frac{\mathrm{e}^{\frac{-\xi^2}{4Dt}}\mathrm{e}^{-t/\tau}}{2\pi}\int_{-\infty}^{\infty}\mathrm{e}^{-Dt(k-\frac{i\xi}{2Dt})^2}\mathrm{d}k,$$

which gives

$$G(\xi,t)=\frac{1}{\sqrt{4\pi Dt}}\mathrm{e}^{-t/\tau}\mathrm{e}^{\xi^2/4Dt}.$$

The temporal Fourier transform of the Greens function is

$$\widetilde{G}(\xi,w)=\frac{1}{D\gamma(w)}\mathrm{e}^{-\gamma(w)\xi},$$

where

$$\gamma(w)=\sqrt{(1+iw\tau/D\tau)},$$

which is a frequency dependent impedance. We can make the simplification that the connection point is at constant distance along the dendritic tree (i.e. $\xi=\xi_0$). This approach can easily be generalised to cover a so-called quasi-active membrane by the replacement of $\gamma(w)$ with the function defined in [74]. A quasi-active membrane is a description of neural tissue that describes resonances associated with the linearisation of the sodium and potassium currents in the HH model. Using the constant connection point, it is possible to calculate the function

$$P(t)=\sum_{k\in\mathbb{Z}}\widetilde{G}(\xi_0,w_k)\mathrm{e}^{iw_kt},\qquad\text{where}\qquad w_k=2\pi k/T,$$

where $P(t)$, like the last chapter, is the function that represents the external input to a neuron (i.e. from other neurons). As before the function is also periodic in T.

4.2.3 Discrete Network With Dendritic Synaptic Kernel

Using the dendritic synaptic kernel it is also possible to re-visit the earlier work and look at a small discrete network. Using a simple two McKean neuron network

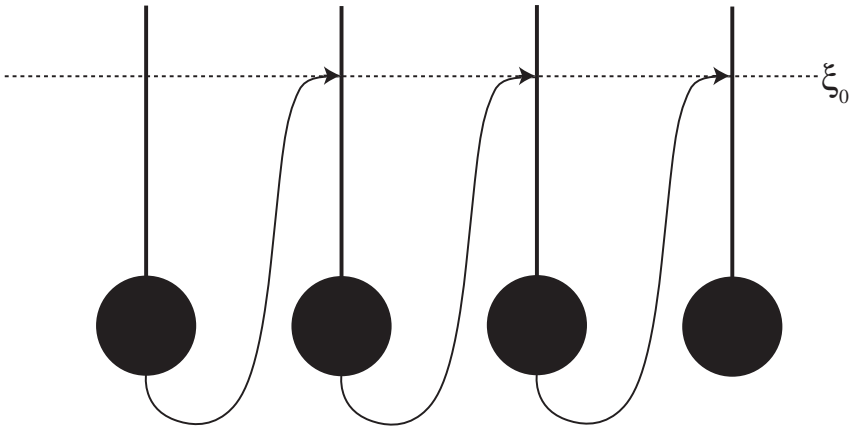

Figure 4.2.3: A network with the idealised dendritic structure. Each neuron receives signals at constant point ξ_0.

with identical dendritic coupling we can construct a bifurcation diagram of phase locked solutions with varying synaptic connection point ξ_0. In figure (4.2.4) we show a pattern of stability exchange. As in the previous chapter, when looking at a discrete delay, we see an exchange and re-exchange of stability of solutions, in this case with increasing dendritic contact point ξ_0. In some sense it would seem that delays arising from diffusion along the dendritic tree can give rise to effects similar to those of discrete communication delays. In figure (4.2.5) we show a corresponding plot for the stability of the synchronous solution in the (I, ξ) parameter plane. Since the period of oscillation is a monotonically decreasing function of I this *checkerboard* pattern of stability is also expected to hold in the (Ω, ξ) parameter plane.

To understand the generation of the checkerboard pattern of stability for the synchronous solution of the two neuron network it is useful to consider the simple case that $R(\theta) = -\sin 2\pi\theta$ (i.e. the only non-zero Fourier coefficients of $R(\theta)$ are

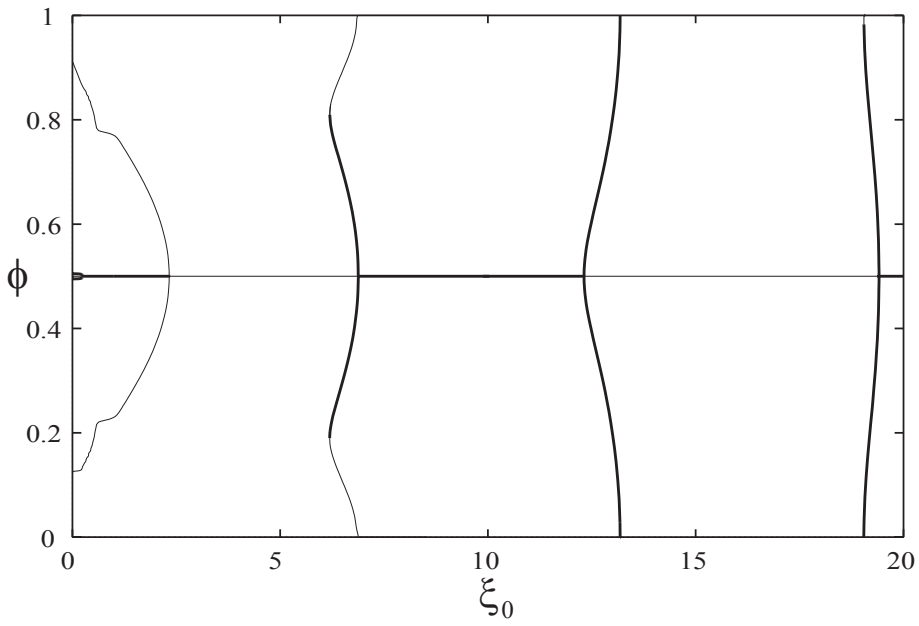

Figure 4.2.4: Relative phase bifurcation diagram for two coupled McKean neurons, with idealised dendritic structure. Excitatory synaptic input occurs at a distance ξ_0 from the soma. Note the exchange of stability of the anti-synchronous states as a function of the dendritic contact distance.

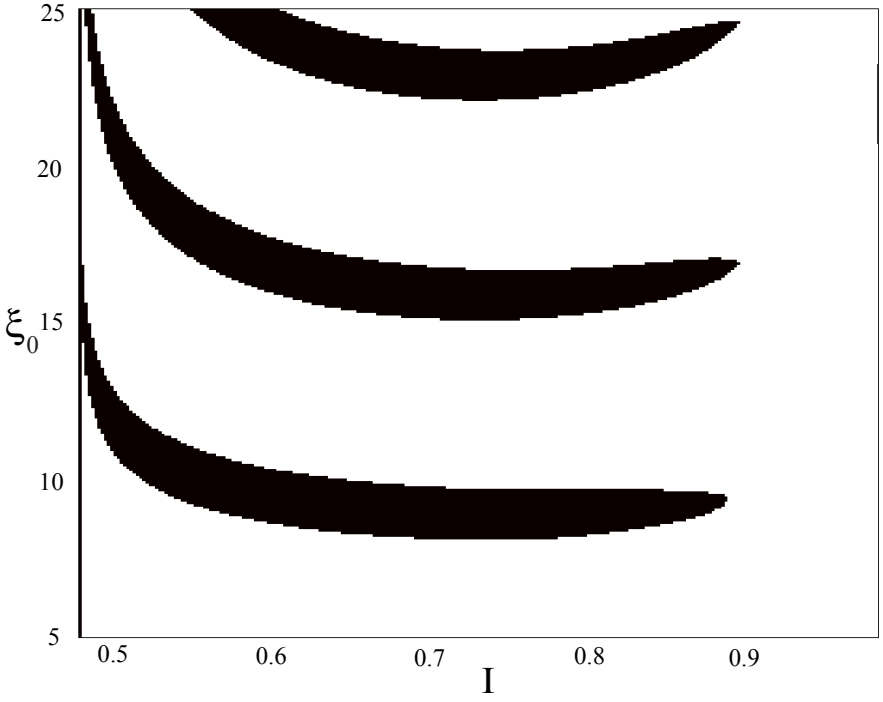

Figure 4.2.5: Stability (black) of the synchronous state for two coupled Mckean neurons in the (I, ξ_0) parameter plane for $D = 1$ (diffusion coefficient of dendritic cable) and $\tau = 1$ (dendrite cell membrane time constant). ξ_0 represents the distance along the dendrite of the synapse from the soma and I is the input current. Note the periodicity of the stability diagram as a function of dendritic interaction distance.

$R_{\pm 1} = \pm i/2$). This might be regarded as a first crude approximation to the Fourier series representation of the response function for the Hodgkin-Huxley model (with an origin chosen to be on the upswing of the voltage spike). It is a simple matter to show that

$$K(\phi) = -2\epsilon\Omega \sin(2\pi\phi)\mathrm{Re}\,\widetilde{\eta}(2\pi/T), \tag{4.13}$$

and the only solutions are $\phi = 0$ (synchronous) and $\phi = 1/2$ (anti-synchronous). Hence, the stability of the synchronous state is determined solely by the sign of $\epsilon\mathrm{Re}\,\widetilde{\eta}(2\pi/T)$. For a delayed alpha function response we have that

$$\mathrm{Re}\,\widetilde{\eta}(\omega) = \alpha^2 \frac{[\alpha^2 - \omega^2]}{[\alpha^2 + \omega^2]^2} \cos(\omega\tau_d), \tag{4.14}$$

so that stability borders are defined by the zeroes of $(\alpha - 2\pi/T)\cos(2\pi\tau_d/T)$, highlighting the T-periodicity of bifurcation diagrams in the delay parameter τ_d. Moreover, in the absence of discrete delays it is easy to see that the synchronous solution is only stable if $\epsilon < 0$ and $\alpha < 2\pi/T$ (slow inhibition) or $\epsilon > 0$ and $\alpha > 2\pi/T$ (fast excitation). In the dendritic case

$$\mathrm{Re}\,\widetilde{\eta}(\omega) = \frac{\mathrm{e}^{-a(\omega)\xi}[a(\omega)\cos(b(\omega)\xi) - b(\omega)\sin(b(\omega)\xi)]}{D[a(\omega)^2 + b(\omega)^2]}, \tag{4.15}$$

where $a(\omega)$ and $b(\omega)$ are given by

$$a(\omega) = \frac{1}{\nu}\sqrt{\frac{1 + \sqrt{1 + (\tau\omega)^2}}{2}}, \tag{4.16}$$

$$b(\omega) = \frac{\mathrm{sign}(\omega)}{\nu}\sqrt{\frac{-1 + \sqrt{1 + (\tau\omega)^2}}{2}}, \tag{4.17}$$

with $\nu = \sqrt{D\tau}$. Hence stability borders are defined by $\tan[b(2\pi/T)\xi] = a(2\pi/T)/b(2\pi/T)$. Here we see that for fixed T bifurcation diagrams will have a periodicity of $\pi/b(2\pi/T)$ in the dendritic contact distance ξ_0.

4.3 Continuous Networks With Dendritic Effects

It is possible to introduce further dendritic effects into the continuum framework. In the presence of dendrites the distance between pre and post synaptic neurons will be a function of the dendritic contact point ξ_0 as well as the separation distance y. The actual length of the distance between two points is $\sqrt{|y|^2 + \xi_0^2}$. However this

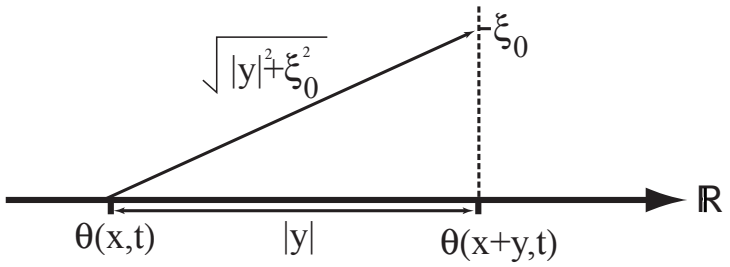

Figure 4.3.1: More complex notion of neuron interaction.

can make the calculation of the integrals difficult. In the interest of simplicity therefore we take $D(y) = (|y| + |\xi_0|)/v$. Dendritic processing then introduces a further discrete delay into the interaction form and shifts the phase interaction function by an amount $|\xi_0|/v$.

As before the model has a one parameter family of travelling wave solutions defined by $\theta(x,t) = \widetilde{\Omega}t + \beta x$, where

$$\widetilde{\Omega}(\beta) = \Omega + \epsilon \int_{-\infty}^{\infty} w(y) H(\beta y - (|y| + |\xi_0|)/v) \mathrm{d}y, \tag{4.18}$$

where $\omega = 1/T$ A linear stability analysis shows that these solutions are stable if Re$\lambda(p) < 0$, where

$$\lambda(p) = \epsilon \int_{-\infty}^{\infty} w(y) H'(\beta y - (|y| + |\xi_0|)/v)[\mathrm{e}^{ipy} - 1] \mathrm{d}y. \tag{4.19}$$

As before the neutrally stable mode $\lambda(0) = 0$ exists, and is associated with perturbations by constant phase-shifts and so is excluded in the definition of linear

stability.

For convenience we now write $H(\theta) = \sum_k H_k \mathrm{e}^{2\pi i k(\theta - |\xi_0|/v)}$.

When $w(y) = w(|y|)$ it is simple to show that

$$\lambda(p) = \epsilon \sum_k H'_k \mathrm{e}^{-2\pi i |\xi_0| k/v} [\widetilde{w}(p + 2\pi k\beta_+) - \widetilde{w}(2\pi k\beta_+) + \widetilde{w}(-p + 2\pi k\beta_-) - \widetilde{w}(2\pi k\beta_-)], \tag{4.20}$$

where $\beta_\pm = \pm\beta - 1/v$, $H'_k = 2\pi i k H_k$ and $\widetilde{w}(p)$ is as in equation (4.6).

We will choose the exponential weight distribution used earlier. Due to the fact that the larger the dendritic coordinate ξ_0 the larger the delay in the system, we would expect to see a periodic exchange of stability in the solution. This is because as ξ_0 increases the delay will reach the period of the travelling waves T and as the waves are periodic, the solutions would then repeat. Indeed just such a scenario is depicted in figure (4.3.2), where we plot the stability of the synchronous solution in the (β, ξ) plane for the Hodgkin-Huxley model. Once again qualitatively similar periodic behaviour is found for the McKean model and is shown in figure (4.3.3).

4.4 Conclusions

Phase interaction functions have been calculated explicitly for McKean networks and numerically for Hodgkin-Huxley networks. In both cases we have made use of Fourier techniques for the practical calculation of the stability of travelling wave solutions in the continuum limit. We showed that an exponential or square synaptic weight function gave us the same travelling wave stability pictures for both the McKean and Hodgkin-Huxley models. This has more readily allowed us to establish that the nature of stability for these travelling waves in McKean and Hodgkin-

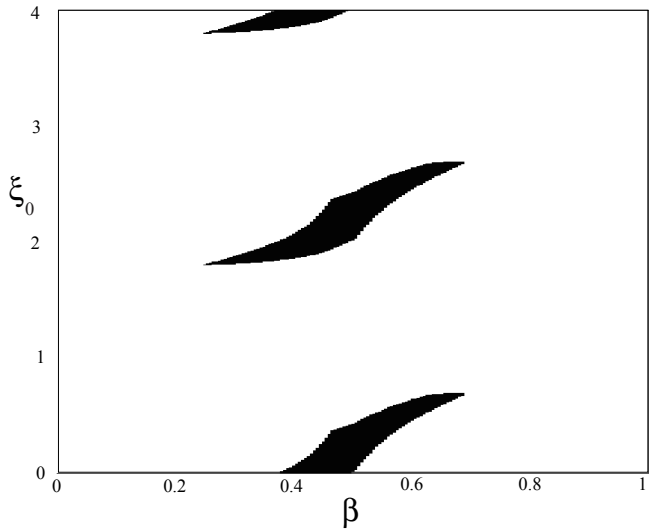

Figure 4.3.2: Region of stability (black) for the travelling wave solution in the (β, ξ) parameter plane, for a continuum Hodgkin-Huxley model with axo-dendritic interactions and an exponential synaptic footprint. Here excitatory synaptic inputs occur at a distance ξ from the soma and the velocity of action potential propagation is taken as $v = 2$. Note the periodicity of the stability diagram as a function of the dendritic contact point.

Huxley networks is entirely consistent.

We also looked at the complicated structure of the dendritic tree. We had to simplify the structure to enable the solution of the wave stability equations. It was shown that a dendrite in this simplification, acts like a discrete delay. This idea makes logical sense as the delay will have the same effect if it arrives one period later due to the periodicity of the equations.

The limitation of this chapter is that all the results are in the weak coupling regime. Although weak coupling theory can shed light on the role of synaptic and dendritic processing on issues such as synchrony, it cannot answer questions about

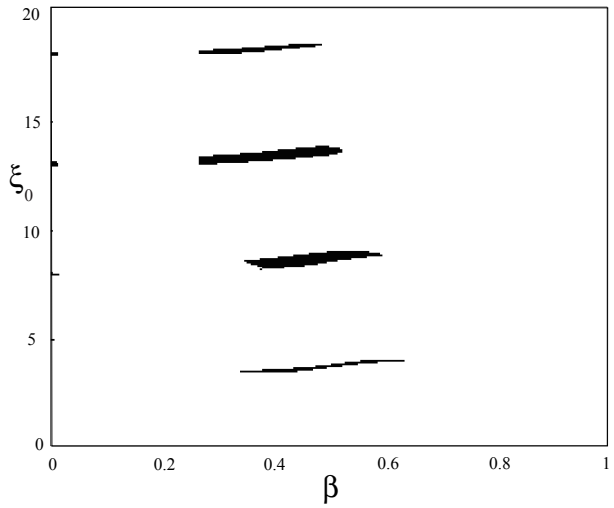

Figure 4.3.3: Region of stability (black) for the travelling wave solution in the (β, ξ) parameter plane, for a continuum McKean model with axo-dendritic interactions and an exponential synaptic footprint. Here excitatory synaptic inputs occur at a distance ξ from the soma and the velocity of action potential propagation is taken as $v = 2$. Note the periodicity of the stability diagram as a function of the dendritic contact point.

instabilities arising in the strong coupling regime.

Chapter 5

Half-Centers

In biology there are many examples of rhythm generating networks. These networks or Central Pattern Generators (CPG) are used widely to model rhythmic behaviour such as heartbeats [75] and locomotion [76]. One way in which these rhythms can be generated is by the use of reciprocal inhibition using a mechanism known as post inhibitory rebound (PIR) [77, 78]. The definition of post inhibitory rebound is an active process in which the excitability of a neuron is enhanced temporarily following a period of voltage depression (hyper-polarisation). If a model with PIR can also fire by anode break excitation [79], it can generate an action potential. In fact any excitable model with a generic cubic nullcline (eg. reduced HH, FHN, McKean) can fire this way. Firing by anode break excitation can be explained in the McKean case using geometric ideas and is illustrated in figure (5.0.1). The system is stable at equilibrium point A. If the system receives a constant inhibitory signal the v nullcline will effectively be shifted and the equilibrium point will become point C. In the limit $\mu \to 0$ the system will instantaneously move to point B and evolve toward the equilibrium point C. If the inhibitory signal lasts sufficiently that the system has evolved below w_{min} then when the inhibition is released the system can only evolve back to equilibrium (A) by a large excursion (action po-

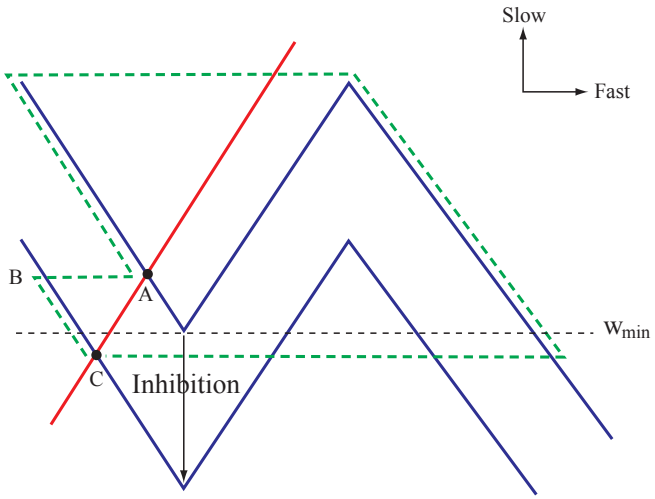

Figure 5.0.1: Phase plane of the McKean model showing the principle of anode break excitation. After inhibition the system can only reach equilibrium again if it makes a large excursion (action potential). In this diagram the fast variable is the voltage and the slow is the gating variable.

tential).

In the previous chapters the models discussed have been oscillatory and only weakly coupled. However, it is possible to create a self-sustained anti-synchronous rhythm using two excitable neurons with strong inhibitory coupling, illustrated in figure (5.0.2). This two neuron network can be constructed in such a way that an inhibitory signal is generated when one neuron fires such that it inhibits the other and with sufficient strength and duration that the second neuron will fire as the inhibition is released. This construction is known as a Half-Center and will fire ad infinitum once one neuron fires.

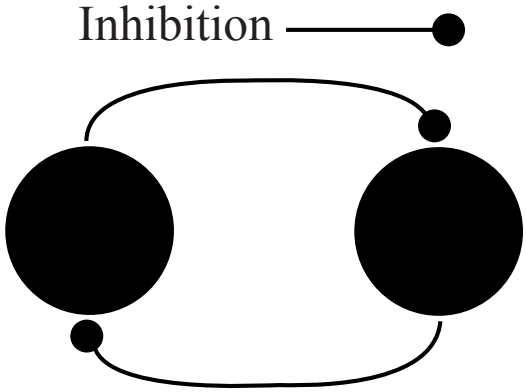

Figure 5.0.2: Illustration of the half-center construction.

5.1 Half-Center McKean

In the case of the McKean model in the limit $\mu \to 0$ as in chapter 2, it is possible to calculate the conditions for a half-center rhythm to exist. If we take two McKean neurons, in the absence of coupling, each neuron has the equation

$$\dot{w_j} = -\beta w_j + A + S_j \qquad j = 1, 2.$$

We introduce external signals $X_j(t)$ which as before we take to be of the form

$$X_j(t) = \sum_{m=0}^{\infty} \eta(t - T_j^m). \tag{5.1}$$

For clarity, in this section we choose to work with Heaviside or *on/off* synapses of the form $\eta(t) = g\Theta(t)\Theta(\tau - t)$, where g is some constant. In this case the synapse has a zero rise and fall time with amplitude $g < 0$ It effectively shifts the v nullcline by g on the time interval $(T^m, T^m + \tau)$. Using this simple form for the synapse has the advantage that we can describe the state of neuron j by using the labels S_j (as done in chapter 3) and χ_j. We introduce a binary variable χ_j which takes the value

1, while there is an inhibitory signal, or 0 when there is no signal. This means that we can write dynamics in the form

$$\dot{w_j} = -\beta w_j + A + S_j + g\chi_j, \tag{5.2}$$

$$v_j = S_j + A + v_0 - g\chi_j - w_j, \tag{5.3}$$

where $\chi_j = 1$ if $T_j^m < t < T_j^m + \tau$. If we just consider one of the neurons, the index notation can be ignored. Assuming that there is no change in the state (i.e. (S, χ) remains fixed) the equations of motion can easily be integrated

$$t - t_0 = \frac{1}{\beta} \ln \left[\frac{-\beta w(t_0) + A + S + g\chi}{-\beta w(t) + A + S + g\chi} \right], \tag{5.4}$$

$$w(t; w(t_0), t_0, S, \chi) = w(t_0) \mathrm{e}^{\beta(t-t_0)} + \frac{A + S + g\chi}{\beta} \left[1 - \mathrm{e}^{\beta(t-t_0)} \right]. \tag{5.5}$$

In the excitable state, the fixed point $(v^*(\chi), w^*(\chi))$ lies on a branch with $S = 0$ and

$$w^*(\chi) = \frac{1}{\beta}[A + g\chi]. \tag{5.6}$$

If the system is inhibited whilst in the state $(S, \chi) = (0, 0)$, it will only rebound if it is inhibited with a strong enough current for sufficient duration. The strength of the inhibition must be large enough to ensure that $w^*(1) < w_{min} = A + v_0 - a/2$ where w_{min} is as in figure (5.1). From (5.6) we obtain the condition

$$|g| > \beta w_{min} + A. \tag{5.7}$$

Moreover for an initial state (v, w) with $(S, \chi) = (0, 0)$, we must have that the duration of the inhibition τ greater than the time it takes to evolve to less than w_{min}. That is $\tau > T(w)$, where

$$T(w) = \frac{1}{\beta} \ln \left[\frac{-\beta w + A + g}{-\beta w_{min} + A + g} \right]. \tag{5.8}$$

Assuming the conditions for rebound are met, it is possible to calculate the time spent in the state $(S, \chi) = (1, 0)$, after the inhibition is released. Under the assump-

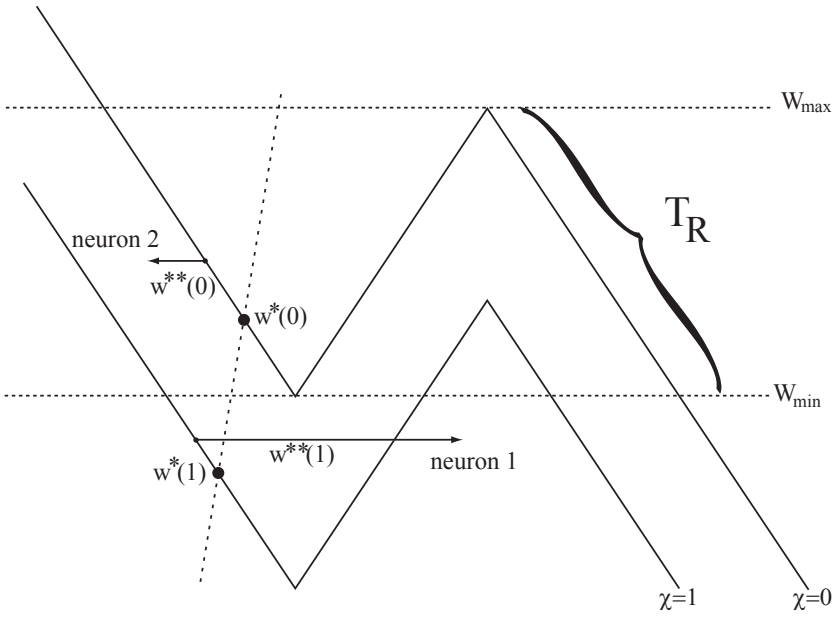

Figure 5.1.1: Nullcline structure of the McKean model showing the construction of a half-center. Neuron 1, heading toward $w^*(1)$, is released from inhibition at point $w^{**}(1)$ and is fires due to anode break excitation. This in turn inhibits neuron 2 which is heading toward point $w^*(0)$, at point $w^{**}(0)$ and then heads toward $w^*(1)$. This process then repeats ad infinitum.

tion that no other inhibitory signal is received and that it starts with initial conditions (v, w), the rebound time on $S = 1$ is given by

$$T_R(w) = \frac{1}{\beta} \ln \left[\frac{-\beta w + A + 1}{-\beta w_{max} + A + 1} \right], \tag{5.9}$$

where $w_{max} = w_{min} + 1/2$ is the maximum value of the of the voltage nullcline in the state $(S, \chi) = (1, 0)$. We now calculate the response of the system initially in the state $w_0 \in [w_{max}, w^*(0)]$ at $t = 0$ with $(S, \chi) = (0, 0)$ for a Δ periodic train of square pulses ($T^m = m\Delta$), assuming that the system relaxes back to the state $(S, \chi) = (0, 0)$ in a time Δ. It will relax in this time if $\Delta > \tau + T_R$. Moreover it is guaranteed if

$\Delta > \tau + T_R(w^*(1))$, no matter what the initial conditions on $(S, \chi) = (0, 0)$. Recall (6.16), starting at $t = 0$, $w = w_0$, after time τ then $w = w(\tau; w_0, 0, 0, 1)$. The rebound time is given by $T_R = T_R(w(\tau; w_0, 0, 1))$ and the value after a period Δ is simply given by

$$w(\Delta; w_{max}, \tau + T_R(w_0), 0, 0). \tag{5.10}$$

Hence it is simple to write a map for $w_{m+1} = w((m+1)\Delta; w_m, m\Delta, 0, 0)$ in the form

$$w_{m+1} = \lambda_1 w_m + \lambda_2 \equiv F(w_m), \tag{5.11}$$

where

$$\begin{aligned}
\lambda_1 &= (A - \beta)\lambda_3, \\
\lambda_2 &= \frac{(A+1)(\beta - A)\lambda_3}{\beta w_{max}} + \frac{A}{\beta}, \\
\lambda_3 &= \frac{w_{max}\mathbf{e}^{-\beta(\Delta - \tau)}}{-\beta w_{max} + A + 1}.
\end{aligned}$$

From the above it is clear that there is a fixed point at $\lambda_2/(1 + \lambda_1)$ and it is stable if $|\lambda_1| < 1$ This gives a condition on Δ as

$$\Delta > \frac{1}{\beta} \ln \left| \frac{(A - \beta) w_{max} \mathbf{e}^{\beta\tau}}{-\beta w_{max} + A + 1} \right| > T(w_{max}) + T_R(w^*(1)). \tag{5.12}$$

If we consider that the times T^m correspond to those at which a McKean neuron makes the transition from $S = 0$ to $S = 1$, signalling the onset of a synaptic pulse, then it is possible for two McKean neurons coupled via reciprocal inhibitory synapses (of the type just discussed) to generate a robust anti-phase rhythm. We shall assume $\tau > T(w_{max})$ and $|g| > \beta w_{min} + A$, so that rebound firing is always possible. Imagine a system of two McKean neurons such that neuron 1 makes a transition to $S = 1$ whilst the other is in state $(S, \chi) = (0, 0)$. If $T_R(w^*(1)) < \tau$ then neuron 1 will reach the state $(S, \chi) = (0, 0)$, before it receives the inhibitory input following the rebound firing of 2. The process may then repeat ad-infinitum, so

that an asymptotically stable periodic limit cycle of period $\Delta = 2\tau$ is expected. The point at which the transition $(S, \chi) = (0, 1) \rightarrow (1, 0)$ is easily calculated as $w^{**}(1) = w(\tau; w^{**}(0), 0, 0, 1)$ to give

$$w^{**}(1) = w^{*}(1) + \mathrm{e}^{\beta\tau}[w^{**}(0) - w^{*}(1)]. \tag{5.13}$$

We may now write the orbit for neuron 1 in the form $w_1(t) = w(t)$. For neuron 2 $w_2(t) = w(t - \tau)$ (i.e. Phase shifted by 1/2)

$$w(t) = \begin{cases} w(t; w^{**}(0), 0, 0, 1), & 0 < t < \tau, \\ w(t; w^{**}(1), \tau, 1, 0), & \tau < t < \tau + T_R(w^{**}(1)) \\ w(t; w_{max}, \tau + T_R(w^{**}(1)), 0, 0), & \tau + T_R(w^{**}(1)) < t < 2\tau \end{cases} \tag{5.14}$$

For convenience we have chosen the origin of the time such that $w(0) = w^{**}(0)$. The geometric interpretation of w_{max},w_{min},$w^{*}(0)$,$w^{*}(1)$,$w^{**}(0)$ and $w^{**}(1)$ can be seen in figure (5.1). The half-center trajectory may be parameterised by a phase variable $\theta \in [0, 1)$ such that $\theta(t) = t/\Delta = t/2\tau$. Hence, for some Δ periodic function Γ we may write

$$w(t) = \Gamma_w(\theta(t)), \tag{5.15}$$

$$v(t) = \Gamma_v(\theta(t)) = \Lambda_w(\theta(t)) + S + A + v_0 - g\chi. \tag{5.16}$$

Hence

$$\dot{w}(t) = \Omega\frac{\mathrm{d}\Gamma_w}{\mathrm{d}\theta} = G(\theta) \equiv G(\Lambda(\theta); S, \chi), \tag{5.17}$$

$$\dot{v}(t) = \Omega\frac{\mathrm{d}\Gamma_v}{\mathrm{d}\theta} = -G(\theta) + \Omega\frac{\mathrm{d}S}{\mathrm{d}\theta} + g\Omega\frac{\mathrm{d}\chi}{\mathrm{d}\theta}. \tag{5.18}$$

Using (5.14) and proceeding as in chapter 2, we find

$$G(\theta) = \begin{cases} \mathrm{e}^{-\beta\theta\Delta}[A + g - \beta w^{**}(0)], & 0 < \theta < \theta_u \\ \mathrm{e}^{-\beta(\theta-\theta_u)\Delta}[A + 1 - \beta w^{**}(1)], & \theta_u < \theta < \theta_d \\ \mathrm{e}^{-\beta(\theta-\theta_d)\Delta}[A - \beta w_{max}], & \theta_d < \theta < 1 \end{cases} \tag{5.19}$$

Where the introduced vales $\theta_{u,d}$ are the points on the periodic orbit where jumps in the value of S occur, i.e. $\theta_u = 1/2$ and $\theta_d = \theta_u + T_R(\Gamma(\theta_u))/2\tau$.

For later convenience we switch to using L(eft) and R(ight) labels and write $w_L = w_1$ and $w_R = w_2$ In the same way that a weak external input was applied to the McKean model in chapter 2, we can apply one to the half-center McKean network such that $v_L \to v_L + \epsilon X_L(t)$ and $v_R \to v_R + \epsilon X_R(t)$. This leads to the system given by $\dot{w}_L = G(w_L; S, \chi) + \epsilon X_L(t)$, $\dot{w}_R = G(w_R; S, \chi) + \epsilon X_R(t)$. Since (w_L, v_L) and (w_R, v_R) are the same except for a phase shift of $1/2$ it is natural to work with just (w_L, v_L).

Proceeding as in chapter 2 we can calculate the response function $R(\theta)$

$$R(\theta) = \Omega \left[\frac{1}{G(\theta)} + \kappa_d \delta(\theta - \theta_d) + \kappa_u \delta(\theta - \theta_u) + \kappa_0 \delta(\theta) \right], \tag{5.20}$$

where $\theta = \theta_L$ The last three terms in (5.20) represent the contributions arising from jumps in the value of v. The constants $\kappa_{d,u,0}$ may be calculated by demanding that $\theta(t)$ evolve smoothly even when jumps in v occur. This is guaranteed upon choosing

$$\kappa_u = \left(\frac{1}{G(\theta_u^+)} - \frac{1}{G(\theta_u)} \right), \quad \kappa_d = \left(\frac{1}{G(\theta_d^+)} - \frac{1}{G(\theta_d)} \right), \quad \kappa_0 = \left(\frac{1}{G(0)} - \frac{1}{G(1)} \right). \tag{5.21}$$

As before in chapter 2 we can calculate the response function

$$R(t/\Delta) = \begin{cases} R_1(t) = \Omega \mathrm{e}^{\beta t} / \left[A + g - \beta w^{**}(0) \right] & t/\Delta \mod 1 \in [0, \theta_u) \\ R_2(t) = B R_1(t) \mathrm{e}^{-\beta \theta_u \Delta} & t/\Delta \mod 1 \in (\theta_u, \theta_d) \\ R_3(t) = C R_1(t) \mathrm{e}^{-\beta \theta_d \Delta} & t/\Delta \mod 1 \in (\theta_d, 1) \end{cases} \tag{5.22}$$

where

$$\begin{aligned} B &= \frac{A + g - \beta w^{**}(0)}{A + 1 - \beta (w^{**}(1))}, \\ C &= \frac{A + g - \beta w^{**}(0)}{A - \beta w_{max}}. \end{aligned} \tag{5.23}$$

The response function is plotted in figure (5.1.2).

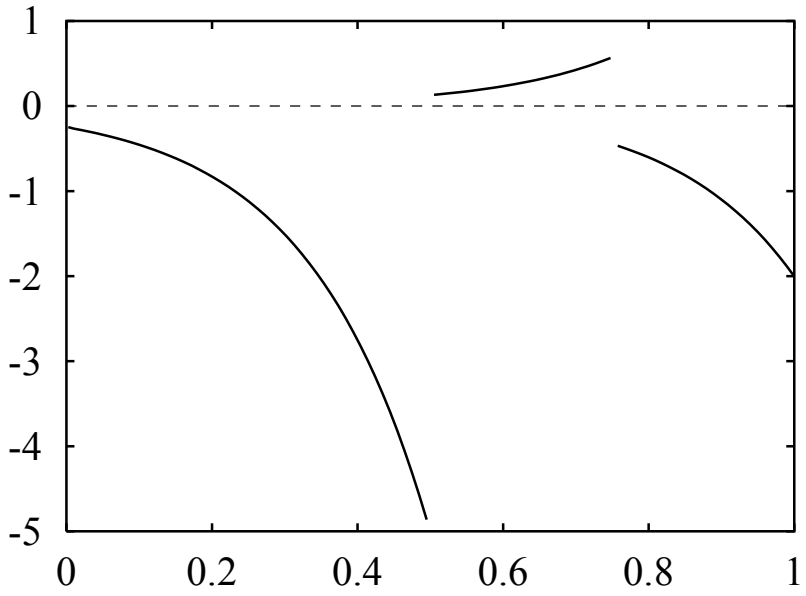

Figure 5.1.2: The three piece response function of the half-center McKean model.

It is worth noting that this form for the response function can be put into the Fourier form used in chapter 3.

5.2 Half-Center Simulations

It is possible to explore half-center systems for Hodgkin-Huxley and McKean neurons ($\mu \not\to 0, \epsilon \not\to 0$) and compare their behaviour with our theory. We choose to consider on/off synapses for McKean as above and difference of exponential synapses for Hodgkin-Huxley. In this way we can compare a mathematically simple half-center (McKean) and a biologically realistic half-center (Hodgkin-Huxley). The reason for choosing the difference of exponential synaptic kernel rather than the alpha function as before is because it gives the ability to control the rise and fall time of the synapse separately. This allows more control when changing the duration of the inhibitory signal.

The difference of exponential synaptic kernel has the form

$$\eta(t) = \left(\frac{1}{\alpha} - \frac{1}{\beta}\right)^{-1} [\exp(-\alpha t) - \exp(-\beta t)]. \tag{5.24}$$

Here α (β) is the inverse rise (fall) time of the synapse. As in chapter 3 may write the input in the form $I_s(t) = g\sum_m \eta(t - T_m) \equiv gs$ where

$$\dot{s} = x \tag{5.25}$$

$$\dot{x} = -(\alpha+\beta)x - \alpha\beta s + \alpha\beta \sum_m \delta(t - T^m), \qquad s(0) = 0, \quad x(0) = \alpha\beta. \tag{5.26}$$

It is worth noting that if $\alpha = \beta$ then the difference of exponentials kernel becomes the alpha function kernel : $\alpha^2 t \mathrm{e}^{-\alpha t}$.

In figure (5.2.1) there is a comparison of the alpha function and difference of exponentials synaptic kernels. It shows that it enables greater control over the shape,

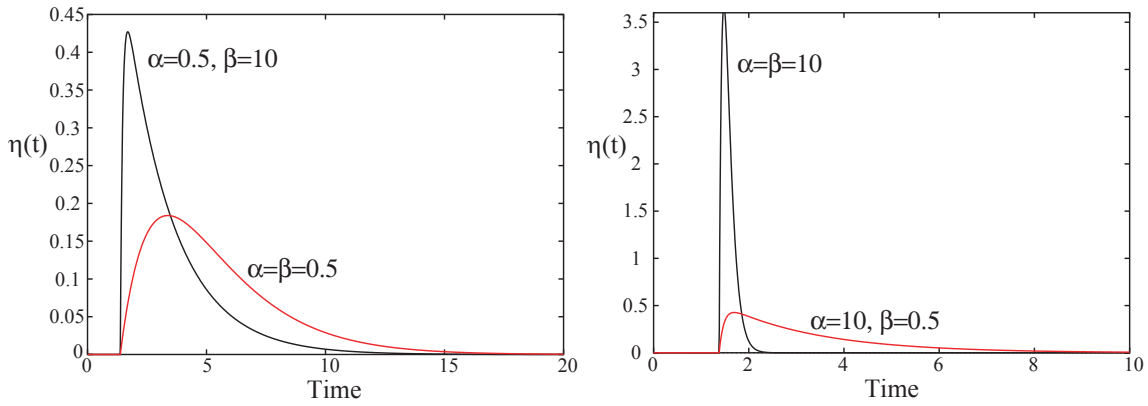

Figure 5.2.1: A comparison of alpha function and difference of exponentials. When $\alpha = \beta$ the difference of exponentials synaptic kernel is the same as the alpha function.

this is useful for matching experimental post synaptic potentials. It has the disadvantage that it is not as simple and as such can not be easily solved explicitly.

Figures (5.2.2) and (5.2.3) show the anti-synchronous rhythm of the half-centers. The anti-synchronous solutions are robust to both system perturbations and parameter changes (apart from changing the synaptic properties too far from the already defined strength and duration requirements). This stable half-center rhythm persists for a substantial region of parameter space and whilst it is impractical to track the boundaries certain qualitative conditions can be given. To obtain this half-center rhythm the individual models have to be able to fire due to anode break excitation, and the inhibitory signals have to be strong (proportional to the spike amplitude) and have sufficient duration (proportional to the uncoupled period of the model in its oscillatory regime). The half-center rhythm with the inhibition superimposed over it can be seen in figure (5.2.4). This shows the relative strength and duration of the inhibition to that of the resulting action potentials. It is clear that this meets the conditions outlined above.

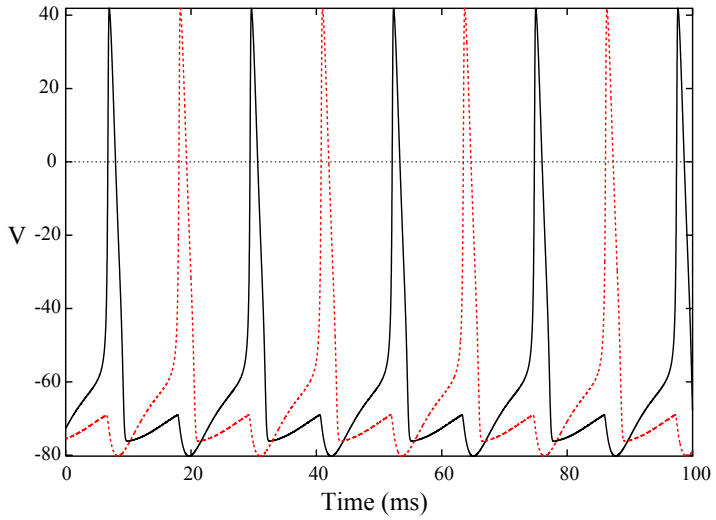

Figure 5.2.2: The half-center rhythm for two Hodgkin-Huxley neurons with only strong mutual inhibition. The inhibitory synapses are modelled with difference of exponentials synaptic kernel. Here $\alpha = 10$, $\beta = 0.5$ and $I = 0$.

Figures (5.2.3) and (5.2.5) show that on/off and difference of exponentials synaptic kernels give qualitatively the same behaviour for the McKean model. The action potentials have different voltage magnitudes due to the difference in synaptic kernel between the two. However the characteristic shape is maintained and this suggests that making the simplification of on/off synapses is reasonable. Moreover since the McKean half-center with on /off synapses can be solved explicitly, it gives a way of predicting behaviour in the biologically realistic model.

5.2.1 Voltage Dependant Synapses

Another common way to represent synaptic interactions is through a system of differential equations based on the presynaptic potential [80]. In this case if v_{pre} is

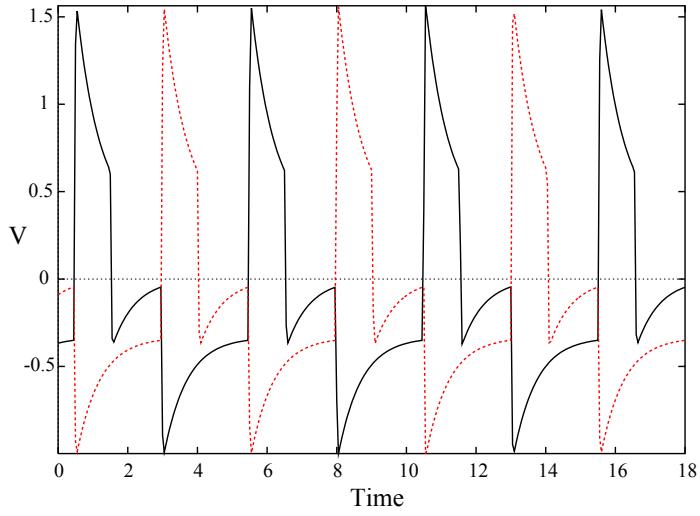

Figure 5.2.3: The half-center rhythm for two McKean neurons with only strong mutual inhibition. The inhibitory synapses are modelled with on/off synapses. Here $\tau = 2.5$, the strength $g = 1$ and $I = 0$.

the potential of the presynaptic cell then $s(t)$ satisfies an ODE such that

$$\frac{\mathrm{d}s}{\mathrm{dt}} = \alpha(1-s)h(v_{\text{pre}} - v_{\text{thr}}) - \beta s, \tag{5.27}$$

or

$$\frac{\mathrm{d}s}{\mathrm{dt}} = \alpha(1-s)h(v_{\text{pre}} - v_{\text{thr}}) - \beta h(v_{\text{thr}} - v_{\text{pre}})s.$$

Here α and β are constants and $h(v)$ is a saturating threshold function such as

$$h(v) = \frac{1}{1+\exp(-v/v_s)}.$$

As $v_s \to 0$, $h(v)$ approximates a Heaviside step function. The above model is often referred to as a *direct* synapse since it is activated as soon as a membrane potential crosses the threshold v_{thr} (at least for the case $v_s \to 0$). To better represent the range of synapse dynamics observed biologically it is sometimes necessary to consider

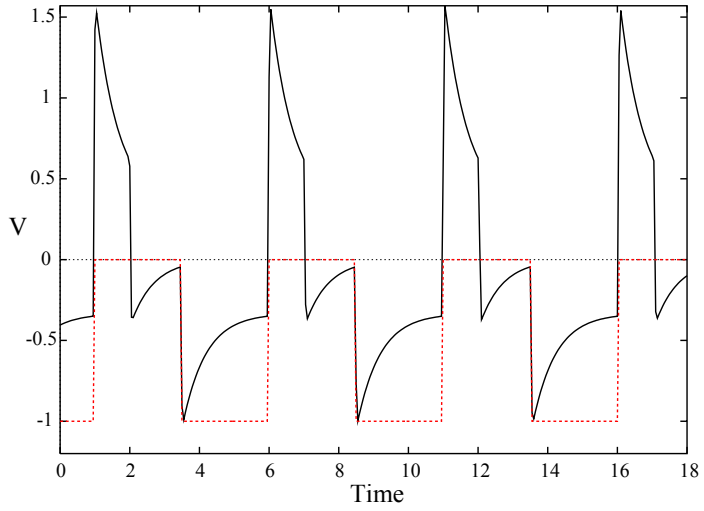

Figure 5.2.4: A comparison of the spikes of the half-center McKean model and the inhibitory on/off synapses that facilitate the half-center rhythm.

models of the form

$$\frac{\mathrm{d}x}{\mathrm{dt}} = \alpha_x(1-x)h(v_{\text{pre}} - v_{\text{thr}}) - \beta_x x,$$
$$\frac{\mathrm{d}s}{\mathrm{dt}} = \alpha(1-s)h(x - x_{\text{thr}}) - \beta s.$$

The effect of such an *indirect* synapse is to introduce a delay in the onset of response, determined by the time it takes for the x variable to cross x_{thr} after v_{pre} crosses v_{thr}. Another example of an indirect synapse is the phenomenological model of *slow* GABA_B inhibition [81]. Synaptic gating is described with a pair of differential equations

$$\frac{\mathrm{d}x}{\mathrm{dt}} = \alpha_x(1-x)h(v_{\text{pre}} - v_{\text{thr}}) - \beta_x h(v_{\text{thr}} - v_{\text{pre}})x,$$
$$\frac{\mathrm{d}s}{\mathrm{dt}} = \alpha(1-s)x^4 - \beta s.$$

Here x represents the activation level of some G-protein.

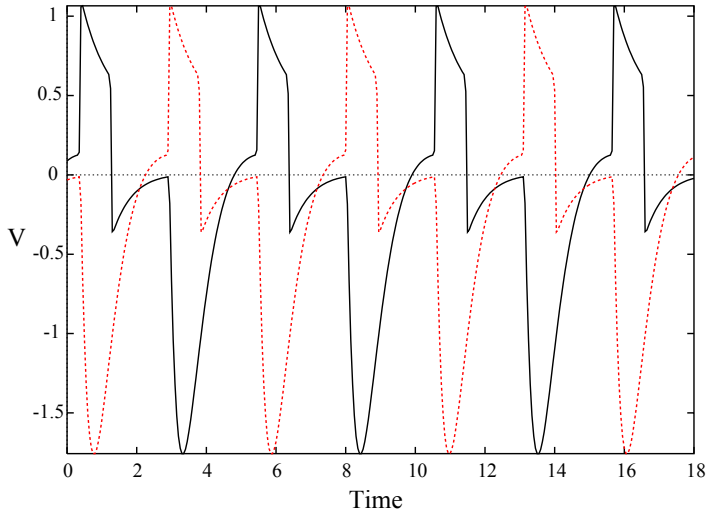

Figure 5.2.5: The half-center rhythm for two McKean neurons with only strong mutual inhibition. The inhibitory synapses are modelled with difference of exponentials synaptic kernel. Here $\alpha = 3$, $\beta = 1$ and $I = 0$.

the synaptic response is dominated by the action potential time threshold). One final voltage gated synapse that can mimic an alpha-function is given by

$$\frac{1}{\alpha}\frac{\mathrm{d}x}{\mathrm{dt}} = -x + h(v_{\text{pre}} - v_{\text{thr}}),$$
$$\frac{1}{\alpha}\frac{\mathrm{d}s}{\mathrm{dt}} = -s + x.$$

Simulations With Voltage Dependant Synapses

We choose to use the voltage dependant synapse as defined in (5.27). This can be seen as analogous to the difference of exponentials synaptic kernel seen earlier. Figure (5.2.6) shows the half-center rhythm generated with voltage gated synapses, the action potential shape is very similar to that of figure (5.2.2). A comparison of

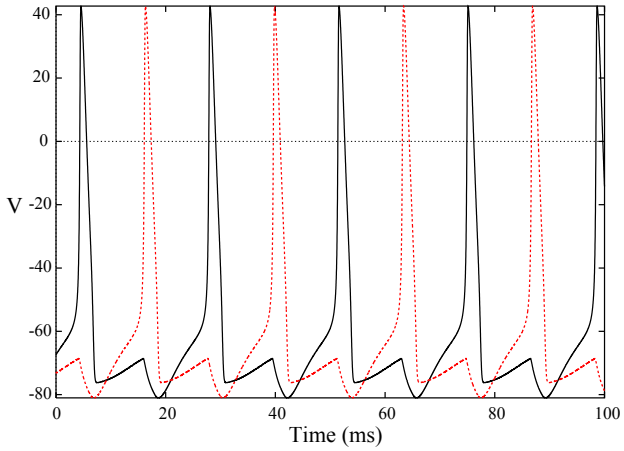

Figure 5.2.6: The half-center rhythm for two Hodgkin-Huxley neurons with only strong mutual inhibition. The inhibitory synapses are modelled with difference of exponentials voltage dependant synapses. Here $\alpha = 10$, $\beta = 0.5$ and $I = 0$.

the action potentials can be seen in figure (5.2.7). It can be seen that the period varies slightly however the shape and magnitude is consistent. This shows that there is very little difference between the two choices of synapse type.

The McKean half-center with voltage dependent synapses is shown in figure (5.2.8) These figures show that the half-center rhythm still exists with voltage dependent synapses.

Conclusions About Half-Centers

It has been shown that the half-center rhythm exists independently of the model and the type of synapse. It is a system that can be constructed for any model that can fire by anode break excitation. It is also a system that is robust to small voltage perturbations. Considering a half-center as a single unit is therefore reasonable.

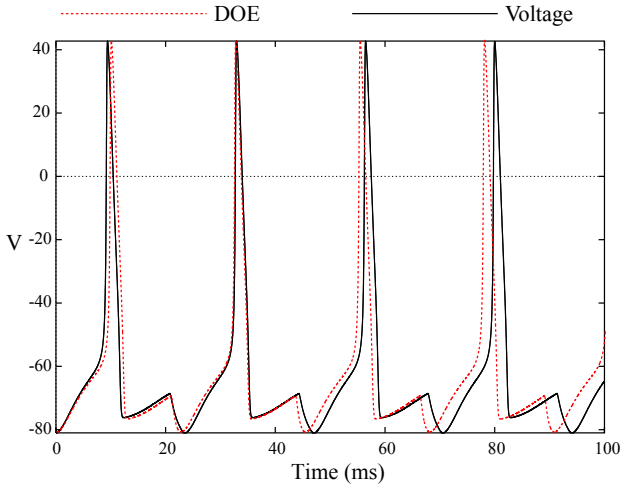

Figure 5.2.7: A comparison of the action potential of the HH half-center with a DOE voltage dependant synapses. Here $\alpha = 10$, $\beta = 0.5$ and $I = 0$ for both.

5.3 A Network Of Half-Centers

Consider two half-centers coupled with weak coupling as shown in figure (5.3.1). There is more complexity in considering coupling in the half-center 'unit' than for considering that of a neuron. With the half-center we have the notion of left and right, this increases the possible number of connections. We shall adopt the notation from figure (5.3.1) that is $L(R)$ for the left (right) side of the half-center and $A(B)$ for the half-center above (below). There are obviously many choice of connection even for a two half-center network and it is not practical to investigate every type. With an eye on future work we shall consider connections as illustrated in figure (5.3.2)

Here the connections are uni-directional and the synapses are a combination of inhibitory (for diagonal connections) and excitatory (for straight connections). Work done on a similar structure by Roberts et al. [82], used detailed biological models,

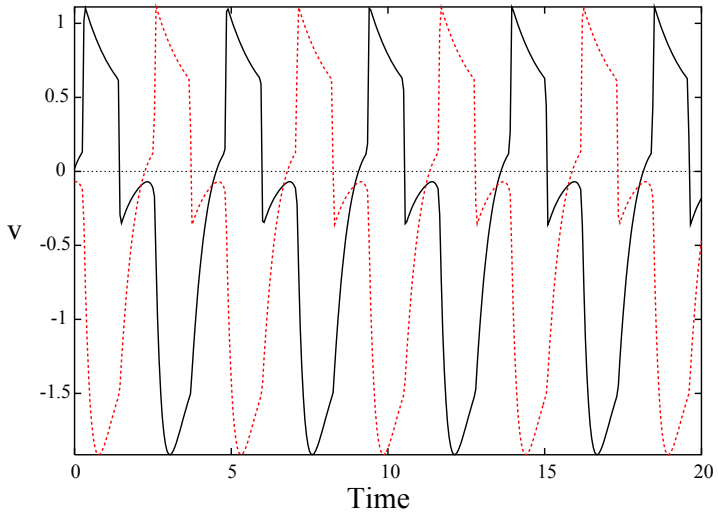

Figure 5.2.8: The half-center rhythm for two McKean neurons with only strong mutual inhibition. The inhibitory synapses are modelled with difference of exponentials voltage dependent synapses. Here $\alpha = 3$, $\beta = 1$ and $I = 0$.

Hodgkin-Huxley with four types of DOE synapses. This work showed that this structure produced phase locking. For weak coupling there is a phase locked state with a small phase difference between the top and the bottom half centers.

5.3.1 McKean Half-Center Network

It is a simple task to simulate this network, figure (5.3.3) shows a McKean half-center network exhibiting phase locked state with a small phase difference between half-centers It is also obviously possible to simulate this construction with a Hodgkin-Huxley half center as seen in figure (5.3.4)

This also shows that there is a small phase difference across the network. How-

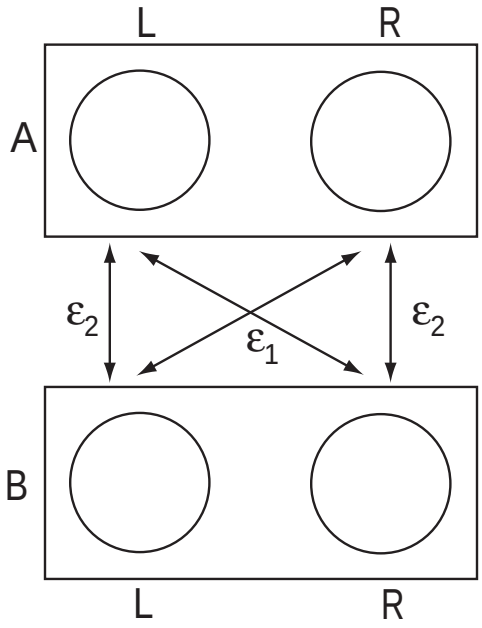

Figure 5.3.1: An illustration of the possible connections for a two half-center network. With ipsi-lateral (same side) coupling ϵ_2) and contra-lateral (opposite side) coupling ϵ_1.

ever in the work by Roberts $et\ al$, it was seen that the phase difference between half centers becomes smaller as the coupling is increased. For a critical strength of the coupling the system becomes synchronous and as coupling strength is increased further the phase locked state is destroyed. This behaviour is seen in the Hodgkin-Huxley model but it is not evident in the McKean model. This suggests that the McKean model does not produce all of the behaviour of the Hodgkin-Huxley model.

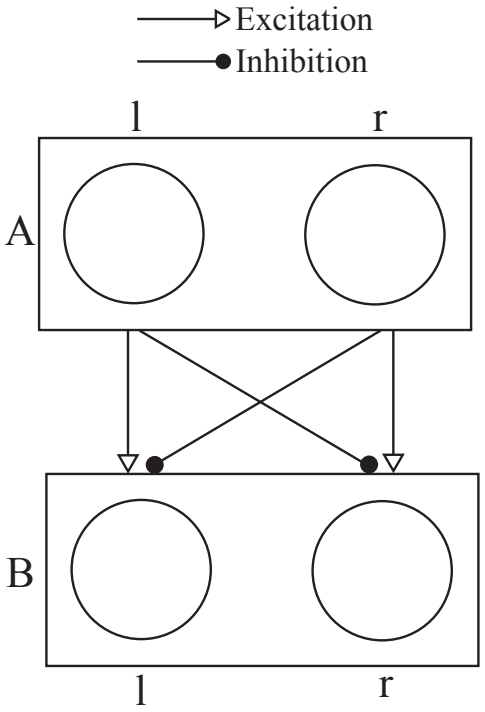

Figure 5.3.2: Connections for a two half-center network.

5.4 Conclusions

In this chapter we showed that it was possible to create an oscillatory network with non-oscillatory neurons using only inhibitory synapses and with no external input. We showed that this structure is robust to voltage and parameter perturbation. These half-center structures can be thought of as a robust anti-synchronous rhythm generator. The rhythm relies on reciprocal inhibition and anode break excitation.

It was shown that in a uni-directional weakly coupled network of half-centers, there was a phase locked state. This phase locked state had a small phase difference between half-centers. This suggests that in a chain of uni-directionally coupled neurons would exhibit a phase difference between each half-center, generat-

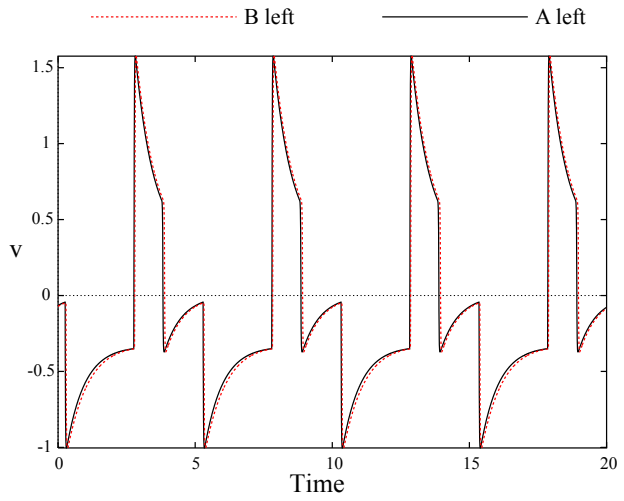

Figure 5.3.3: The phase locked solution of the left side of the McKean half center network. There is a small phase difference between A left and B left.

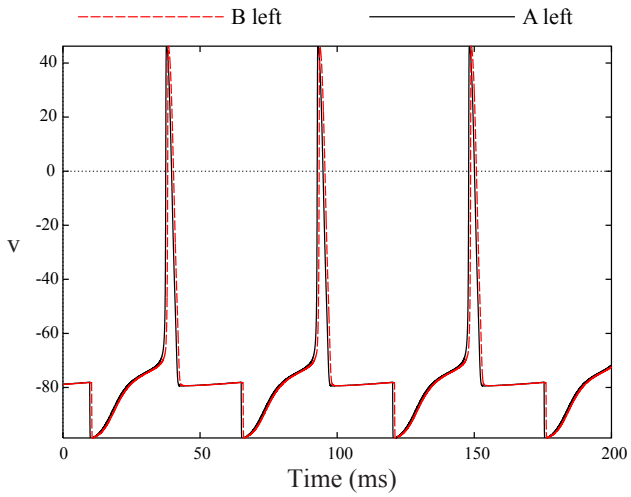

Figure 5.3.4: The phase locked solution of the left side of the HH half center network. There is a small phase difference between A left and B left.

ing a wave across the chain. However when the McKean half-center network was simulated it was shown that it did not respond to changing of coupling strength

in the same way as either the HH half-center or the simulations by Roberts $et\ al$. This shows that the McKean model does not match the Hodgkin-Huxley model in this respect. This discrepancy prompts the construction of a new model in the next chapter, which more closely mimics the HH model.

The swimming motion generated in spinal cord of small swimming vertebrates is one area that could benefit from a network of half-center models. This is because the two sides of the spinal cord exhibit such an anti-synchronous rhythm. Modelling of the spinal cord using a network of half-centers is the focus of the next chapter.

Chapter 6

Locomotion In The Embryonic Xenopus Tadpole

6.1 Background

The study of neural systems that arise in biology is an inherently complicated undertaking. Nervous systems such as those seen in mammals and other large animals are so massive as to be experimentally and mathematically hard to study. Progress can be made if the focus is changed to simple animals. Locomotion in walking animals is studied [83] but much more is done looking at locomotion in animals such as the lamprey [84] [85] and the tadpole [86] [87] [88]. The tadpole is of particular interest because it is the simplest vertebrate, but conclusions about the mechanisms for locomotion in larger vertebrates such as humans can be made. With modern equipment such as the patch clamp, detailed voltage readings can be taken from motor neurons during fictive swimming. Extensive biological experiments and numerical simulations as well as anatomical and immunocytochemical analysis, have been performed by Professor A.Roberts and his colleagues in the

biology department at Bristol university [89], [82],[76]. They study the Xenopus hatchling "clawed toad" tadpole, an example of which is shown in figure (6.1.1).

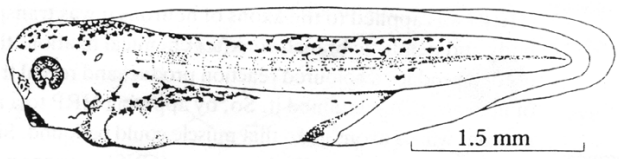

Figure 6.1.1: A caricature of the Xenopus hatchling tadpole, reproduced with permission from A.Roberts [89].

When the tadpole is touched on any part of its body its first response is to swim away from the point of contact as in figure (6.1.2). Swimming can also be initiated by a rapid changing of the light levels over the tadpole, which can be sensed by the tadpoles pineal eye. This swimming motion can stop on its own but more often than not the tadpole stops when it comes in contact with the surface of the water or the side of the tank. In this case it attaches itself using mucus excreted by a cement gland on the front of its head. Once attached it stays there for around a day while its body matures further.

The frequency of swimming tends to be around $10 - 20$Hz and passes down the body at about 5cms^{-1}. This ability to swim when first hatched is interesting but more surprising is that the animal can still swim even if its brain is removed. This suggests that swimming is an innate ability of the spinal column and not controlled by the brain. Moreover, this swimming motion has a wavelength approximately equal to that of the body length.

From the late 1970's it was discovered that horseradish peroxidase [90] [91] [92], when applied to a neurons axon, would be transported throughout the neuron.

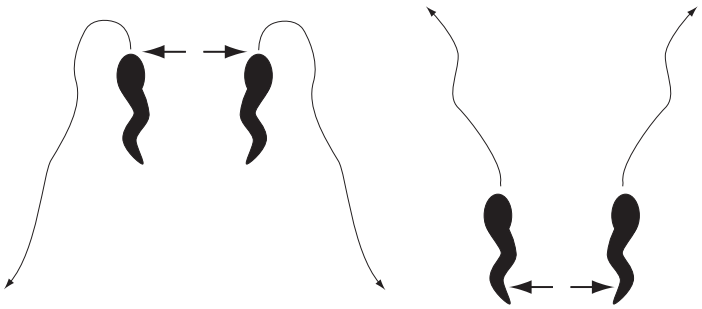

Figure 6.1.2: The tadpole will swim away from the contact point even if that means reversing the direction of swimming.

This allows the anatomy of neuronal structures to be studied in detail, enabling the identification of both neuron type and connections within the spinal cord. Using this method Roberts $et\ al.$ [93] have been able to identify eight distinct neuron classes in the hatchling tadpole. These include the Rohon-Beard neurons (which innervate the skins nerve endings) and the motor neurons (which innervate the swimming muscles). Neither of these can generate the swimming motion of the tadpole. The other neurons, known as interneurons are thought to be responsible for generating the swimming rhythm.

To study the anatomy in better detail the tadpoles are immobilised with a toxin such as α-bungarotoxin which blocks the synapses between the nerves and the muscles. This allows the tadpole to be dissected and its spinal cord to be exposed. Electrodes can then be placed to record the discharge from the axons of the motor neurons. When the tadpole is stimulated directly in the spinal cord it can be seen that there is an anti-synchronous rhythm generated contra-laterally (across the spinal cord). Figure (6.1.3) shows actual voltage recordings from motor neurons on either side of the cord during swimming. It can also be observed that the spikes occur at slightly different times rostra-caudally (head to tail), specifically at later times in the caudal (tailward) direction. The anti-synchronous rhythm and

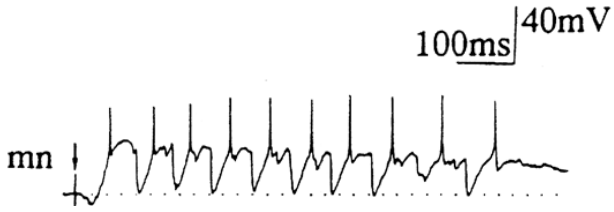

Figure 6.1.3: Voltage trace of the motor neuron output from the 'swimming' Xenopus hatchling tadpole, reproduced with permission from A.Roberts [82].

the slight phase difference down the tadpoles length seem to match those seem in actual swimming and so it is known as 'fictive' swimming.

In many vertebrates neurons in the central nervous systems tend to fire bursts of inputs. However the tadpole only fires a single impulse even after being depolarised for a long time. So that an insight into the behaviour of the spinal cord can be obtained, it is useful to model the whole cord using neuron models with simple spiking (non-bursting) behaviour.

As well as the types of neurons as mentioned above, the anatomical structure of the Xenopus tadpole has been identified [94]. The interneurons which generate the anti-synchronous rhythm run the length of the spinal cord. The connections can be ascending or descending and figure (6.1.4) shows soma positions and axon projections of neurobiotin-filled interneurons in the tadpole. This shows that across the tadpole the axons of both ascending and descending interneurons project far away from the soma. This indicates that connections between quite distant interneurons exist and their could be many connections between them with $en\ passent$ synapses. This means that when creating a realistic biological simulation, the coupling should be non nearest neighbour coupling. It also means that, as discussed in chapter 3, the delays incurred by signals travelling down axons is not insignificant

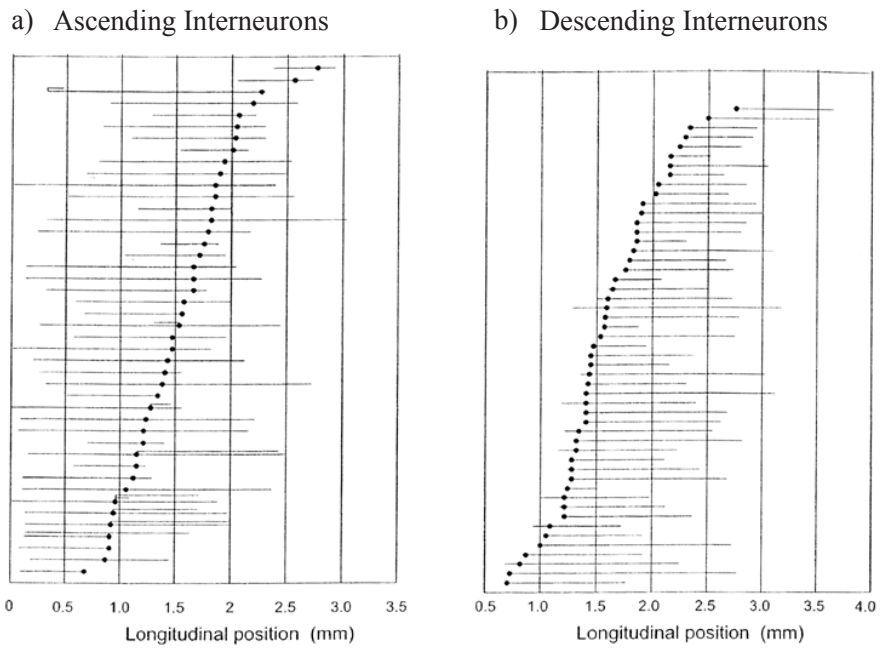

Figure 6.1.4: Soma positions and axonal projections for neurobiotin-filled interneurons in the Xenopus hatchling tadpole. Distances are measured from hindbrain. Reproduced with permission from A.Roberts [94].

for these interneurons.

This does present the important question, how many of these properties are essential for this very specific form of motion. Numerical simulations by Roberts $et\ al.$ [82] use various types of synapses with anatomically realistic connections. The neuron models they use are in fact various parameter regimes of the Hodgkin-Huxley model. For these simulations the network and model properties are assigned with the use of the anatomical and experimental data that the group gathers from their experiments. For example, it is known that synaptic excitation in the tadpole, as well as in other vertebrates, is mediated by glutamate. It has two components, a fast component mediated by non-NMDA (AMPA/kainate) recep-

tors and a slow component mediated by NMDA receptors [95]. Synaptic reciprocal inhibition between the left and right sides of the spinal cord is mediated by glycine [96]. It has also been shown that when the cement gland is stimulated the swimming can be stopped by the release of GABA which inhibits the spinal motor neurons [97, 98].

A lot of insight into the basic mechanisms for locomotion in small vertebrates has been made using mathematical analysis of chains of simple oscillators [99] (where waves are interpreted as swimming). Numerical simulations using biophysical models and structures matching those seen in the biology [82], give insight into neuron and synapse effects. It is clearly desirable to simplify both the model and the construction used in detailed biological simulations but maintain more biological realism than the mathematically tractable simple chains. The aim is to identify the critical conditions required to produce the swimming behaviour observed, whilst maintaining as many links to the biology as possible. This prompts the work in this chapter, to try to simulate chains and find the balance between simplicity and biological realism. It should enable a better understanding of the mechanisms for the swimming motion. The first place to start is to choose a model for the neurons of the chains.

6.2 New 2 Variable Model Of An Excitable Neuron

The McKean model captures many of the qualitative features of more biophysical models, like reduced Hodgkin-Huxley in chapter 2, but not the quantitative ones. For this reason it is worthwhile constructing a new model that better matches some of the behaviour seen in the HH model. The most obvious way in which the McKean model does not match the biologically realistic HH model (or its reduced form, see chapter 2), is that the voltages and timescales are not of comparable mag-

nitudes. A way to address this is to fit a piecewise linear voltage nullcline to the cubic one of the reduced HH model. This fitting can be seen in figure (6.2.1). When fitting the nullcline a choice of input must be made. Looking to the next section, where we use the model in its excitable regime, we choose zero input.

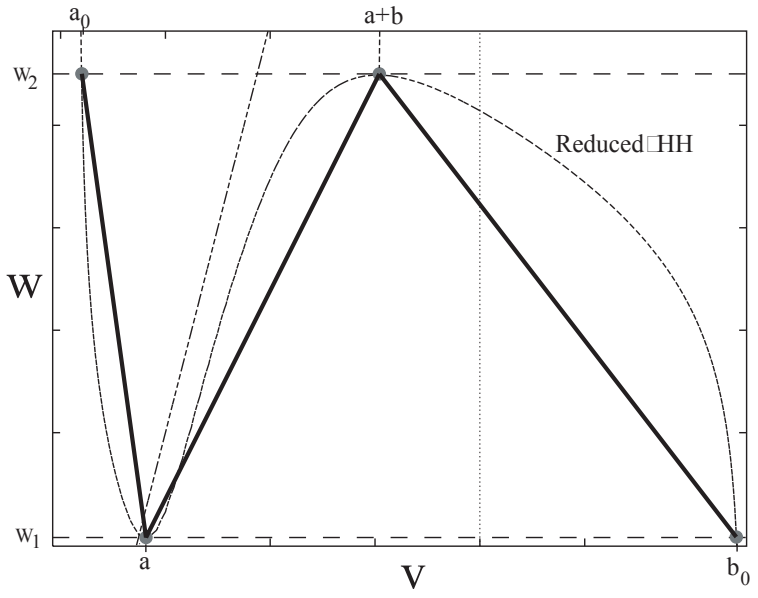

Figure 6.2.1: It is possible fit the nullcline structure using 4 points (a_0, w_2),(a, w_1),$(a + b, w_2)$ and (b_0, w_1). $I = 0$ for the fitting process

Another difference between the McKean model and the (reduced) Hodgkin-Huxley model is in their response to input. When current is added to the HH model as illustrated in figure (6.2.2), the v nullcline does not shift evenly for all v. If we interpret the v nullcline as three branches of a cubic, we can see that the left branch moves when some current is applied whereas the right branch is almost invariant

This behaviour is not seen in the McKean model but can be incorporated into a new model by constructing a piecewise linear nullcline for which the right branch is unaffected by input. This structure can be seen in figure (6.3.7). We have equations

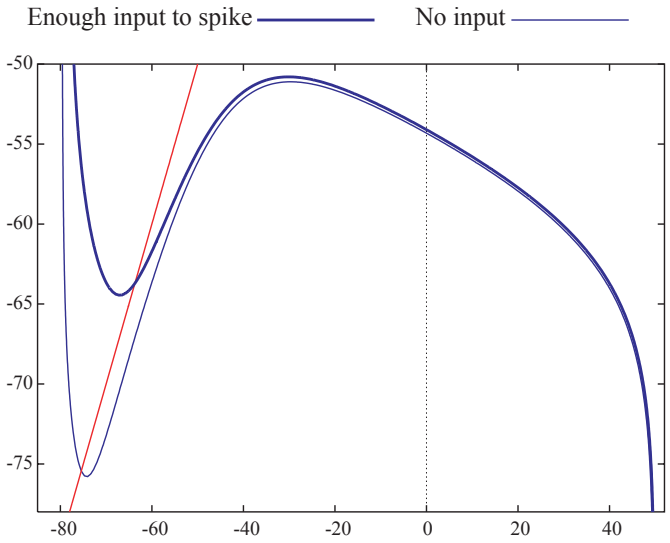

Figure 6.2.2: Under current injection some parts of the nullcline alter substantially, whilst others are almost invariant.

of the form,

$$\mu_1 \dot{v} = f(v, I_T) - w - w_0, \tag{6.1}$$

$$\mu_2 \dot{w} = v - \gamma w - v_0, \tag{6.2}$$

where $I_T = (I + \epsilon X(t))$. The time scales μ_1 and μ_2 can be altered to fit the timescale of the reduced HH model for a specific value of I. The function $f(v)$ is given by

$$f(v, I_T) = \begin{cases} w_2 + \rho I_T - (v - a_0)m_1, & v < a; \\ gv + c, & a < v < a + b; \\ w_2 - (v - (a + b))m_2, & v > a + b. \end{cases} \tag{6.3}$$

This leaves the right branch invariant under input as desired. The gradients of the left (right) branch m_1 (m_2) are given by

$$m_1 = (w2 - w1)/(a - a_0) \qquad \text{and} \qquad m_2 = (w_2 - w_1)/(b_0 - (a + b)).$$

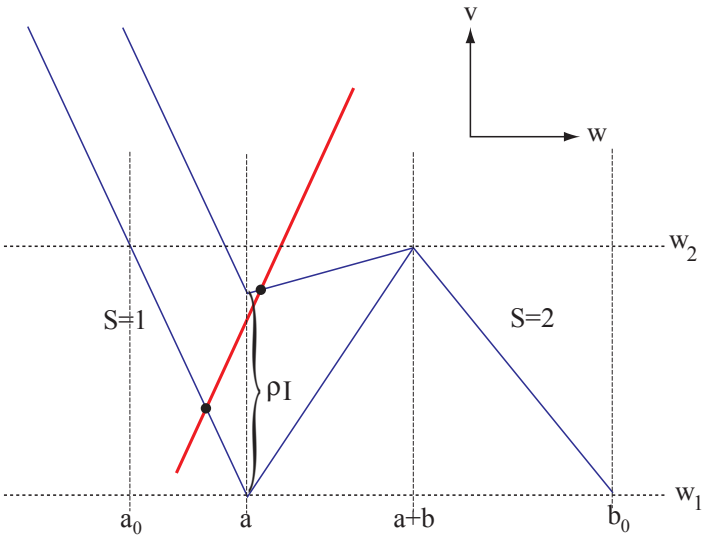

Figure 6.2.3: Construction of the new piece-wise linear model also showing the effect of constant input ρI to the nullcline branches.

The magnitude of the input is controlled by ρ. It is calculated from the Hopf bifurcation point I_* (as defined in chapter 2). This means that this new model and the reduced HH have the same I_* value. Also μ_1 and μ_2 are fitted from the period of the action potentials at I_* because in the next section the model will be used in the excitable regime (i.e. $I_T < I_*$). We also have the condition that the center branch connects the left and right branches which is guaranteed upon choosing

$$g = (w_2 - (w_1 + \rho I_T))/b,$$
$$c = 0.5(w_1 + w_2 + \rho I_T - (2a + b)g).$$

We shall call this model the modified McKean (MM) model. A comparison of the action potentials produced by the modified McKean model and Hodgkin-Huxley model is shown in figures (6.2.4) and (6.2.5).

The action potentials of the modified McKean model mimic those of the Hodgkin-Huxley model. There is one limitation of this modified model, namely that the

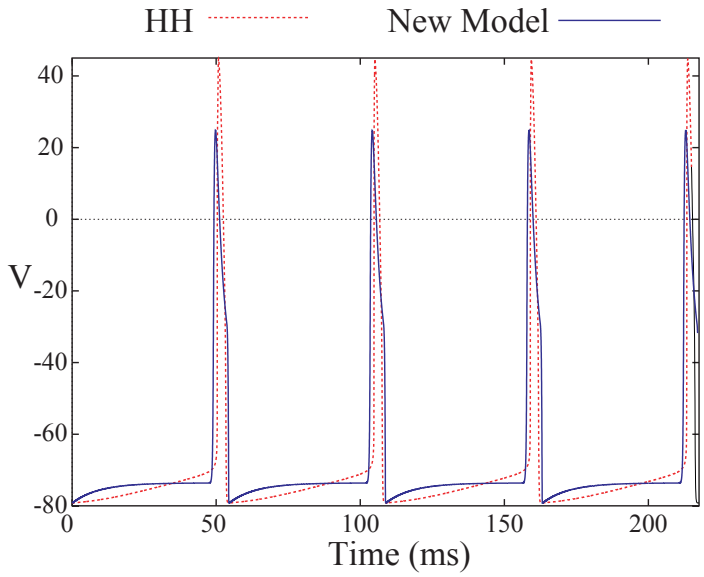

Figure 6.2.4: A comparison of the spike trains produced by the modified McKean model and the Hodgkin-Huxley model, input $I = I_*$ for both.

input I_T must not be sufficient to make the left branch of the v nullcline at $v = a$ higher than the right branch at $v = a + b$, which gives the physiologically realistic condition $I_T < (w_1 - w_2)/\rho$.

As with the normal McKean model in chapter 2 we consider the singular limit $\mu_1 \ll \mu_2$. We label the nullclines as $S = 1(2)$ for the left (right) branches, so that the voltages $v_1(v_2)$ on these branches are given by

$$v_1 = \frac{1}{m_1}\left[\rho I_T + w_2 + a_0 m_1 - w - w_0\right], \tag{6.4}$$

$$v_2 = \frac{1}{m_2}\left[w_2 + (a+b)m_2 - w - w_0\right]. \tag{6.5}$$

The slow dynamics take the usual form

$$\dot{w}_S \equiv G(w;S) = -\beta_S w + A_S,$$

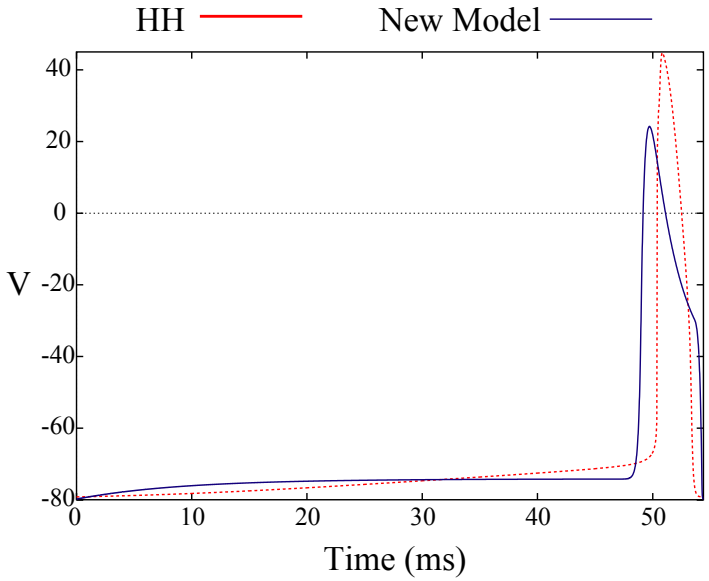

Figure 6.2.5: An action potential comparison of the modified McKean model and the Hodgkin-Huxley model, input $I = I_*$ for both.

where

$$\beta_1 = (\gamma + 1/m_1)/\mu_2, \qquad \beta_2 = (\gamma + 1/m_2)/\mu 2,$$

$$A_1 = ([\rho I_T + w_2 + a_0 m_1 - w_0]/m_1 - v_0)/\mu_2, \tag{6.6}$$

$$A_2 = ([w_2 + (a+b)m_2 - w_0]/m_2 - v_0)/\mu_2. \tag{6.7}$$

In the oscillatory regime the period of oscillation is $T = T_1 + T_2$, where

$$T_1 = \int_{w_2}^{w_1} \frac{1}{G(w;1)} dw = \frac{1}{\beta_1} \ln \left[\frac{(-\beta_1 w_2 + A_1)}{(-\beta_1 w_1 + A_1)} \right], \tag{6.8}$$

$$T_2 = \int_{w_1}^{w_2} \frac{1}{G(w;2)} dw = \frac{1}{\beta_2} \ln \left[\frac{(-\beta_2 w_1 + A_2)}{(-\beta_2 w_2 + A_2)} \right]. \tag{6.9}$$

Without any input ($\varepsilon = 0$) the oscillatory solution is

$$w(t) = \begin{cases} w_2 \exp(-\beta_1 t) + \frac{A_1}{\beta_1}[1 - \exp(-\beta_1 t)], & t \in [0, T_1); \\ w_1 \exp(-\beta_2 (t - T_1)) + \frac{A_2}{\beta_2}[1 - \exp(-\beta_2 (t - T_1))], & t \in (T_1, T), \end{cases}$$

$$v(t) = \begin{cases} -w(t)/m_1 + F_1, & t \in [0, T_1); \\ -w(t)/m_2 + F_2, & t \in (T_1, T), \end{cases}$$

where $(v(t), w(t)) = (v(t+T), w(t+T))$ and $F_1 = A_1 + v_0$,$F_2 = A_2 + v_0$.

This system can be parameterised by a phase variable in the same way as chapter 2. The response function can therefore be calculated and is given by

$$R(\theta) = \Omega \left[\frac{C_S}{G(\theta; S)} + \kappa(0)\delta(\theta) + \kappa(\theta_T)\delta(\theta - \theta_T) \right], \tag{6.10}$$

where

$$C_S = \frac{1 + m_S^2}{1 + m_S},$$

and

$$\kappa(0) = \left[\frac{C_1}{G(0;1)} - \frac{C_2}{G(1;2)} \right], \tag{6.11}$$

$$\kappa(\theta_t) = \left[\frac{C_2}{G(\theta_T;2)} - \frac{C_1}{G(\theta_T;1)} \right], \tag{6.12}$$

and

$$G(\theta; S) = \begin{cases} e^{-\beta_1 \theta T}[A_1 - \beta_1 w_2] & S = 1; \\ e^{-\beta_2 T(\theta - \theta_T)}[A_2 - \beta_2 w_1] & S = 2. \end{cases} \tag{6.13}$$

We have that $S = 1$ for $\theta \in [0, \theta_T)$ and $S = 2$ if $\theta \in (\theta_T, 1)$ (where $\theta_T = T_1/T$ as in chapter 2). The response function of the modified McKean model is plotted in figure (6.2.6). Note that the major difference to chapter 2 is the presence of the coefficients C_S in the equations for $R(\theta)$.

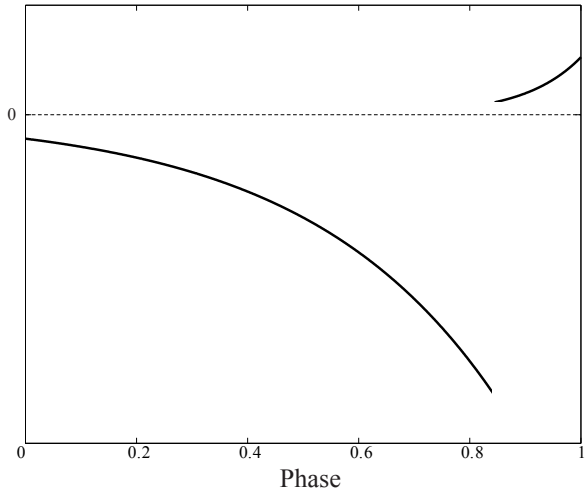

Figure 6.2.6: Response function of the modified McKean model.

6.3 Modified McKean Half-Center Model

It is interesting to revisit the half-center discussion of chapter 5 for this new model. The half center rhythm can be seen in figure (6.3.1). The half-center rhythm (not in singular limit) generated in figure (6.3.1) is obtained using on/off synapses. However, the action potentials generated are similar to those of the HH half-center seen in chapter 5 which used a difference of exponential synaptic kernel.

6.3.1 Feedback and Shunts

In biological simulations it is common to use voltage shunts, of the form

$$X(t) = g(v - v_s) \sum_m \eta(t - T^m)$$

where v_s is the reversal potential. The sign of the reversal potential relative to the steady state v^* determines whether the synapse is excitatory ($v_S > v^*$) or inhibitory

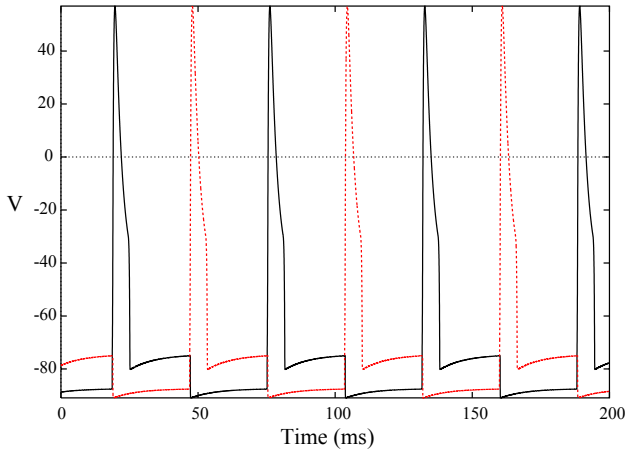

Figure 6.3.1: Half-center rhythm generated by the modified McKean model with on/off inhibitory coupling.

$(v_S < v^*)$. Shunts give more biologically realistic synaptic effects and so we use them in Hodgkin-Huxley simulations from now on.

The HH model with shunts can be seen in figure (6.3.2).

In the work by A Roberts and his colleagues it is clear that many neurons in the Xenopus tadpole have self feedback. Moreover this feedback is nearly always slow (compared to inhibition) and excitatory. We will therefore utilise slow excitatory self feedback in networks from now on.

In their work they have simulated voltage traces for a sophisticated half-center structure with a combination of excitatory and inhibitory synapses. The trace can be seen in figure (6.3.4).

To keep a simple form for the modified McKean half-center we make the approximation that in a stable spiking rhythm the slow excitation can be modelled as a positive constant. The affect of adding feedback to a half center construction can

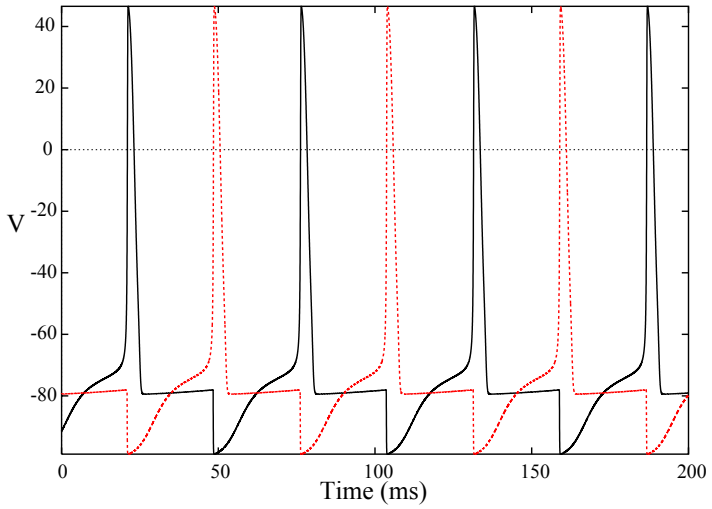

Figure 6.3.2: The half-center rhythm for two Hodgkin-Huxley neurons with only strong mutual inhibition. The inhibitory synapses are modelled with difference of exponentials synaptic kernel. Here $\alpha = 10$, $\beta = 0.5$ and $I = 0$.

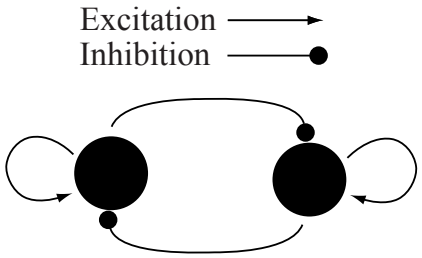

Figure 6.3.3: Two Neurons connected with either inhibitory or excitatory synapses.

be seen in simulations of both Hodgkin-Huxley and modified McKean Models in figures (6.3.5) and (6.3.6).

It is clear that slow feedback changes the shape of the post-synaptic voltage giving more defined plateaus. This gives a much better agreement with the experimental

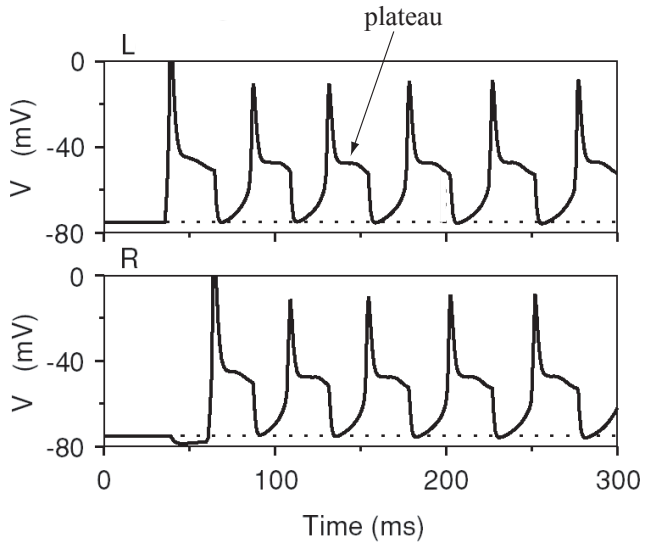

Figure 6.3.4: Simulated voltage trace by A Roberts and colleagues using four neurons with a combination of excitatory and inhibitory synapses (reproduced with permission from A. Roberts [82]).

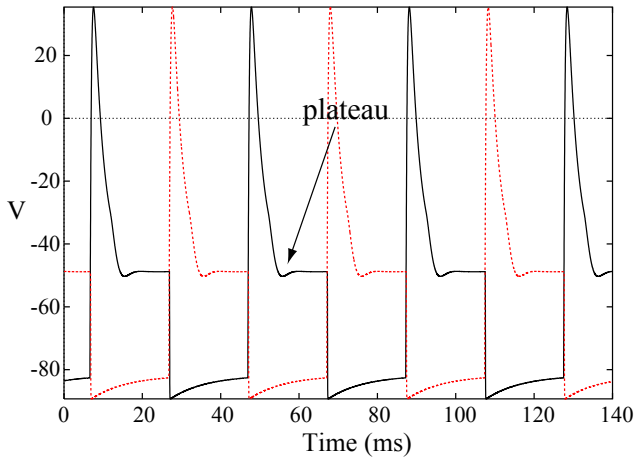

Figure 6.3.5: Half-center rhythm generated by the modified McKean model with on/off inhibitory coupling and constant excitatory feedback.

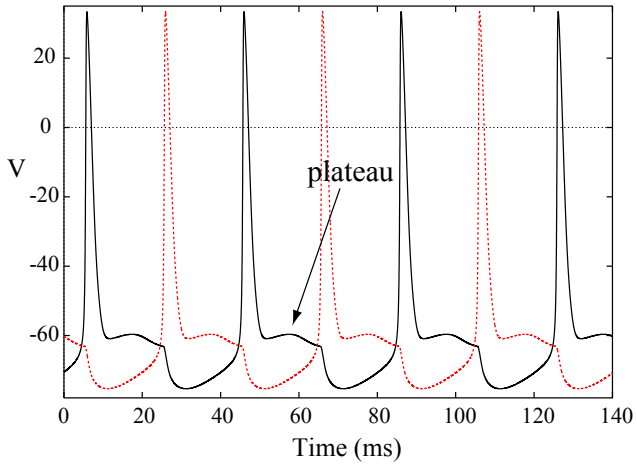

Figure 6.3.6: Half-center rhythm generated by the Hodgkin-Huxley model with inhibitory coupling and slow excitatory feedback (both using difference of exponential synaptic kernel and shunts).

results seen in figure (6.3.4). With an investigation into changing the parameters it would also seem that feedback makes the rhythm more robust to voltage and parameter perturbation than with only inhibition.

6.3.2 Exact Solution Of Half-Center

As mentioned above the idea of feedback can be taken as a constant background excitation E. When the opposing neuron fires there is a constant inhibition I for time τ. This means for this system the total input term I_T has the form $I_T = E + I\chi$ where χ is 1 during the inhibition and 0 otherwise. There are therefore three states defined by (S, χ). In effect this means that A_S from the single neuron model (6.6) and (6.7), becomes $A_{S,\chi} = \{(1,0),(1,1),(2,0)\}$.

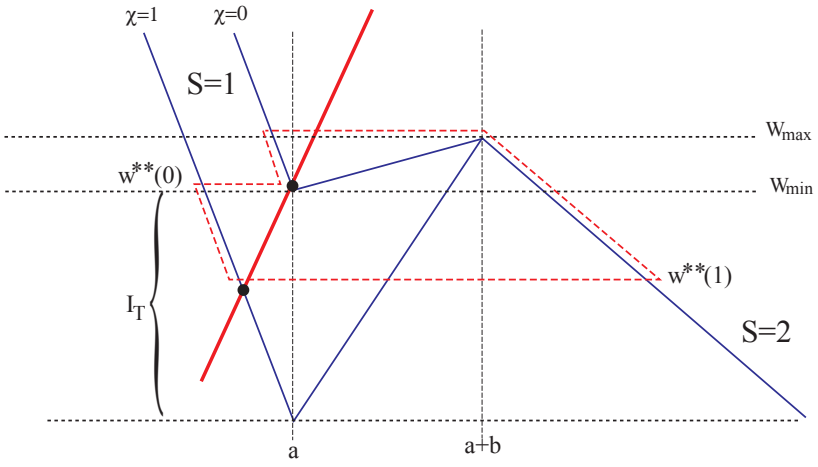

Figure 6.3.7: Construction of the modified McKean half-center. The system undergoes inhibition at point $w^{**}(0)$ on branch $(1,0)$ and the system moves to branch $(1,1)$ the system evolves toward the new equilibrium and but at some point $w^{**}(1)$ the inhibition is released and the system moves to branch $(2,0)$.

Hence, as in chapter 5, we write

$$\dot{w}_S \equiv G(w;S;\chi) = -\beta_S w + A_{S,\chi}. \tag{6.14}$$

Assuming there is no change in the state ((S,χ) remains fixed) then

$$t - t_0 = \frac{1}{\beta_S} \ln\left[\frac{-\beta_S w(t_0) + A_{S,\chi}}{-\beta_S w(t) + A_{S,\chi}}\right], \tag{6.15}$$

$$w(t;w(t_0),t_0,S,\chi) = w(t_0)\mathrm{e}^{-\beta_S(t-t_0)} + \frac{A_{S,\chi}}{\beta_S}\left[1 - \mathrm{e}^{-\beta_S(t-t_0)}\right]. \tag{6.16}$$

Generalising the approach of chapter 5 it is possible to the calculate the response

function. Without loss of generality we choose $\beta_1 = \beta_2 = \beta$), this gives

$$R(\theta) = \Omega \left[\frac{1}{G(\theta)} + \kappa_d \delta(\theta - \theta_d) + \kappa_u \delta(\theta - \theta_u) + \kappa_0 \delta(\theta) \right]$$

where

$$G(\theta) = \begin{cases} \mathrm{e}^{-\beta\theta\Delta}[A_{1,1} - \beta_1 w^{**}(0)], & 0 < \theta < \theta_u \\ \mathrm{e}^{-\beta(\theta-\theta_u)\Delta}[A_{2,0} - \beta_2 w^{**}(1)], & \theta_u < \theta < \theta_d \\ \mathrm{e}^{-\beta(\theta-\theta_d)\Delta}[A_{1,0} - \beta_1 w_{max}], & \theta_d < \theta < 1 \end{cases}$$

and

$$\kappa_u = \left(\frac{1}{G(\theta_u^+)} - \frac{1}{G(\theta_u)} \right), \qquad \kappa_d = \left(\frac{1}{G(\theta_d^+)} - \frac{1}{G(\theta_d)} \right), \qquad \kappa_0 = \left(\frac{1}{G(0)} - \frac{1}{G(1)} \right).$$

As in chapter 5 we define

$$R(t/\Delta) = \begin{cases} R_1(t) = \Omega \mathrm{e}^{\beta t} / \left[A_{1,1} - \beta_1 w^{**}(0) \right] & t/\Delta \bmod 1 \in [0, \theta_u) \\ R_2(t) = \Omega \mathrm{e}^{\beta t} \mathrm{e}^{-\beta\theta_u\Delta} / \left[A_{2,0} - \beta w^{**}(1) \right] & t/\Delta \bmod 1 \in (\theta_u, \theta_d) \\ R_3(t) = \Omega \mathrm{e}^{\beta t} \mathrm{e}^{-\beta\theta_d\Delta} / \left[A_{1,0} - \beta w_{max} \right] & t/\Delta \bmod 1 \in (\theta_d, 1) \end{cases} \tag{6.17}$$

The response function of the modified McKean half-center model is plotted in figure (6.3.8).

Using this response function it it possible, using the same method of chapter 3, to calculate the interaction function for the half-center network proposed in chapter 5 explicitly. It was shown in chapter 5 that the McKean model did not reproduce the biologically realistic simulations by Roberts $et\ al$.

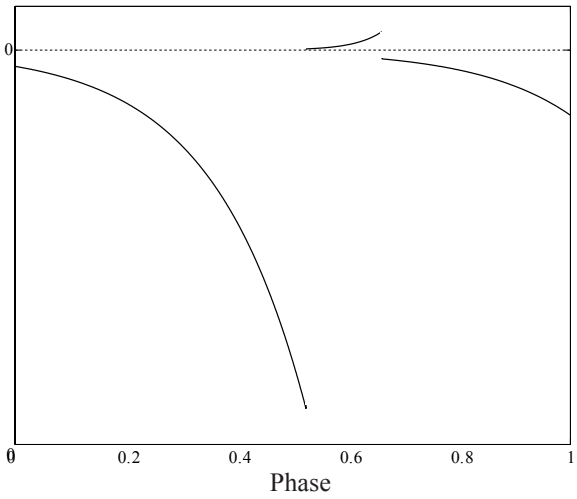

Figure 6.3.8: Response function of the modified McKean half-center model.

6.3.3 Modified McKean Half-Center Network

It is possible to calculate the explicit interaction function in the same way in chapter 3. Using the setup as shown in (5.3.2) two half center oscillators have the form

$$\dot{\theta}_1 = \Omega, \tag{6.18}$$

$$\dot{\theta}_2 = \Omega + R(\theta_2)X_L(t) + R(\theta_2 + 1/2)X_R(t), \tag{6.19}$$

Here X_L and X_R represent the synaptic inputs to the effective left and right side of the couple from neuron 1. If we assume that these synaptic inputs can be modelled as a convolution of incoming spike train with some synaptic response kernel.

$$X_L = \sum_m \eta_E(t - T_m^1) + \eta_I(t - T_m^1 + \Delta/2), \tag{6.20}$$

$$X_R = \sum_m \eta_I(t - T_m^1) + \eta_E(t - T_m^1 + \Delta/2). \tag{6.21}$$

As before T_m^1 represents the time of the mth spike from oscillator 1 and η_I (η_E) are the inhibitory (excitatory) synapses. Introduce the phase $\theta_n = \phi_n + \Omega t$, we have that $T_m^1 = (m - \phi_1)\Delta$. We can use the theory of averaging to give

$$\frac{\mathrm{d}\phi_1}{\mathrm{dt}} = 0, \tag{6.22}$$

$$\frac{\mathrm{d}\phi_2}{\mathrm{dt}} = \varepsilon H(\phi_1 - \phi_2) + O(\varepsilon^2). \tag{6.23}$$

The interaction function has four parts, one for each synapse.

$$H(\phi) = \frac{1}{\Delta}\int_0^{\Delta} R(t/\Delta)P_E(t + \phi\Delta) + R(t/\Delta)P_I(t + (\phi + 1/2)\Delta), \tag{6.24}$$

$$+ R(t/\Delta + 1/2)P_I(t + \phi\Delta) + R(t/\Delta + 1/2)P_E(t + (\phi + 1/2)\Delta)\mathrm{d}t. \tag{6.25}$$

Using the alpha function coupling we can calculate this function explicitly

Using the explicit form for the interaction function we can explore the relationship between the strength of coupling. Figure (6.3.9) shows the variation of the phase locked solution with the strength of combined ipsi-lateral and contra lateral coupling. It also shows that the network predicts the behaviour seen in the simulations. The discrepancy between the results as coupling increases is due to the explicit results being in the regime of $\mu \to 0$ and of weak coupling. This agrees with the results seen by Roberts $et\ al.$ [82] that the phase locked solution has a small phase difference that decreases to zero at a critical value and then the solution is lost as coupling strength increases. Although the solution shown in figure (6.3.9) tends to zero, it does so away from the weak coupling regime and as such the solution is no longer valid.

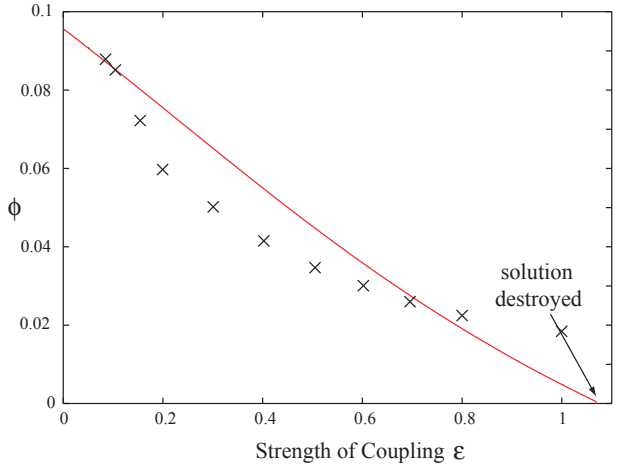

Figure 6.3.9: The effect of strength of combined ipsi-lateral and contra lateral coupling on the phase locked solution. The solid line shows the solution predicted by the explicit half-center network equations, the crosses mark results obtained by simulations of the same system.

6.4 Chain Of Oscillators

Weakly coupled oscillator arrays can be used to model many physical and biological systems [100] [61] [101, 102, 103, 104, 105] Systems such as swimming in the Xenopus tadpole discussed earlier, and are often modelled using a one dimensional chain. This is illustrated in figure (6.4.2).

These chains can produce travelling wave solutions which can be interpreted as the swimming motion that these animals exhibit. These travelling waves can be shown to exist even with only nearest neighbour coupling (although in the real animals the connections tend to be far from nearest neighbour). Work with non-nearest neighbour coupling shows travelling wave solutions exist [106], as well as more advanced behaviour such as S-waves. An S-wave is where the front section

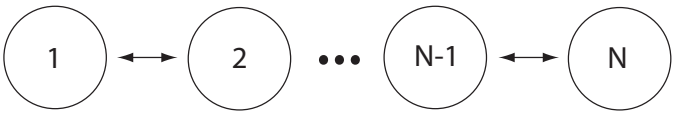

Figure 6.4.1: Notion of a simple N neuron chain with bi-directional coupling.

of a body contracts on one side, whilst the back contracts on the other. It is associated with later stages of animal development in animals such as the salamander [99]. Under the assumption of weak coupling and limiting the focus to nearest neighbour coupling, each oscillator can be reduced to a one dimensional phase variable. Consider a chain of size $n+1$, general phase equation that can be written in the form

$$\dot{\theta}_i = \omega_i + \epsilon \left[H^+(\theta_{i+1}, \theta_i) + H^-(\theta_{i-1}, \theta_i) \right] \qquad i = 1, ..., n+1 \tag{6.26}$$

Where the functions $H^{\pm}$ are 2π periodic, ω_i are the uncoupled frequencies and $\epsilon \ll 1$. We also have the boundary condition

$$H^+(\theta_{n+2}, \theta_{n+1}) \equiv 0 \equiv H^-(\theta_0, \theta_1) \tag{6.27}$$

Under the assumption of weak coupling we can apply the theory of averaging as in chapter 3. Therefore $H^{\pm}(\theta_i, \theta_j)$ can be written as $H^{\pm}(\theta_j - \theta_i)$. Using the identity $\phi_i = \theta_{i+1} - \theta_i$, (6.26) can be written as

$$\dot{\phi}_i = \Delta_i + \epsilon \left[H^+(\phi_{i+1}) - H^+(\phi_i) - H^-(-\phi_{i+1}) + H^-(-\phi_i) \right] \qquad i = 1, ..., n \tag{6.28}$$

Here $\Delta_i = \omega_{i+1} - \omega_i$ are variations in frequencies between oscillators and the boundary conditions (6.27) become

$$H_n^+(\phi_{i+1}) \equiv 0 \equiv H^-(-\phi_0).$$

For large n it is possible to approximate (6.28) by a partial differential equation (P.D.E.), which can be considered as a continuum limit. It can be shown that this continuum limit behaves like the original system. The P.D.E. predicts that phase locking is not sustained for arbitrarily large frequency gradients and this can lead to frequency plateaus [107] [61]. Critical points of (6.28) are associated with time independent solutions to this P.D.E., which is a nonlinear singularly perturbed two-point boundary value problem. For certain $H^{\pm}$ this can be solved uniquely and an extensive review is given in [**?**].

6.4.1 Simple Example

Following the example in [108], we can choose a simple $H^{\pm}$. It is then possible to simulate (6.28) which can give and idea of what to expect from more complicated $H^{\pm}$ functions. Imagine a chain of $n+1$ neurons, From (6.28), we can consider the equations to have the form.

$$\begin{aligned}
\dot{\phi}_1 &= \omega_1 + H^+(\phi_2) - H^+(\phi_1) + H^-(-\phi_1), \\
\dot{\phi}_i &= \omega_i + H^+(\phi_{i+1}) - H^+(\phi_i) + H^-(-\phi_i) - H^-(-\phi_{i-1}), \\
\dot{\phi}_n &= \omega_n - H^+(\phi_n) + H^-(-\phi_n) - H^-(-\phi_{n-1}),
\end{aligned}$$

Where ,

$$H^+(\phi) = H^-(\phi) = 0.5 * \cos(\phi) + \sin(\phi). \tag{6.29}$$

It has been seen already in chapter 3 that the interaction function can be written as a Fourier series. Hence (6.29) can be considered as a first approximation to a more complicated interaction function. First consider the simple case where there is no frequency gradient across the chain (i.e. ω_i for all i), figure (6.4.2) shows the

solution with $n = 36$. This shows the that the phase differences ϕ_i spread across the

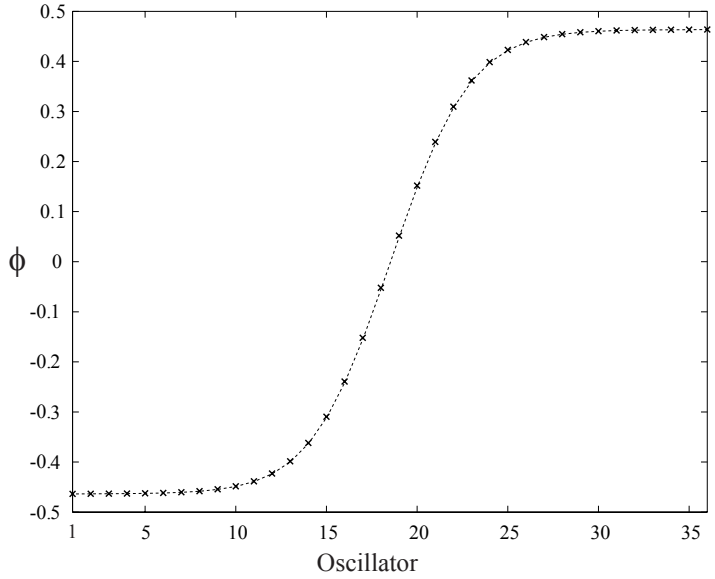

Figure 6.4.2: Relative phases of the phase locked solution of 37 oscillators.

chain. However it is common to have a frequency gradient in a chain of oscillators and much work is performed in this area [109].

If we give this simple system a frequency gradient we can see in figure (**??**) that it results in a significant boundary effect. This characteristic shape is widely seen in chains with a frequency gradient across it, and for simple systems these boundary layers can be explicitly calculated [108]. There is a limitation of this chain theory, there is no idea of sides (left / right) in such a chain. It is desirable to re-examine this theory with a notion of left and right.

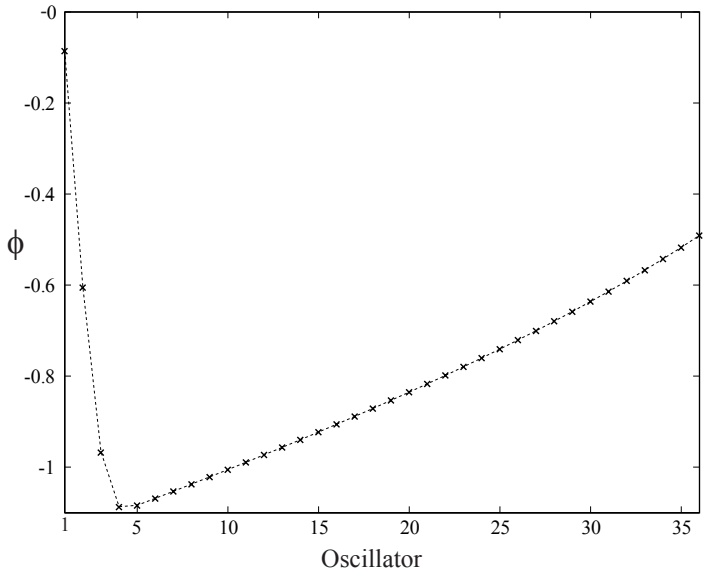

Figure 6.4.3: Relative phases of the phase locked solution of 37 oscillators with a frequency gradient.

6.5 Travelling Waves In A Half-Center Chain

In order to model the spinal cord of the tadpole, we must get our queues from biological experiments. In systems such as that of the spinal cord of tadpoles, the motor neurons on opposite sides of the cord which oscillate with a robust anti-phase rhythm during swimming. This suggests the use of the half-center construction to better model the two distinct sides of the spinal cord, rather than with a single neuron model or single pool of neurons for both sides.

Mimicking the real neuronal connections and construction seen in the tadpole is a difficult undertaking, even for the simple models we have. The approximate con-

nections, axon lengths and neuron density for the length of the body are roughly known from experimental work [94]. However trying to ascertain what information is critical, so that it is possible to simplify the connections, is a real challenge. Simulating a chain of neurons with all the different connection possibilities would be useful to find how simple the model can get, but would be a mammoth undertaking. The investigation will therefore be focused on the construction of vertical connections being excitatory and diagonal connections being inhibitory, the form chosen in chapter 5 for a small network. This limitation is reasonable as there is some biological evidence for this choice [76]. We would expect to see travelling wave solutions for this form.

6.5.1 Chain Of Half-Centers

In the tadpole there are distinct left and right sides to the spinal cord. There is motivation therefore to construct a chain of half-centers as this would allow the retention of the notion of a left and a right side. This construction is illustrated in figure (6.5.1).

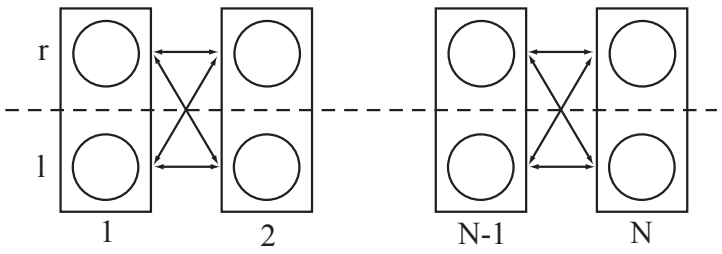

Figure 6.5.1: Illustration of a bi-directional coupling in a chain of half-centers.

In the last chapter we saw that for a network of two half-centers, the interaction

function could be calculated. Moreover the interaction function can be split into sub functions for each direction of connection. We also only have to regard one side of the cord if we assume weak coupling between half-centers because one side will be exactly out of phase with the other (i.e. $H_L(\phi) = H_R(\phi - 1/2)$). Considering just the left side, we can write from equation (6.27)

$$\begin{aligned}
\dot{\phi}_1 &= H^+(\phi_2) - H^+(\phi_1) + H^-(-\phi_1), \\
\dot{\phi}_i &= H^+(\phi_{i+1}) - H^+(\phi_i) + H^-(-\phi_i) - H^-(-\phi_{i-1}), \\
\dot{\phi}_{N-1} &= -H^+(\phi_{N-1}) + H^-(-\phi_{N-1}) - H^-(-\phi_{N-2}),
\end{aligned}$$

where each function $H^{\pm} = H_L^{\pm} + H_R^{\pm}$ can be thought of as the input from the above left (H_L^+), above right (H_R^+), below left (H_L^-) and below right (H_R^-). These interaction functions can either be calculated explicitly (such as in the case of the modified McKean model with alpha function coupling), or we can use a Fourier expansion (such as was shown for the Hodgkin-Huxley model in chapter 3).

All of the mathematical tools are now in place to make a model of the tadpole.

6.5.2 Results Of Half-Center Chains

From (**??**) we have a set of equations and using the method in chapter 3 with the response function (6.17) we can calculate the interaction function for the half-center MM. We can also use brute force simulations for both a Hodgkin-Huxley and MM half-center chain. From the results obtained in sub-section (6.17) with a simple interaction function, we would expect to see a travelling wave solutions.

Exact Results

Using the interaction function for the modified McKean model we can simulate a bi-directional chain with excitatory ipsi-lateral and inhibitory coupling contra-lateral, nearest-neighbour coupling. The relative phases of the phase locked solution of 36 half centers can be seen in figure (6.5.2). This shows that a chain of

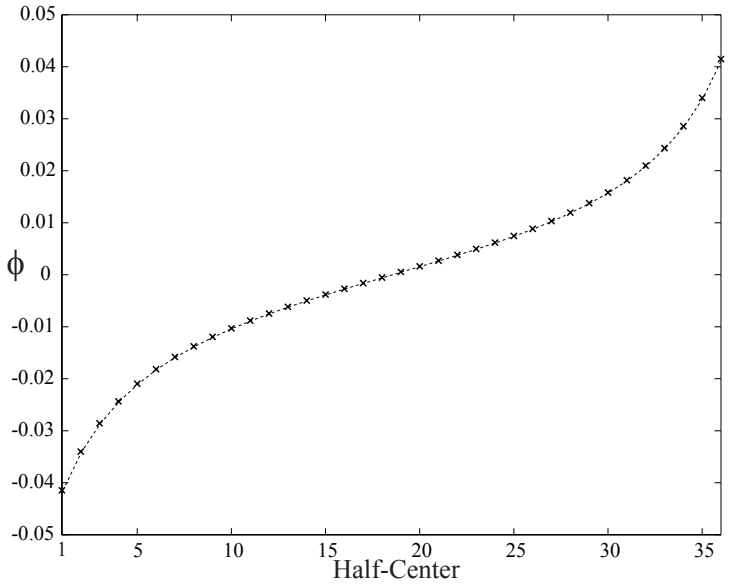

Figure 6.5.2: Relative phases of the phase locked solution of a chain of 37 MM half-centers.

half-centers produces a travelling wave solution.

It is possible to introduce a small frequency gradient into this system as in section (6.4.1). As the gradient is small (in magnitude and gradient) then it doesn't invalidate the assumptions made in the calculation of the interaction function. The relative phases of the phase locked solution of 36 half centers with a small frequency gradient can be seen in figure (6.5.3). This shows a similar boundary effect as with the simple example, except that the boundary effect is less pronounced.

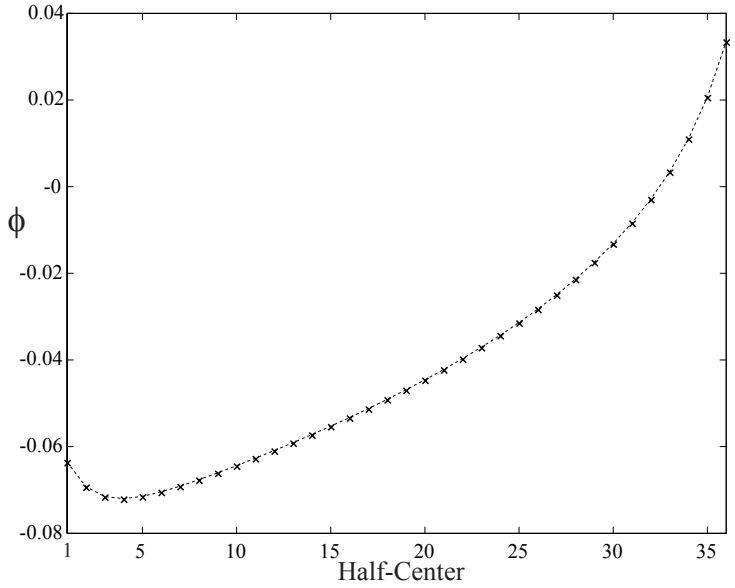

Figure 6.5.3: Relative phases of the phase locked solution of a chain of 37 MM half-centers with a small frequency gradient.

The subtlety of the boundary effect is in part down to the small size of the frequency gradient.

Simulation Results

As well as the exact solution it is also possible to simulate chains. We have written a MATLAB program to simulate a half-center chain with modified McKean or Hodgkin-Huxley models. These use shunts and differential of exponential synapses. We now can compare this biologically realistic chain with the mathematically tractable exact solution. Figures (6.5.4) and (6.5.5) show the simulation results of Hodgkin-Huxley and McKean half center chains. These show that the distribution of the relative phases of the HH and MM are consistent with each other in the sense that $\phi < 0$ for N¡18 and $\phi > 0$ for N¿18. This correlation is expected as the MM model

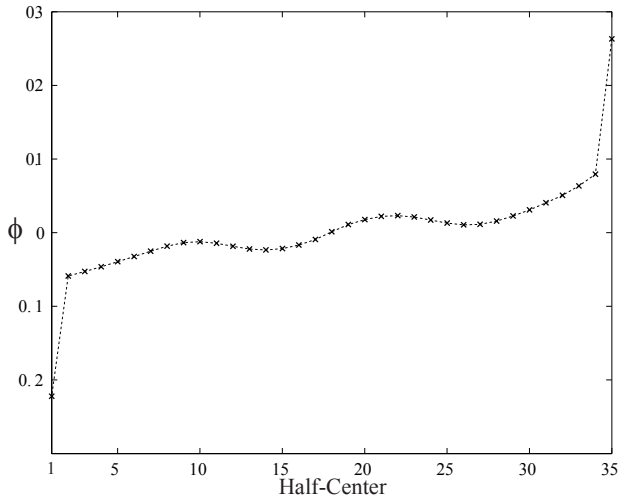

Figure 6.5.4: Relative phases of the phase locked solution of a simulated chain of 36 Hodgkin-Huxley half-centers. Contra-lateral and ipsi-lateral coupling strengths $= 0.5$..

was constructed to mimic the HH model and all of the connection and synaptic parameters are the same for both simulations. The MM and HH results are also similar to those of the exact solution for MM.

There are two reasons why there is a small disagreement between the exact solution of MM and the simulations of MM. Firstly the exact solution has on/off inhibitory synapses and a constant background excitation whereas the simulations

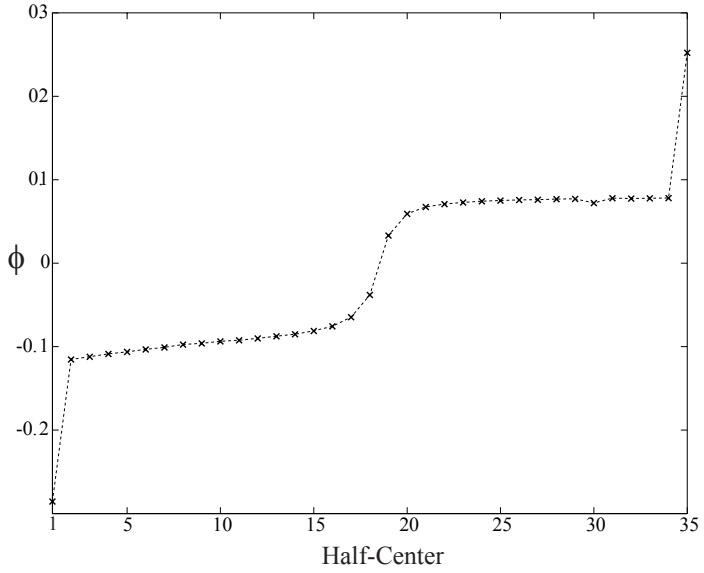

Figure 6.5.5: Relative phases of the phase locked solution of a simulated chain of 36 MM half-centers. Contra-lateral and ipsi-lateral coupling strengths $= 0.5$.

have both excitatory and inhibitory difference of exponentials synapses. Secondly the coupling strengths in the simulations are large but by assumption they are not for the explicit solution. These results do show however, that the simplifications made to the half-center chain to enable the calculation of the interaction function have not drastically changed the resulting travelling wave behaviour.

In these simulations it is possible to create the property of the wavelength being equal to the bodylength. This can be achieved by adjusting the frequency of the top and bottom oscillators [110] [105].

6.5.3 Frequency Gradient

For the Modified McKean model, one method of slightly changing the period of the oscillations is to change the value of the parameter μ_2 by some small amount (see equations (6.8) and (6.9)). If the amount of this variable is changed too much then it moves away from the HH like behaviour. This is a simple way of exploring what happens if there is some small frequency gradient in the system. Figure (6.5.6) shows the effect of a small frequency gradient on the relative phase distribution of a MM half-center chain.

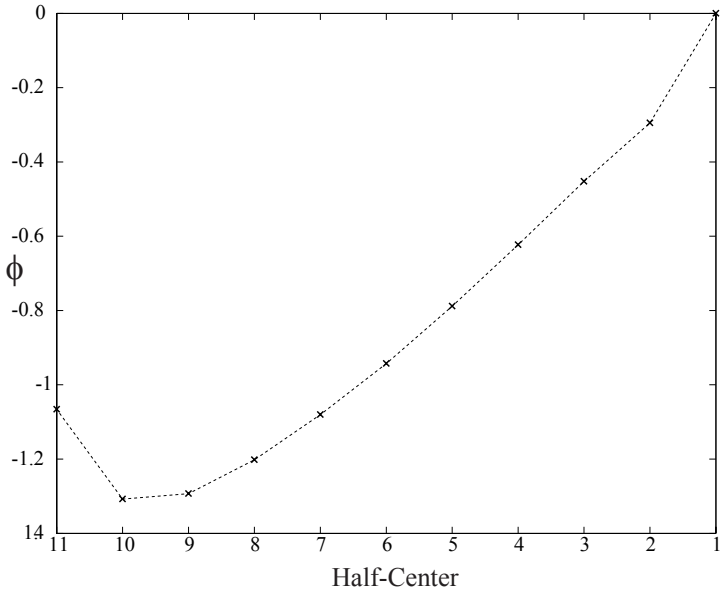

Figure 6.5.6: The effect of a small frequency gradient on the relative phase distribution of a MM half-center chain with 12 half-centers.

6.5.4 Oscillator Death

It is clear from the assumptions made to calculate the interaction function that the exact solution cannot tell us anything about the behaviour away from the weak coupling regime. However it is possible using the brute force simulations to investigate what happens as the strength of coupling is increased. It has been shown that under strong coupling, a chain can exhibit oscillator death [41] [111]. This is where large interactions cause the cessation of oscillations. This was seen in the simulations of both HH and MM models when the excitatory ipsi-lateral coupling was increased to the magnitude of the coupling within the half-center. This does not happen when increasing the inhibitory contra-lateral coupling. Oscillator death in the HH case can be seen in figure (6.5.7) where the system started in a robust half-center rhythm.

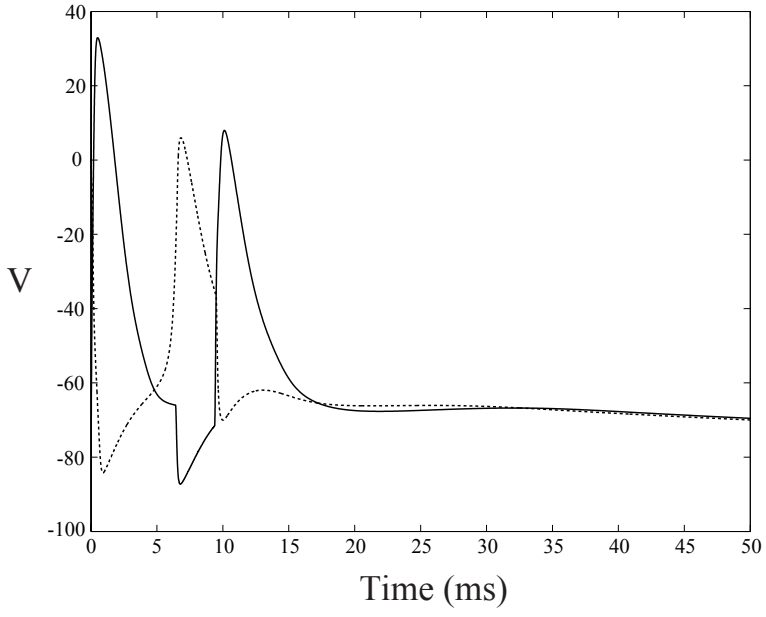

Figure 6.5.7: Oscillator death through strong ipsi-lateral and contra-lateral coupling in a chain of Hodgkin-Huxley half-centers.

This is one method can be used to stop the oscillation of the chain of half-centers. This suggests that a large signal propagating the whole spinal cord of the tadpole, could be one method of stopping the swimming motion.

6.6 Conclusions

In this chapter the neuro-chemistry and anatomy of the hatchling Xenopus tadpole was reviewed. A new model was then defined, one that had the advantage of being mathematically tractable but that was fitted to the phase plane and timescales of the reduced HH model. The model was named the modified McKean model. This MM model was then used to create a half-center oscillator and it was shown that this construction was also analytically tractable under the assumption of on/off synapses. This allowed the explicit calculation of the interaction function for the weakly coupled half-center network proposed in chapter 5. It was shown that the MM model was consistent with the results of Roberts $et\ al$, where the McKean model had not been.

A chain of oscillators was then proposed and a review of simple oscillator chains results was given. We then proposed a half-center chain as a useful model of the tadpole spinal cord. With a wealth of biological data, the construction of the chain was limited to an anatomically motivated simplification. With this construction the phase dynamics were solved explicitly for the MM model in the weak coupling limit. It was then shown that direct simulations for MM and HH with the same network construction but away from the weak coupling limit yielded results consistent with the exact solution. This approach was a combination of a new model of a spiking neuron, a simple half-center construction (with on/off synapses) and the theory of coupled oscillator chains.

Chapter 7

Conclusions and Further Work

7.1 Conclusions

In this thesis the focus of the work has been on investigating the necessity of using a realistic, albeit complicated, system such as Hodgkin-Huxley to model biological systems. Whilst there is no doubt that if quantifiable biological data is needed the Hodgkin-Huxley model is best, in a lot of situations it is the qualitative behaviour that is of interest. The work in this thesis has illustrated the fact that more simple models can replicate the behaviour seen in more complicated models. Of particular interest has been the McKean model as it is the simplest model that can generate action potentials.

For small networks the McKean model has been shown to accurately replicate the behaviour of the Hodgkin-Huxley model. With the restriction of strong relaxation and weak coupling, it was shown that the powerful machinery of coupled oscillator theory could be used to study phase-locked states in synaptically coupled McKean networks.

The study of real neural networks, which typically possess thousands of neurons, presents a highly non-trivial challenge. To make progress in this direction a continuum description was adopted. This allowed the study of large network properties without having to solve an impractical number of equations. Phase interaction functions for McKean and Hodgkin-Huxley networks were calculated. The use of Fourier techniques further enabled the practical calculation of the stability of travelling wave solutions in the continuum limit. We showed that an exponential or square synaptic weight function gave us the same travelling wave stability pictures for both the McKean and Hodgkin-Huxley models. This has more readily allowed us to establish that the nature of stability for these travelling waves in McKean and Hodgkin-Huxley networks is entirely consistent. We also looked at the dynamics of the dendritic tree. It was shown that a simplified notion of a dendrite acts like a discrete delay. This was attributed to the periodicity of the equations defining a phase-locked state.

Next we showed that it was possible to create an oscillatory network with non-oscillatory neurons using only inhibitory synapses and with no external input. Moreover this was found to be robust to noise and parameter perturbation. We explained that the rhythm relies on reciprocal inhibition and anode break excitation. It was shown analytically that in a uni-directional weakly coupled network of half-centers, there was a phase locked state with a small phase difference between half-centers. Interestingly this was in agreement with results of simulations by Roberts $et\ al$ [82].

This suggested that a chain of uni-directionally coupled neurons would exhibit a phase difference between each half-center, generating a wave across the chain. Unfortunately the McKean half-center network was shown not to match the behaviour of the Hodgkin-Huxley half-center network. This discrepancy prompted the construction of a new model to more closely mimic the Hodgkin-Huxley model.

This modified McKean model was shown to mimic the Hodgkin-Huxley model very closely, both quantitatively and qualitatively.

We then focussed on the work of Roberts $et\ al$. [95, 89, 87], on the modelling of the spatially extended tadpole. In their work they simulate sections of the spinal cord in great detail using the Hodgkin-Huxley model. It was shown in the last chapter that the modified McKean model could replicate the same behaviour as the Hodgkin-Huxley model in a chain of half-centers. Importantly the network equations for the modified McKean model were found to generate swimming waves consistent with those seen in fictive swimming. The fact that this model successfully mimics the Hodgkin-Huxley model whilst being mathematically tractable is a great benefit.

7.2 Future Work

There are several areas that could be continued in further work. One obvious place to start would be to investigate the new model that was described in the last chapter in greater detail. It would be of interest to investigate the small network and continuum behaviour of this model along the lines of chapters 3 and 4.

There is increasing interest in networks with strong coupling [74, 59] [8] [112]. It would be interesting to see what progress could be made with this new model even if purely by simulation, since there is no general theory for strongly coupled oscillators.

Looking at non-nearest neighbour coupling would be of interest as it can be seen that the axon projections in the tadpole can be of significant length [94]. In this case the use of techniques in chapter 4, where we explicitly incorporated axonal delays,

might be useful.

Finally we are in an ideal position to study further aspects of tadpole dynamics, not just the swimming motion. In particular the onset of bursting behaviour seen during struggling [88]. This is clearly a driven system that could easily be treated with the modelling framework that has been developed in this thesis. There is now an extensive suite of MATLAB programs (which were in development for several months) available for just such a purpose and it is planed that these will be used by members of Alan Roberts group at the university of Bristol. This code will also be freely available on the world wide web.

Chapter 8

Appendices

8.1 Appendix A - Model Parameters

Hodgkin-Huxley

In chapters 2-5 Hodgkin-Huxley parameters, unless otherwise stated, are :-

$C = 1$, $g_L = 0.3$, $g_K = 36$, $g_{Na} = 120$, $v_L = -54.402$, $v_K = -77$, $v_{Na} = 50$

$$a_m A = -4,\ a_m B = -0.1,\ a_m C = -1,\ a_m D = 40,\ a_m F = -10$$
$$a_h A = 0.07,\ a_h B = 0,\ a_h C = 0,\ a_h D = 65,\ a_h F = 20$$
$$a_n A = -0.55,\ a_n B = -0.01,\ a_n C = -1,\ a_n D = 55,\ a_n F = -10$$
$$b_m A = 4,\ b_m B = 0,\ b_m C = 0,\ b_m D = 65,\ b_m F = 18$$
$$b_h A = 1,\ b_h B = 0,\ b_h C = 1,\ b_h D = 35,\ b_h F = -10$$
$$b_n A = 0.125,\ b_n B = 0,\ b_n C = 0,\ b_n D = 65,\ b_n F = 80$$

In chapter 6 the Hodgkin-Huxley parameters, unless otherwise stated, are :-

$C = 1$, $g_L = 0.3$, $g_K = 36$, $g_{Na} = 120$, $v_L = -74.48$, $v_K = -79.755$, $v_{Na} = 50$

$$a_m A = -5,\ a_m B = -0.1,\ a_m C = -1,\ a_m D = 50,\ a_m F = -10$$
$$a_h A = 0.07,\ a_h B = 0,\ a_h C = 0,\ a_h D = 75,\ a_h F = 20$$
$$a_n A = -0.1625,\ a_n B = -0.0025,\ a_n C = -1,\ a_n D = 65,\ a_n F = -10$$
$$b_m A = 4,\ b_m B = 0,\ b_m C = 0,\ b_m D = 75,\ b_m F = 18$$
$$b_h A = 1,\ b_h B = 0,\ b_h C = 1,\ b_h D = 45,\ b_h F = -10$$
$$b_n A = 0.03125,\ b_n B = 0,\ b_n C = 0,\ b_n D = 75,\ b_n F = 80$$

FitzHugh-Nagumo

Unless otherwise stated the FitzHugh-Nagumo model parameters are :-

$a = 0.25$, $\mu = 0.005$, $\gamma = 0.5$, $v_0 = 0$, $w_0 = 0$

McKean

Unless otherwise stated the McKean model parameters are :-

$a = 0.25$, $\mu = 0.01$, $\gamma = 0.5$, $v_0 = 0$, $w_0 = 0$

Modified McKean

Unless otherwise stated the McKean model parameters are :-

$a = -74.2$, $b = 44.45$, $a_0 = -80$, $b_0 = 48.96$, $w_1 = -75.8$, $w_2 = -51.1$

$\gamma = 0.5$, $\mu_1 = 0.1$, $\mu_2 = 11.2818$, $\rho = 0.68$, $v_0 = 0$, $w_0 = 0$

8.2 Appendix B - XPP Code

```
############################################################

# Hodgkin-Huxley model with chapter 6 parameters.
par C=1,gL=0.3,gK=36,gNa=120,VL=-74.48,VK=-79.755,VNa=50
par J=20



par amA=-5, amB=-0.1, amC=-1, amD=50, amF=-10,
par ahA=0.07, ahB=0, ahC=0, ahD=75, ahF=20
par anA=-0.1625, anB=-0.0025, anC=-1, anD=65, anF=-10
par bmA=4, bmB=0, bmC=0, bmD=75, bmF=18
par bhA=1, bhB=0, bhC=1, bhD=45, bhF=-10
par bnA=0.03125, bnB=0, bnC=0, bnD=75, bnF=80

alpham(x)=(amA+amB*x)/(amC+exp((x+amD)/amF))
alphah(x)=(ahA+ahB*x)/(ahC+exp((x+ahD)/ahF))
alphan(x)=(anA+anB*x)/(anC+exp((x+anD)/anF))
betam(x)=(bmA+bmB*x)/(bmC+exp((x+bmD)/bmF))
betah(x)=(bhA+bhB*x)/(bhC+exp((x+bhD)/bhF))
betan(x)=(bnA+bnB*x)/(bnC+exp((x+bnD)/bnF))

taum(x)=1.0/(alpham(x)+betam(x))
```

```
taun(x)=1.0/(alphan(x)+betan(x))
tauh(x)=1.0/(alphah(x)+betah(x))
minfty(x)=alpham(x)*taum(x)
ninfty(x)=alphan(x)*taun(x)
hinfty(x)=alphah(x)*tauh(x)
v'=1.0/C*(-gL*(v-VL)-gK*n*n*n*n*(v-VK)-gNa*h*m*m*m*(v-VNa)+J)
m'=1.0/(taum(v))*(minfty(v)-m)
n'=1.0/(taun(v))*(ninfty(v)-n)
h'=1.0/(tauh(v))*(hinfty(v)-h)
@meth=rungekutta,dt=0.01,total=50,maxstore=10000000
@done
############################################################

# McKean Model
par a=0.25,mu=0.01,I=0.0,gamma=0.5, w0=0, v0=0

f(x)=heav(a/2-x)*(-x)+heav(x-a/2)*heav((1+a)/2-x)*(x-a)+heav(x-(1+a)/2)*(1-x)
v'=1.0/mu*(f(v)- w-w0 +I )
w'=v-gamma*w -v0
@ meth=rungekutta,dt=0.01,total=20
@ done
############################################################

#McKean Half-Center Model
#Simulation of two square-pulse coupled McKean neurons with reciprocal inhibition
#tau is duration of IPSP
par I=0.0,w0=0,v0=0,gamma=0.5,a=0.25,epsilon=1,mu=0.01,tau=2.5
beta=1+gamma
```

```
v1(0)=0
v2(0)=1
w1(0)=-1
w2(0)=0
X[1..2](0)=0

global 1 {v1-(1+a)/2}{X1=1}
global 1 {v2-(1+a)/2}{X2=1}

f(x)=-x*heav(a/2-x) + (x-a)*heav(x-a/2)*heav((1+a)/2-x) +(1-x)*heav(x-(1+a)/2)

v1'=1.0/mu*(f(v1)-w1-w0+I-epsilon*heav(X2))
v2'=1.0/mu*(f(v2)-w2-w0+I-epsilon*heav(X1))
w1'=v1-gamma*w1-v0
w2'=v2-gamma*w2-v0
X[1..2]'=-heav(X[j])/tau

@meth=stiff,dt=0.01,total=20
@done
###############################################################

#Modified McKean Model
# all pars in the first line are fitted to HHR (chapter 6 figure (6.2.1))
par a=-74.2,b=44.45,a0=-80,b0=48.96,w1=-75.8,w2=-51.1
par mu1=0.1,mu2=11.2818,I=2.6,rho=0.68,w0=0,v0=0
#rho is a input scaling constant to better match the
#effect of current on the nullclines of HHR
par thr=-35,d1=0,d2=0
```

```
global 1 {v-thr}{d1=d2;d2=t}
aux period=d2-d1
# simple period of oscillation calculator

g=(w2-(w1+rho*I))/b
c=0.5*(w1+w2+rho*I-(2*a+b)*g1)
gamma=1
m1=(w2-w1)/(a-a0)
m2=(w2-w1)/(b0-(a+b))

f(x)=(w2+rho*I-(x-a0)*m1)*heav(a-x) + (g*x+c)*heav(x-a)*heav(a+b-x)
+(w2-(x-(a+b))*m2)*heav(x-b-a)

v'=(1/mu1)*(f(v) - w-w0)
w'=(1/mu2)*(v-gamma*w-v0)

@ meth=rungekutta,dt=0.01,total=100,maxstore=1000000
@ done
###############################################################
```

Bibliography

[1] A T Winfree. Biological rhythms and the behaviour of populations of coupled oscillators. *J. Theor. Biol.*, 16:15–42, 1967.

[2] A T Winfree. *The Geometry of Biological Time*. Springer-Verlag, New York, 1980.

[3] G B Ermentrout. An adaptive model for synchrony in the firefly Pteroptyx Malaccae. *Journal of Mathematical Biology*, 29, 1991.

[4] G B Ermentrout. Firefly synchrony. *Nature*, 353, 1991.

[5] R E Mirollo and S H Strogatz. Synchronization of pulse-coupled biological oscillators. *SIAM Journal on Applied Mathematics*, 50:1645–1662, 1990.

[6] S H Strogatz. From Kuramoto to Crawford: Exploring the onset of synchronization in populations of coupled oscillators. *Physica D*, 143:1–20, 2000.

[7] B Van Der Pol and J Van Der Mark. The heartbeat considered as a relaxation oscillator and an electrical model of the heart. *Philos. Mag*, 6:763–775, 1928.

[8] D W Storti and R H Rand. Dynamics of two strongly coupled relaxation oscillators. *SIAM Journal On Applied Maths*, pages 56–67, 1986.

[9] B Braaksma and J Grasman. Critical dynamics of the Bonhoeffer-van der Pol equation and its chaotic response to periodic stimulation. *Physica D*, 68:265–280, 1993.

[10] Yulia Timofeeva. *Oscillations And Waves In Single And Multi-Cellular Systems With Free Calcium*. PhD thesis, Department of Mathematical Sciences Loughborough University, 2003.

[11] J Marchant X-P Sun, N Callamaras and I Parker. A continuum of insp3-mediated elementary Ca2+ signaling events in xenopus oocytes. *Journal of Physiology (London)*, 509:67–80, 1998.

[12] H Berger. Heber rechestorungen bei herderkrankengen des grosshirns. *Arch. Psychiatr. Nervenkr.*, 78:238–263, 1926.

[13] B Hille. *Ionic Channels of Excitable Membranes*. 1991.

[14] M R Dawson. *Minds and Machines: Connectionism and Psychological Modeling*. 2003.

[15] C M Gray. Synchronous oscillations in neuronal systems : Mechanisms and functions. *Journal Of Computational Neuroscience*, 1:11–38, 1994.

[16] N Kopell and G B Ermentrout. Symmetry and phaselocking in chains of weakly coupled oscillators. *Physica D*, 39:623–660, 1986.

[17] P R Roelfsema, A K Engel, P Konig, and W Singer. Visuomotor integration is associated with zero time-lag synchronizationamong cortical areas. *Nature*, 385:157161, 1997.

[18] Stuart, Spruston, and Hausser. *Dendrites.* Oxford University Press, 1999.

[19] L Hodgkin and A F Huxley. A quantitative description of membrane and its application to conduction and excitation in nerve tissue. *Journal of Physiology (London)*, 116:449–472, 1952.

[20] A L Hodgkin and A F Huxley. A qualitative description of membrane current and its application to conduction and excitation in nerve. *Journal of Physiology (London)*, 117:500–544, 1952.

[21] R FitzHugh. Mathematical models of excitation and propagation in nerve tissue. *In Biological Engineering*, 116:1–85, 1969.

[22] R FitzHugh. Impulses and physiological states in models of nerve membrane. *Biophysical Journal*, 1:445–466, 1961.

[23] J Nagumo, S Arimoto, and S Yoshizawa. An active pulse transmission line simulating nerve axon. *Proceedings of the Institute of Radio Engineers*, 50:2061–2070, 1962.

[24] R A Gray. Termination of spiral wave breakup in a FitzHugh-Nagumo model via short and long duration stimuli. *Chaos*, 12, 2002.

[25] L Lapicque. Recherches quantatives sur l'excitation electrique des nerfs traitee comme une polarization. *J Physiol Pathol Gen*, 9:620–635, 1907.

[26] H P McKean. Nagumo's equation. *Advances in Mathematics*, 4:209–223, 1970.

[27] G B Ermentrout. Type I membranes, phase resetting curves and syncrony. *Neural Computation*, 8, 1996.

[28] G B Ermentrout. XPP. http://www2.pitt.edu/∼phase/.

[29] G B Ermentrout. *Simulating, Analyzing, And Animating Dynamical Systems : A Guide To Xppaut For Researchers and Students.* SIAM, 2002.

[30] A L Hodgkin and W A H Rushton. The electrical constants of a crustacean nerve fibre. *Proc. Roy. Soc. Lond. B. Bio.*, 133, 1946.

[31] A L Hodgkin. Ionic exchange and electrical activity in nerve and muscle. *Arch. Sci. Physiol.*, 3, 1949.

[32] A F Huxley A L Hodgkin and B Katz. Ionic currents underlying activity in the giant axon of the squid. *Arch Sci Physiol*, 3, 1949.

[33] A L Hodgkin and A F Huxley. Propagation of electrical signals along giant nerve fibres. *Proc. Roy. Soc. Lond. B. Bio.*, 140, 1952.

[34] J Hugenard and D A McCormick. *Electrophysiology Of The Neuron.* Oxford University Press, 1996.

[35] Bard Ermentrout. Neural networks as spatio-temporal pattern forming systems. *Rep. Prog. Phys.*, 61:353–430, 1998.

[36] C Morris and H Lecar. Voltage oscillations in the barnacle giant muscle fiber. *Journal of Biophysics*, 35:193–213, 1981.

[37] L F Abbott. A network of oscillators. *Journal of Physics A*, 23:3835–3859, 1990.

[38] J Keener and J Sneyd. *Mathematical Physiology*. Springer-Verlag, 1998.

[39] J P A Foweraker, D Brown, and R W Marrs. Discrete time simulation of the oscillatory and excitable forms of a FitzHugh-Nagumo model applied to the pulsatile release of luteinising releasing hormone. *Chaos*, 5:200–208, 1995.

[40] W Gerstner and W M Kistler. *Spiking Neuron Models: Single Neurons, Populations, Plasticity.* Cambridge University Press, 2002.

[41] G B Ermentrout and N Koppel. Oscillator death in systems of coupled neural oscillators. *SIAM Journal on Applied Maths*, pages 125–146, 1990.

[42] G B Ermentrout and N Kopell. Multiple phase interaction and averaging in systems of coupled neural oscillators. *Journal of mathematical biology*, pages 195–217, 1991.

[43] P Glendinning. *Stability, Instability and Chaos: An Introduction to the Theory of Nonlinear Differential Equations (Cambridge Texts in Applied Mathematics).* Cambridge University Press, 1994.

[44] S Coombes and P C Bressloff. Mode-locking and arnold tongues in integrate-and-fire neural oscillators. *Physical Review E*, 60(2):2086–2096, 1999.

[45] S Coombes. Liapunov exponents and mode-locked solutions for integrate-and-fire dynamical systems. *Physics Letters A*, 255:49, 1999.

[46] S Coombes, M R Owen, and G D Smith. Mode-locking in a periodically forced integrate-and-fire-or-burst neuron model. *Physical Review E*, 64, 2001.

[47] D T W Chik, S Coombes, and Z D Wang. Clustering through post inhibitory rebound in synaptically coupled neurons. *Physical Review E*, 70:011908, 2004.

[48] A Pikovsky, M Rosenblum, and J Karthy. *Synchronization*. Cambridge University Press, 2001.

[49] H R Wilson and J D Cowan. Excitatory and inhibitory interactions in localized populations of model neurons. *Biophysical Journal*, 12:1–24, 1972.

[50] H R Wilson and J D Cowan. A mathematical theory of the functional dynamics of cortical and thalamic nervous tissue. *Kybernetik*, 13:55–80, 1973.

[51] S Amari. Homogeneous nets of neuron-like elements. *Biological Cybernetics*, 17:211–220, 1975.

[52] S Amari. Dynamics of pattern formation in lateral-inhibition type neural fields. *Biological Cybernetics*, 27:77–87, 1977.

[53] J D Cowan. History of concepts and techniques. *Intelligent Systems*, 3:375–400, 2004.

[54] R L Beurle. Properties of a mass of cells capable of regenerating pulses. *Philosophical Transactions of the Royal Society London B*, 240:55–94, 1956.

[55] James M. Weimann, Petra Skiebe, Hans-Georg Heinzel, Cristina Soto, Juan Carlos Jorge-Rivera Nancy Kopell, and Eve Marder. Modulation of oscillator

interactions in the crab stomatogastric ganglion by crustacean cardioactive peptide. *Journal of Neuroscience*, 17, 1997.

[56] F C Hoppensteadt and E M Izhikevich. *Weakly connected neural networks*. Springer-Verlag, 1997.

[57] J Guckenheimer and P Holmes. *Nonlinear Oscillations, Dynamical Systems, and Bifurcations of Vector Fields*. Springer, 1983.

[58] S Coombes. Phase locking in networks of synaptically coupled mckean relaxation oscillators. *Physica D*, 160:173–188, 2001.

[59] P C Bressloff and S Coombes. Dynamics of strongly coupled spiking neurons. *Neural Computation*, pages 91–129, 2000.

[60] G B Ermentrout and N Kopell. Oscillator death in systems of coupled neural oscillators. *SIAM Journal on Applied Mathematics*, 50:125–146, 1990.

[61] P C Bressloff and S Coombes. Travelling waves in chains of pulse-coupled integrate-and-fire oscillators with distributed delays. *Physica D*, 130:232–254, 1999.

[62] P C Bressloff and S Coombes. A dynamical theory of spike train transitions in networks of integrate-and-fire oscillators. *SIAM Journal On Applied Maths*, pages 820–841, 2000.

[63] P C Bressloff. Mean-field theory of globally coupled integrate-and-fire neural oscillators with dynamic synapses. *Physical Review E*, 60:2160–2170, 1999.

[64] S Coombes and G J Lord. Intrinsic modulation of pulse-coupled integrate-and-fire neurons. *Physical Review E*, 56(5):5809–5818, 1997.

[65] S Coombes and G J Lord. Desynchronization of pulse-coupled integrate-and-fire neurons. *Physical Review E*, 55(3):R2104–R2107, 1997.

[66] S Coombes and A H Osbaldestin. Period adding bifurcations and chaos in a periodically stimulated excitable neural relaxation oscillator. *Physical Review E*, 63, 2000.

[67] N Fenichel. Persistence and smoothness of invariant manifolds for flows. *Indiana University Mathematics Journal*, 21:193–225, 1971.

[68] P C Bressloff and S Coombes. Dynamics of strongly coupled spiking neurons. *Neural Computation*, 12:91–129, 2000.

[69] T Yoshinaga, Y Sano, and H Kawakami. A method to calculate bifurcations in synaptically coupled Hodgkin-Huxley equations. *International Journal of Bifurcation and Chaos*, 9:1451–1458, 1999.

[70] G B Ermentrout and D Kleinfeld. Travelling electrical waves in cortex: Insights from phase dynamics and speculation on computational role. *Neuron*, pages 33–44, 2001.

[71] S M Crook. *The role of delay in oscillatory models of olfactory cortex*. PhD thesis, University of Maryland, 1996.

[72] S M Crook, G B Ermentrout, M C Vanier, and J M Bower. The role of axonal delay in the synchronization of networks of coupled cortical oscillators. *Journal of Computational Neuroscience*, 4:161–172, 1997.

[73] S Coombes and P Bressloff. Saltatory waves in the spike-diffuse-spike model of active dendritic spines. *Physical Review Letters*, 91:028102, 2003.

[74] P C Bressloff. Resonant like synchronisation and bursting in a model of pulse coupled neurons with active dendrites. *Journal of Computational Neuroscience*, pages 237–249, 1999.

[75] E A Arbas amd R L Calabrese. Slow oscillations of membrane potential in interneurons that control heartbeat in the medicinal leech. *Journal Of Neuroscience*, 7:3953–3960, 1987.

[76] A Roberts and M J Tunstall. Mutual re-excitation with post-inhibitory rebound. *European Journal of Neuroscience*, pages 11–23, 1990.

[77] S Coombes and S H Doole. Neuronal population dynamics with post inhibitory rebound. *Dynamics and Stability Of Systems*, 11:193–217, 1996.

[78] S Coombesa, S H Doole, and C Campbell. Central pattern generation in a model neuronal network with post inhibitory rebound and reciprocal inhibition. *Dynamics and Stability Of Systems*, 11:193–217, 1996.

[79] J J B Jack, D Noble, and R W Tsien. *Electric current flow in excitable cells*. Clarendon Press, Oxford, 1975.

[80] A Destexhe, Z F Mainen, and T J Sejnowski. Synthesis of models for excitable membranes , synaptic transmission and neuromodulation using a common kinetic formalism. *Journal of Computational Neuroscience*, 1:195–231, 1994.

[81] D Golomb, X J Wang, and J Rinzel. Propagation of spindle waves in a thalamic slice model. *Journal of Neurophysiology*, 75:750–769, 1996.

[82] M J Tunstall, A Roberts, and S R Soffe. Modelling inter-segmental coordination of neuronal oscillators. *Journal Of Computational Neuroscience*, 13:143–158, 2002.

[83] G S Cymbalyuk, R Borisyuk, U Meller-Wilm, and H Cruse. Oscillatory network controlling six-legged locomotion. optimization of model parameters. *Neural Networks*, 11:1449–1460, 1998.

[84] J Tegnér, A Lansner, and S Grillner. Modulation of burst frequency by calcium-dependant potassium channels in the lamprey locomotor system. *Journal Of Computational Neuroscience*, 5:121–140, 1998.

[85] J Buchanan. Neural network simulations of coupled locomotor oscillators in the lamprey spinal cord. *Biological Cybern.*, 66:367–374, 1992.

[86] N Dale. Coordinated motor activity in simulated spinal networks emerges from simple biologically plausible rules of connectivity. *Journal Of Computational Neuroscience.*, 14:55–70, 2003.

[87] R Perrins, A Walford, and A Roberts. Sensory activation and role of inhibitory reticulospinal neurons that stop swimming in hatchling frog tadpoles. *Journal Of Neuroscience*, 22:4229–4240, 2002.

[88] S R Soffe. Two distinct rhythmic motor patterns are driven by common premotor and motor neurons in a simple vertebrate spinal cord. *Journal Of Neuroscience*, 13:4456–4469, 1993.

[89] A Roberts. How does a nervous system produce behaviour? a case study in neurobiology. *Scientific Progress*, pages 31–51, 1990.

[90] A O W Stretton and E A Kravitz. Neuronal geometry determination with a technique of intracellular dye injection. *Science*, 162:132–134, 1968.

[91] K Kristensson and Y Olsson. Retrograde axonal transport of protein. *Brain Res*, 29:363–365, 1971.

[92] J H LaVail and M M LaVail. Retrograde axonal transport in the central nervous system. *Science*, 176:1416–1417, 1972.

[93] A Roberts and J D W Clarke. The neuroanatomy of an amphibian embryo spinal cord. *Phil. Trans. Soc. B.*, 296:195–212, 1982.

[94] W C Li, R Perrins, S R Soffe, M Yoshida, A Walford, and A Roberts. Defining classes of spinal interneurons and their axonal projections in hatchling xenopus laevis tadpoles. *Journal Of Comparitive Neurology*, 441:248–265, 2001.

[95] N Dale and A Roberts. Dual-component amino-acid-mediated synaptic potentials: Excitatory drive for swimming in xenopus embryos. *Journal Of Physiology*, 363:35–59, 1985.

[96] S R Soffe. Ionic and pharmacological properties of reciprocal inhibition in xenopus embryo motoneurons. *Journal Of Physiology*, 382:463–473, 1987.

[97] W C Li, R Perrins, A Walford, and A Roberts. The neuronal targets for GABAergic reticulospinal inhibition that stops swimming in hatchling tadpoles. *Journal Of Comp Physiol A*, 189:29–37, 2003.

[98] S R Soffe W C Li and A Roberts. Spinal inhibitory neurons that modulate cutaneous sensory pathways during locomotion in a simple vertebrate. *Journal Of Neuroscience*, 22, 2002.

[99] G B Ermentrout and N Kopell. Inhibition produced patterning in chains of coupled nonlinear oscillators. *SIAM Journal on Applied Mathematics*, 54:478–507, 1994.

[100] T Williams. Phase coupling by synaptic spread in chains of coupled neuronal oscillators. *Science*, 258, 1992.

[101] G B Ermentrout and N Kopell. Symmetry and phaselocking in chains of weakly coupled oscillators. *Commun. Pur. Appl. Math.*, 39, 1986.

[102] W Zhang G B Ermentrout and N Kopell. Multiple coupling in chains of oscillators. *Siam Journal on Mathematical Analysis*, 21, 1990.

[103] G B Ermentrout and N Kopell. Phase-transitions and other phenomena in chains of coupled oscillators. *SIAM Journal on Applied Mathematics*, 50, 1990.

[104] N Kopell G B Ermentrout and T Williams. On chains of oscillators forced at one end. *SIAM Journal on Applied Mathematics*, 51, 1991.

[105] G B Ermentrout and N Kopell. Inhibition-produced patterning in chains of coupled nonlinear oscillators. *SIAM Journal on Applied Mathematics*, 54, 1994.

[106] Liwei Ren and G B Ermentrout. Phase locking in chains of multiple-coupled oscillators. *Physica D*, 143:56–73, 2000.

[107] G B Ermentrout and N Kopell. Frequency plateaus in a chain of weakly coupled oscillators. *SIAM Journal on Applied Mathematics*, 15:215–237, 1984.

[108] G B Ermentrout and L Ren. Monotonicity of phaselocked solutions in chains and arrays of nearest neighbour coupled oscillators. *SIAM Journal on Mathematical Analysis*, 29, 1998.

[109] D Somers and N Kopell. Waves and synchrony in networks of oscillators of relaxation and non-relaxation type. *Physica D*, pages 169–183, 1995.

[110] A H Cohen and T Kiemel. Intersegmental coordination : lessons from modeling systems of coupled non-linear oscillators. *Amer. Zool.*, 33:54–65, 1993.

[111] M He, X Y Ma, and W J Zhang. Oscillation death in systems of oscillators with transferable coupling and time-delay. *Discrete Cont. Dyn. S.*, 7, 2001.

[112] M N Stolyarov, V A Romanov, and E I Volkov. Out-of-phase mixed mode oscillations of two strongly coupled identical relaxation oscillators. *Physical Review E*, pages 163–169, 1996.